Alma Mater Studiorum

Università di Bologna

SCUOLA DI SCIENZE

Dipartimento di Chimica Industriale "Toso Montanari"

Corso di Laurea Magistrale in

CHIMICA INDUSTRIALE

Classe LM-71- Scienze e Tecnologie della Chimica Industriale

Selective photo-oxidation of cellobiose with TiO_2-supported metal nanoparticles

Tesi di laurea sperimentale

CANDIDATO
Erica Lombardi

RELATORE
Dott.ssa Stefania Albonetti

CORRELATORI
Dott. Jose Antonio Lopez-Sanchez
Dott. Luigi Da Và

II sessione

Anno Accademico 2012-2013

KEY WORDS

Photocatalysis

Hydrolysis of biomass

Selective oxidation

Gold and silver nanoparticles

Titania

ACRONIM LIST

CB electronic conduction band of a semiconductor

CCD Charge Coupled Device

ESI ElectroSpray Ionization

HMF 5-Hydroxymethyl-2-furaldehyde

HPLC High Pressure Liquid Chromatography

ICP Inductively Coupled Plasma

ICSD Inorganic Crystal Structure Database

IR Infrared spectroscopy

NHE normal hydrogen electrode

OES Optical Emission Spectrometry

P123 poly (ethylene glycol)-block-poly (propylene glycol)-block-poly (ethylene glycol)

PVA poly (vinyl alcohol)

PVP poly (vinyl pyrrolidone)

RID Refractive Index detector

RSD relative standard deviation

RT room temperature conditions (T=~25°C, P=1atm)

SoP Side on Plasma

TEM Transmission Electron Microscopy

UV Ultra Violet wavelength (100-400nm)

UV-VIS Ultra Violet-Visible spectroscopy

VB electronic valence band of a semiconductor

VIS Visible wavelength (400-800nm)

VWD Variable Wavelength Detector for UV-VIS spectroscopy

WI wetness impregnation method

XRD X-Ray diffractometry

ABSTRACT

Upgrade of biomass to valuable chemicals is a central topic in modern research due to the high availability and low price of this feedstock. For the difficulties in biomass treatment, different pathways are still under investigation. A promising way is in the photodegradation, because it can lead to greener transformation processes with the use of solar light as a renewable resource. The aim of my work was the research of a photocatalyst for the hydrolysis of cellobiose under visible irradiation. Cellobiose was selected because it is a model molecule for biomass depolymerisation studies. Different titania crystalline structures were studied to find the most active phase. Furthermore, to enhance the absorption of this semiconductor in the visible range, noble metal nanoparticles were immobilized on titania. Gold and silver were chosen because they present a Surface Plasmon Resonance band and they are active metals in several photocatalytic reactions. The immobilized catalysts were synthesized following different methods to optimize the synthetic steps and to achieve better performances. For the same purpose the alloying effect between gold and silver nanoparticles was examined.

The training period for the production of this work was done at the University of Liverpool with Dr. J. A. Lopez-Sanchez group.

Summary

OBJECTIVE

The research in photocatalytic transformation of biomass is an interesting and new field because it can lead to greener transformation processes with the use of the principal renewable resource: solar light. For the peculiar biomass structure, the research is only at the beginning and applied to model molecules as cellobiose to understand the reactivity of the chosen catalysts. Furthermore, the reaction mechanisms have still to be completely investigated. In the photocatalytic field, supported metal nanoparticles have attracted interest for their activity in different reactions, in particular in the oxidation of alcohols, leading to the possibility of application of those systems to the transformation of biomass into valuable chemicals.

The aim of my research was the synthesis of noble metal supported nanoparticles and its application in the hydrolysis of cellobiose. The principal product expected by this reaction was glucose, deriving from the break of the β-1,4-glycosidic bond of cellobiose. A new approach to this reaction was followed using light-activated catalysts to perform the reactions under visible irradiation. Within the different semiconductors, titania was selected as a support because it presents catalytic activity in the UV region and its absorption in the visible can be enhanced by semiconductor doping techniques. For that reason, noble metal nanoparticles were immobilized on titania because they can act as electron acceptor in the visible range through their Surface Plasmon Resonance band.[40, 86] Furthermore, they present good activity in several photocatalytic reactions[86, 123] and the electron transfer between the metal nanoparticles and titania bandgap is widely proved.[60, 127]

Two methods were chosen to synthesize the immobilized catalysts. Wetness impregnation was used as a first approach to optimize the synthetic parameters. Moreover, immobilized colloidal nanoparticles were selected for a deeper analysis. The alloying effect between those two metal nanoparticles was also evaluated.

The synthesized catalysts were then tested in the reaction of hydrolysis of cellobiose under visible irradiation and their synthetic features were optimized to try to obtain the best catalytic performances.

1. INTRODUCTION

1.1. Biomass importance

Industrial chemistry of the 20th century and the early 21st century was designed around crude oil, due to the high availability and low prices. However, presently, this strongly focused raw materials base appears to become more reliable in the future, due to international financial and political factors. Therefore worldwide researchers attention has recently focused on the development of novel catalytic processes involving the production of fuels and chemicals from unconventional energy sources. Biomass are found to have the first place in this field, because of their abundance on the heart surface, their rapid growth and the possibility to reuse industrial and agricultural raw materials.[91]

Different techniques have been developed to transform biomass into available fuels as bioethanol, biodiesel and bio-oil. The most widely used between them is bioethanol, derived by food crops as corn and sugarcane. Anyway, one of the major problems of those biofuels is that their production competes with the need for food.[104] This question was solved using for fuel production second generation feedstocks or exploiting lands that are not available for agriculture.

Furthermore, the utilization of cellulose-based biomass is not only driven to energy supplies, also the production of fine chemicals is also a key technology. Polysaccharides as starch and cellulose can be converted into monosaccharides or into oxidation products as 5-hydroxymethyl-2furaldeide (HMF) or levulinic acid which are renewable platform molecules for the synthesis of a variety of chemicals.[104]

1.1.1. Biomass structure and reactivity

Biomass are generated by simple molecules as water, CO_2, O_2 and N_2 linked together by complex biochemical processes (photosynthesis and others) with a productivity of complex substances of ca. 170×10^9tons per year.[132]

The major components of plant biomass are carbohydrates or saccharides (cellulose, hemicelluloses, starch and saccarose) and they are around 75% of the total plant biomass.[87]

The total biomass composition can be subdivided in cellulose, hemicellulose, lignin and other minor constituents. The most important polymer that is part of the carbohydrate fraction is cellulose (ca. 40% of the total biomass composition[132]). It is built up of linearly connected β-(1,4) glucose molecules and, owing to its regular structure, it forms extensive networks with inter and intramolecular hydrogen bonds. Hemicellulose instead it's an amorphous polymer composed of several sugar molecules like glucose, galactose, mannose and xylose (Figure 1) and comprises ca. 25% of the total biomass fraction.[31] A more complex structure has been assigned to lignin, which is an amorphous, insoluble polymer consisting of aromatic and polyaromatic parts (Figure 1). This polymer makes the ca. the 30% of the total mass of biomass.[87] Minor constituents (ca. 5%) include organic extractives as fats, oils, proteins and inorganic compounds.[133, 114] The ratio between the different components can vary highly depending on the type of feedstock considered.

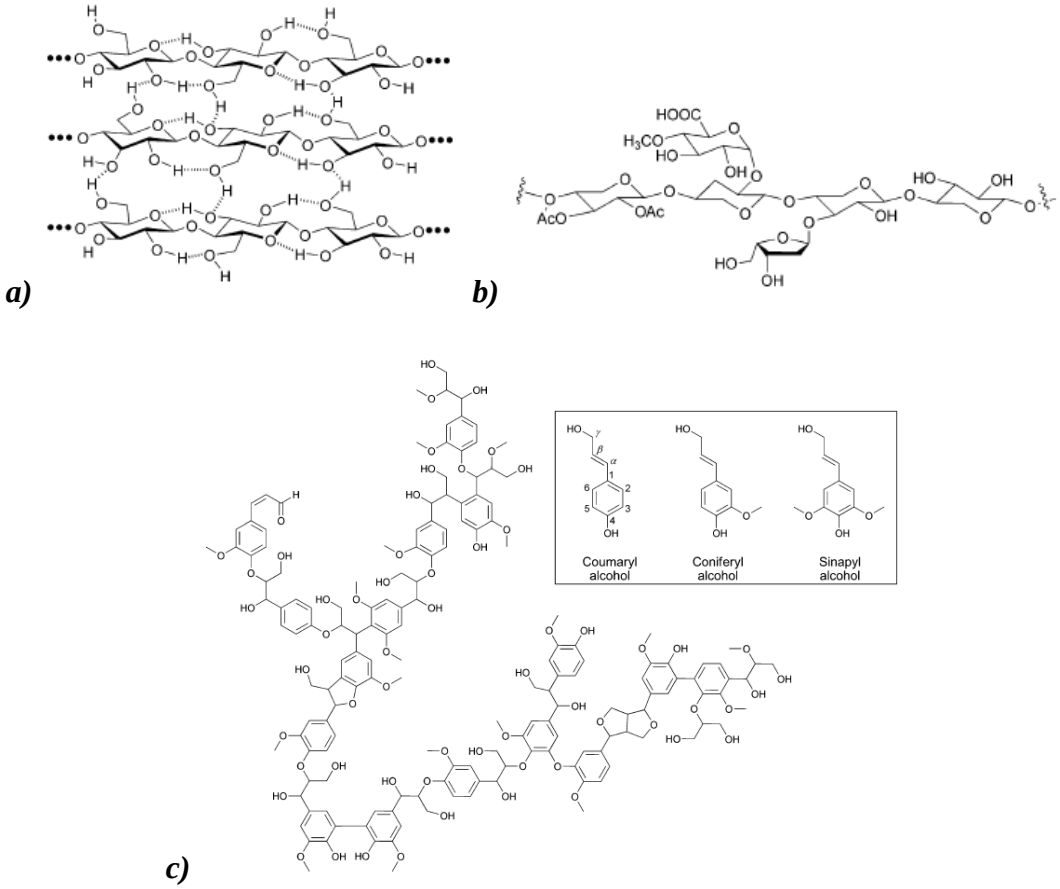

Figure 1: Composition of the different biomass polymers: a) cellulose, b) hemicelluloses and c) lignin and its principal building blocks.[91]

Lignocellulose has obtained increasing attention in the last few years in chemical research due to its structure that leads to the phenomenon known as "biomass recalcitrance". That is because this polymer is naturally build up to resist to microbial and enzymatic deconstruction, hydrolysis and solubilisation so it is hard to treat especially in water environment. On the other hand, those structures are an important energy storages for incoming solar radiation through photosynthesis and represent an alternative pathway for the production of fuels and chemicals. For these reasons, biomasses have been studied hardly recently to try to enhance the catalyst/substrate interactions and to improve the products yields.[91]

1.1.2. Traditional acid catalysis

Cellulose transformation starts from its depolymerisation by hydrolyzing the β-1,4-glicosidic bonds and it is generally developed as an acid catalyzed reaction. This depolymerisation reaction (both with homogeneous and heterogeneous catalysts) can be classified as an heterogeneous reaction because its yield is determined by mass-transfer effects between the insoluble cellulose particles and the aqueous environment where the catalytic system is dissolved. To reduce this rate-limiting step of reaction, cellulose can be pre-treated with mechanical ball milling or several chemical processes. In particular the milling step seems to disrupt cellulose bonds and reduce significantly the crystallinity degree (as reported by XRD analysis) enhancing the solubility of the reagent.[114]

The catalytic tests reported in literature are usually done on lignocellulosic materials, microcrystalline cellulose or cellobiose. The first one is the most complex to analyze because of the wide range of different compounds content, so it is the less used. Microcrystalline cellulose is the crystalline part of biomass and the most difficult to hydrolyze, because it is build up of packed cellulose chains. Cellobiose, instead, is the cellulose dimer and it is used as a standard for depolymerisation studies (Figure 2).

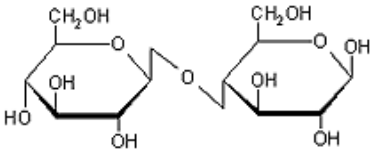

Figure 2: Cellobiose structure, build up by two glucose molecules linked by a β-1,4-glycosidic bond.

From cellulose and hemicellulose reactions not only sugars and sugar alcohols are obtained (glucose, fructose, mannose, xylose...) but also other oxidation, dehydratation and hydrogenation products (HMF, levulinic acid, furfural... Figure 3) that can be further transformed in furan based biofuels, liquid alkenes and valeric biofuels.[125] Those reactions are called "biorefinery processes" and are also catalyzed by acids.[105]

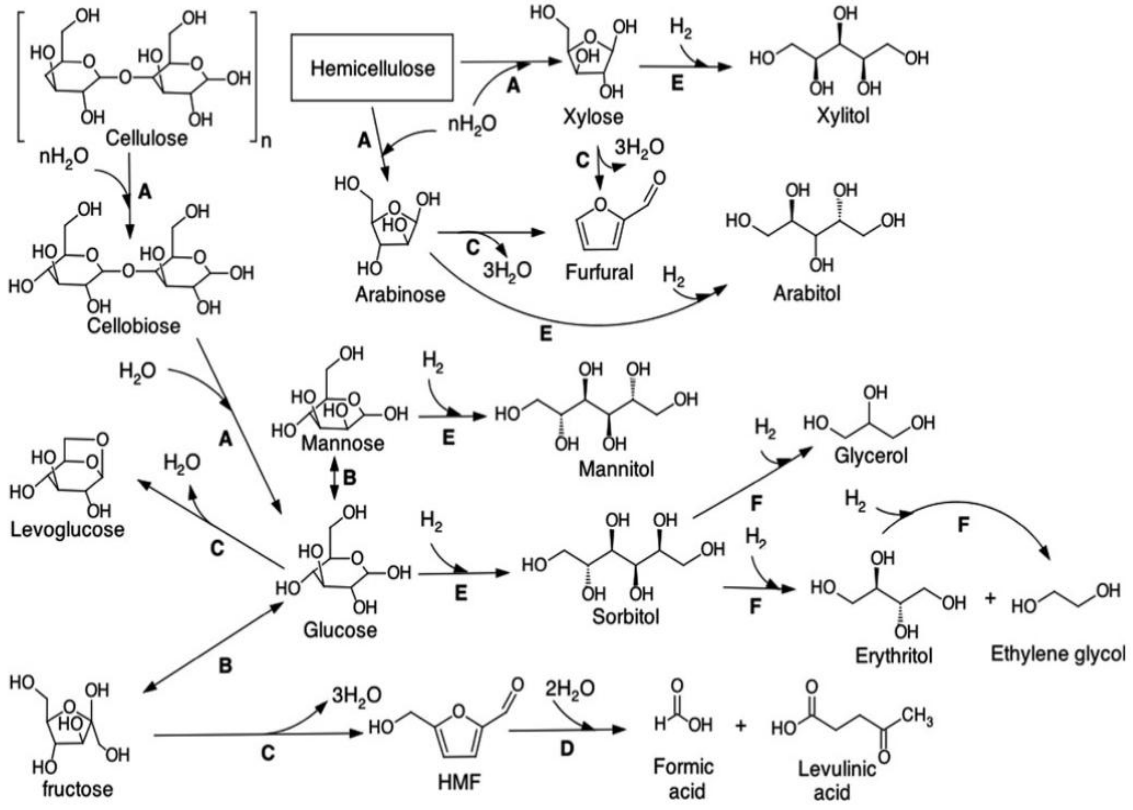

Figure 3: Principal reaction pathways for the conversion of cellulose. The reactions identified are (A) hydrolysis, (B) isomerisation, (C) dehydration, (D) rehydration, (E) hydrogenation and (F) hydrogenolysis.[89]

The attention on furanic derivates has reached high interest because HMF can find application in plastics and polyesters production, pharmaceuticals and diesel-like fuels.[112] The production of this molecule is object of study also in presence of ionic liquids, applying a variety of homogeneous and heterogeneous catalysts. Other furan-like

products obtainable from typical waste biomass sources (as cotton, newspaper and wood) are 5-chloromethyl-furfural (CMF) and 2,5-dimethyltetrahydrofuran (DMTHF) applied for liquid fuels.

Furthermore levulinic acid and its derivatives, such as γ-valeriolactone are important for the production of bioplastic products but do not exhibit the required properties to compete with traditional liquid fuels. In contrast valeric biofuels, which are a new platform of levulinic acid derivates, have been recently proposed as candidate molecule for their fuel properties. In this field, the most promising molecule in this class is pentyl valerate but γ-valeriolactone can also be converted to liquid C8 alkenes (a mixture of n-butenes).[114]

1.1.2.1. Homogeneous and heterogeneous catalysis

Homogeneous catalytic reactions have been the first developed because the catalyst is dissolved in reaction medium, facilitating the interactions with the dispersed solid biomass. Generally they require milder conditions and reactions are very selective. Mineral acids are involved: trifluoroacetic, nitric, phosphoric, hydrochloric and dicarboxylic (oxalic, maleic, fumaric) acids. The principal problem with these catalytic systems is linked to reactor corrosion, neutralization and separation steps that prevent the diffusion of the technologies. The use of sulphuric acid, for example, needs a complex treatment of the reaction products leading to separation, recycling problems and treatment of the high amount of acid waste.[114]

In recent years industrial chemistry has changed its priority with the diffusion of "green chemistry" and "green technology" principles. These dictate that the production of chemicals should reduce its impact on human health and environment. In this scenario reaction catalyzed by mineral acids are not more acceptable for the problems they lead, and it is stimulated the replacement with recyclable, nontoxic solid acids with strong acid sites. From 1940s liquid acids have been replaced with solid acids in the major areas of chemistry like fuel production, bulk chemicals, oil refining and petrochemical industries.[105] Even though the yields of reaction with solid acids are often lower than with mineral acids, these new catalysts have the advantage to be easily separable after reaction by their immobilization on supports or by generating multiphase systems.[91]

Relatively to biomass conversion, in particular to the degradation of cellulose, the main type of active solid acid catalysts studied in literature are: sulfonated active carbons,[80] amorphous carbons bearing SO_3H, COOH and OH groups,[101] silica/carbon nanocomposites,[115] layered $HNbMoO_6$,[104] Ru supported on mesoporous carbon materials (CMKs),[56, 69] sulfonated CMKs,[83] heteropolyacids with polyvalent transition metal salts[114] and magnetic solid acids.[61]

The research on these materials is still in development because, the catalysts need to be selective with high temperatures of reaction and in polar solvents and have to possess strong acidity and a porous structure that allows the access of the sugars in the active sites.[104] Furthermore, they have to be stable in reaction conditions without modification of its structure and deactivation, leading to the challenge of finding catalytic materials that possess adequate hydrothermal stability.[89]

For these reasons also different systems are in analysis to stick to green chemistry principles and find high conversion values with renewable energy resources.

1.2. Nanotechnology and metal nanoparticles

Atoms and molecules have been the principal focus for chemistry in the late 19th and 20th centuries, allowing a deep knowledge in the micrometer size. Nowadays the field of study has moved to the nanometric scale with the analysis of small agglomerates of atoms or molecules in the range of dimension between 1 and 100nm. In this range the properties of materials are different from the atomic size and the bulk of materials, due to the high ratio of surface/bulk atoms, and new characteristics have been discovered as electron confinement and shape importance. For that reason peculiar features can be obtained with different sizes and shapes of the same material in the nanometric dimensions.[32]

One of the most clear examples of this change is offered by metals: their delocalized electrons on the surface in bulk systems are the explanation for the high electrical and thermal conductivity, instead when metal nanoparticles are formed the electrons can move in more confined spaces, leading to completely different properties.[118]

Recent developments in nanopartcle synthesis have permitted a better control in particle dimension and shape, providing more suitable catalysts for specific activities. One of the most interesting aspects is reaching the smallest nanoparticles to enhance the surface to volume ratio so the availability for reaction. This is strictly connected to the activity of those nanosized technologies together with other aspects as surface relationships, intraparticle metal–metal bonding, strength of metal–support interaction, structure and atom packing geometry.[118]

The characterisation of those systems involves different spectroscopic and analytical techniques that permit the classification of the nanoparticles in terms of dispersion on the support, size, defect, structure of the crystal, plasmonic band and oxidation state of the metal. The most widely used techniques for nanoparticle analysis are X-Ray photoelectron spectroscopy (XPS), X-Ray diffraction (XRD) and transmission electron spectroscopy (TEM). Furthermore the support features have to be analyzed, because they affect the activity and availability of immobilised metal nanoparticles. Characterization is done primarily in terms of accessibility of active sites, and even regarding particle dimension, morphology, textural properties (pore volumes and size, micro or mesopore capacity), chemical nature, surface functionality (groups, loading and acidity/basicity), and surface energy characteristics (hydrophobicity/hydrophilicity).[118]

The challenging field of nanoparticles and their application has collected a huge number of publications in the last 20 years, especially in relation to silver and gold that present the more unexpected changes from the bulk metal.[32] Many efforts are devoted to the synthetic step because it presents a variety of challenges that are still not solved, as tuning the dimension, shape and monodispersity. For this reason, different techniques have been developed to enhance the interaction between nanoparticles and substrates or target molecules. In recent years, the number of useful application papers for nanoparticles has grown, strictly related to the increase in knowledge in this field and new synthetic pathways have been found enhancing the activity of this research area. Thus, increasing both the field of synthesis and of application has lead to potentially great applications of those nanotechnology systems in everyday life.[32]

Nanotechnologies are interdisciplinary not only for their usefulness but also in relation to the kind of knowledge necessary to improve their synthesis and enhance exploitation that spaces from physics and biology to chemistry. The principal fields of nanoparticle application are medicine (as delivery system, contrast agents and magnetic resonance imaging [MRI]), for chemical sensors (as electrochemical sensors and biosensors) and in heterogeneous catalysis (oxidations, hydrogenations and C-C coupling reactions).[118]

1.2.1. Synthesis and immobilization methods for metal nanoparticles

There are different methods to synthesize nanoparticles and support them. That is due to the fact that the surface interactions between the metal and the support are specific. Moreover, each method leads to peculiar physicochemical properties as dispersion, size and features of the metal, surface area and pore diameter of the support.

The principal immobilization methods can be listed as: wetness impregnation, deposition-precipitation, graft hybrid, colloids immobilization and nanoparticle encapsulation.[130]

Deposition-precipitation pathway is the most used for industrial syntheses: the metal salt is precipitated in the hydroxide form on the support by changing the pH and subsequently the solid is dried and calcined. Furthermore, this method is largely used when the support is intrinsically acid or basic but the obtained particle size dispersion is highly variable leading to difficulties in specific catalytic applications.[3]

Graft hybrid method enhances metal/support interactions by surface functionalisation of the support but the synthesis is often complex because a large number of steps and reagents are required.

Another method is the encapsulation of preformed nanoparticles into the supporting material during its growth, as in the case of hydrothermal synthesis of mesoporous silica. This leads to a good dispersion of the particles but can infect the structural features of the support itself.

Finally Wetness Impregnation and colloids immobilization are within the most employed in research, because the first one is the simplest way to support metal nanoparticles and the second allows the possibility of tuning synthetic parameters, then are treated in depth in the sequent paragraphs.

1.2.1.1. Wetness impregnation method

Wetness impregnation method have been the first developed to prepare gold based catalysts.[26] Even if the activity of these catalysts is not always as high as following other synthetic pathways[15, 67, 92] it is still widely used to immobilize metal nanoparticles on different supports such as mesoporous materials and metal oxides. That is because this method is simple, it doesn't need high temperatures of reaction and it is not requested any pre-formation of nanoparticles. Also the quantity of metal effectively immobilized on the solid surface is higher compared to other methods such as reduction deposition.[92]

Generally the metal salt solution is added to the substrate, and the drying step allows the loading in the pores of the support by capillary force.[131] The metal is then dried and reduced by calcination in air or under hydrogen atmosphere, confirming the presence of nanoparticles with both pathways. This synthesis leads to big particles with a and poor dispersion on the surface[92] due to the difficulty of controlling thermal activation and reduction in the formation of nanoparticles.[3] Bimodal size distribution or different types of nanostructures are often obtained because the particles grow in the inner part of the channel of the support and on the surface. This is due to the difficulty of controlling the nucleation and growth and to the high mobility of ions during the thermal treatment. Besides, the heating ramp has a fundamental importance in this type of synthesis because acts as a control between thermodynamic and dynamic trends. In detail, thermodynamic

control tends to the formation of large metal crystals (growth) and it is enhanced by a slow heating ramp, instead multinucleation is under dynamic control and leads to smaller particles with a fast ramp. Basic for the determination of size and dispersion is also the pore dimension of the support. That is why mesoporous materials are the most widely studied because they can encapsulate easily big nanoparticles.[102]

Another problem of this method is due to the presence on the catalyst at the end of the synthesis of the counter ion of the metal salt. That is because it can compromise the catalytic activity, especially in the case of chlorine for gold catalysts. This atom can cause the poisoning of the active sites and also enhances sintering of gold nanoparticles. Several modified wetness impregnation methods have been developed to avoid this problem. For example double precipitation with a base allows the deposition of gold in the hydroxide form facilitating the removal of chlorine ion.[15]

1.2.1.2. Catalysts prepared with preformed nanoparticles

Synthesis of sols has been one of the most used techniques to obtain metal nanoparticles because it permits control of size, shape and crystalline phase before embedding the nanoparticles in the support. The principal components of this type of synthesis are the precursors and the solvents. Precursors are surfactants that act as particle size and shape drivers, solvents instead have the aim of enhance the dispersion. The choice of both depends on the desired features of the final product and to the specific properties of the metal/substrate pair. The step of nanoparticle formation is also different within synthetic methods: the most used in the case of metals is thermal reduction because it leads to spherical, monodisperse particles; other pathways are chemical reduction or oxidation, precipitation, sol-gel and galvanic exchange.[3]

Thermal reduction involves the addition of the precursor into a hot solution of solvent and stabilizing agent, sometimes is necessary also the addition of a reducing agent to reach the zero oxidation state of the metal. The strength of the reducing agent is strictly related to the type of metal or precursor used: in the case of a high negative reduction potential a strong reducer is necessary (sodium borohydride or superhydride). Milder ones instead are preferred to enhance the growth step of nanoparticles (carboxylic acids or 1,2-alkanedyols).

Stabilizing agents are named also ligands or surfactants because they prevent nanoparticle aggregation stabilizing the sol from precipitation. They stick to the metal enhancing, with their hydrophilic or hydrophobic part, the interaction with the solvent. Furthermore choosing an appropriate ligand the dimension of the particles and the dispersion of the sol can be controlled because it changes the type of nanoparticle/ligand bond. Covalent interactions are stronger and consent a better stability of the solution but they cannot be easily removed. The opposite is electrostatic binding that suffers more of the system perturbations (temperature, ionic strength, dilution) but allows an ease of replacement with supports or other molecules.[3]

Another type of weak ligand is represented by steric stabilizers, that are often polymers or other high molecular weight molecules with heteroatoms interacting with the nanoparticles. The most used are poly(N-vinyl-2-pyrrolidone) [PVP], poly(vinyl alcohol) [PVA], poly(acryl amide), poly(acrylic acid) and poly(ethyleneimine) with different protective values.[81] In polar solvents the non-toxic PVP is the most used because in part it binds at the metal surface creating the first layer while the excess dissolves in the solution generating a double protective layer that controls the particle size.[49] In some cases the stabilizer can act also as reducing agent, for example with ethylene glycol, but it is necessary the addition of other molecules as PVA to avoid the aggregation of the colloid.[14]

Sol suspension are generally loaded on different types of materials to enhance the dispersion and/or the catalytic activity. The most used immobilization methods are encapsulation and capillary inclusion, obtained generally by simple sonication.[3] Also in this case the specific features of the metal and support pair play a great role leading to a variety of specific synthetic pathways.

1.3. Photocatalysis

Photocatalysis is a branch of chemistry that exploits light radiation to overcome the energy barriers of chemical reactions.[86] Solar light is a renewable source of energy but only in the last century it has been analyzed as a potential motor for chemistry. Photochemical and photophysical processes between light and matter are now under study to become both supplementary and complementary to traditional reactions. Until now the most analyzed applications for photocatalysis are the destruction of pollutants in water[42] and water splitting.[64]

1.3.1. Semiconductors

Semiconductors are nanostructured materials that permit the conversion of light into chemical energy behaving as photocatalysts for light-induced reactions. For that reason their optical characteristics are exploited in different application. The most important feature of those materials is represented by its electronic structure made up of a filled valence band (VB) and an empty conduction band (CB) separated by a gap that permits the excitation of electrons by light of a specific wavelength. Moreover a semiconductor can be used as photocatalyst if the redox potential for the generation of hydrogen and oxygen from water, or for other reactive oxygenated compounds from water (as hydrogen peroxide, hydroxyl, and superoxide radicals) is included between its band gap.[60]

Photoactivation of semiconductors can be explained as shown in Figure 4: incident photons of appropriate wavelength (*hv* equal to the bandgap energy) excite electrons of the solid from the valence to the conduction band generating a "hot" electron/hole pair that acts subsequently as a catalyst.[86]

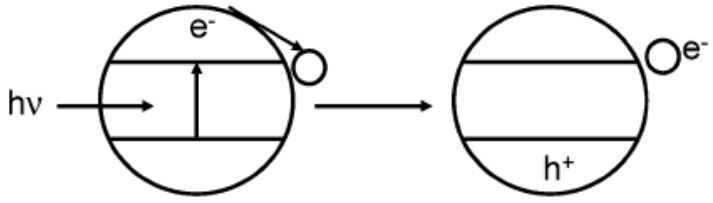

Figure 4: Light excitation of a semiconductor. Electron is expressed as e^- and hole as h^+.[86]

In Figure 5 are shown the bandgap energies of the most employed photocatalysts, which is the difference in electron volts between the lower state of the conduction band and the upper one of the valence band. Energies are referred to the normal hydrogen electrode (NHE). In relation to the material and the pH, the holes present in the valence band, generated from light excitation of the semiconductor, can act as oxidants (between +1V and +3.5V) and the excited electrons in the conduction band can act as reductants (between +0,5V and -1,5V).[42] For the reported semiconductors the energy values reported leads to an excitation that falls in the UV region of the light spectrum.

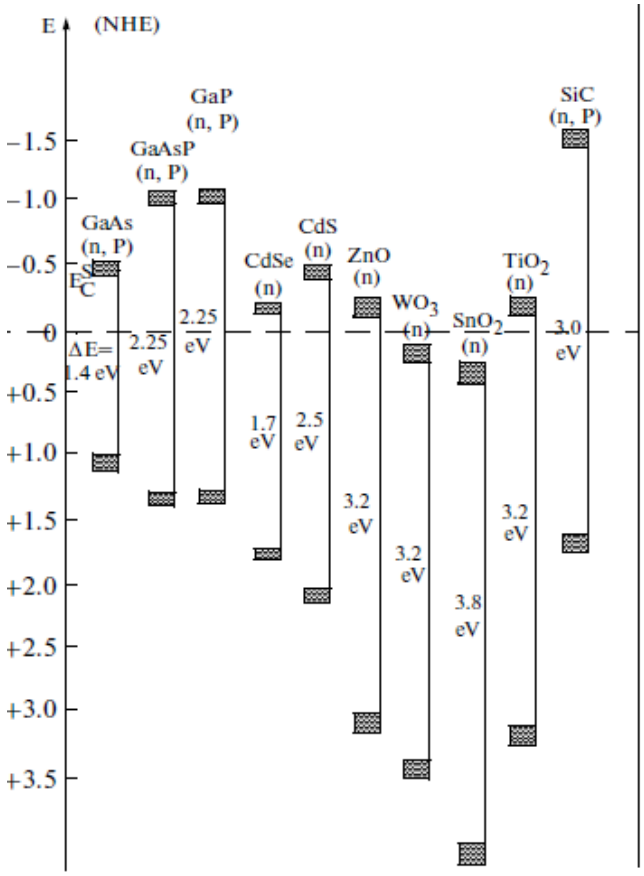

Figure 5: Semiconductor bandgaps in aqueous electrolyte at pH 1.[42]

The possibility of using a semiconductor as a photocatalyst is also strictly related to the ratio between the light excitation and the deactivation process due to the recombination of electrons and holes. For that reason a key factor for the photocatalytic ability is the surface area because it influences the optical properties. A semiconductor with a high surface area has a high density of localized states, that means electronic states with energy between the conduction and the valence band.[77] These states, and unsaturated bonds on the surface, are allowable for electrons as trapping sites and enhance the charge

separation. Also the adsorbed species density is important because it infects the transfer of these trapped charge carriers to form radicals rather than recombine.[43]

Furthermore, other important features of a semiconductor that has to be taken into account are: non toxicity, simple synthetic pathways, low production cost, catalytic effects and solar light activation.[42] Also stability issues have to be considered, especially in water and air-saturated environment.[60] For example some metal sulphides and chalcogenides, even though they present photocatalytic activity, are subject to photocorrosion in water solution and dissolve under irradiation, leading to their not exploitability.[86]

1.3.2. Titania

The first application of titanium dioxide under light irradiation started from a paper published in 1972 by Fujishima and Honda in which they demonstrated that water could be photolized electrochemically under UV light by immerging a titania photoanode in combination to a Pt counter electrode in an aqueous electrolytic solution.[36] Since then, advanced studies have been undertaken on the applications of titania in water purification and solar light activated catalyst, due to the most specific features of this material: non toxicity, low cost, photocorrosion stability and above all its potential bandgap. Furthermore, titania can be recycled by immobilisation on glass, fibers, activated carbons, sand and inorganic crystals.[60]

Titania has also another advantage as a semiconductor: annihilation of excited electrons and holes doesn't happen quickly letting them reacting with other molecules in solution. The movement of electrons in the conduction band happens faster than hole jumping from neighbour sites. That lets the possibility for charge carriers to migrate to the metal oxide surface where reactions happen.[86]

This reactivity can be proved comparing the time of excitation of electrons under UV light to their relaxation into the valence band. The first one is in the order of femtoseconds (10^{-15}s),[21] instead the second one occurs within ca. 10^{-14}s (Figure 6). That means that more carriers are produced than the annihilated one. Those are then able to move within the band and are vulnerable to different processes:[84]

1. Arrive at the surface of the solid and react with the other molecules in solution (direct photocatalytic reaction)
2. Be lost by recombination in the bulk of the solid (bulk recombination)
3. Be trapped in surface states and undergo the same processes as (1.) with other molecules in the surroundings ore recombine (2.) (photocatalytic reaction via surface states and surface recombination)

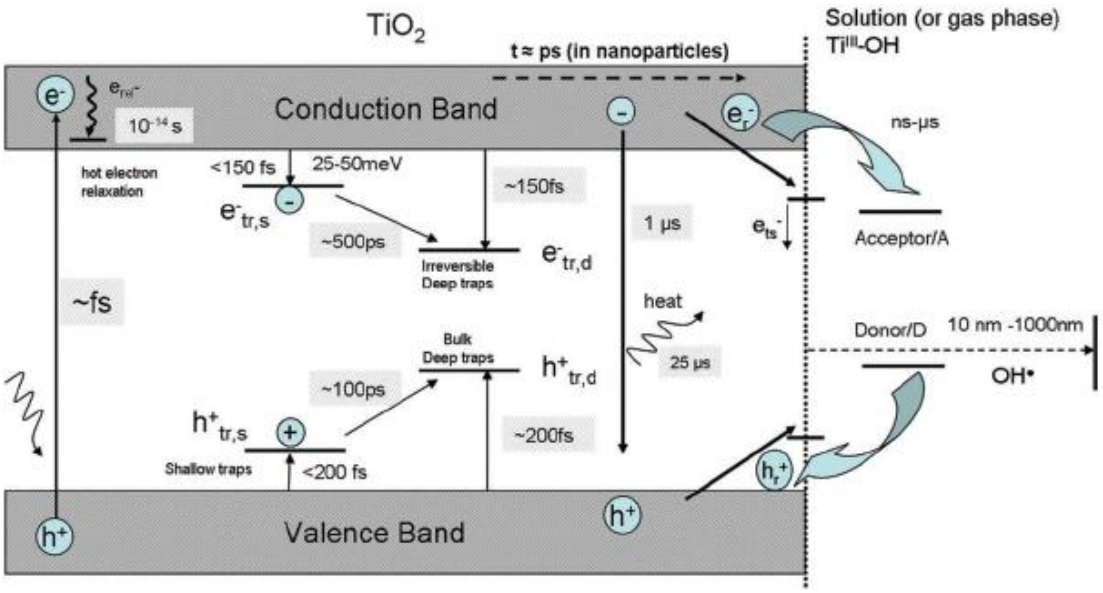

Figure 6: Typical time scales in photocatalytic process on TiO_2 as an indication on kinetic reaction values on titania surface.[84]

The electrons produced by UV radiation in the conduction band can present a mild reducing ability (E_{red} ca. -0.3V), instead holes in the valence band can act as strong oxidizers (E_{ox} ca. +3.0V)[66] towards the molecules adsorbed on the surface, as O_2 or H_2O. This electrostatic potential consent the reduction by excited electrons of acceptors as oxygen to superoxide ($^{\bullet}O_2^-$) and the subsequent formation of hydroperoxide radicals (HOO•) and other oxygenated reactive species. On the other hand, surface holes can oxidize absorbed water and titanol groups (superficial TiO-H) generating hydroxyl ($^{\bullet}$OH) and titanoxyl (TiO$^{\bullet}$) radicals (Scheme 1).[86] Although the hydrophilicity of titania is not very high and few molecules are adsorbed onto its surface from the solution or ambient moisture, they are fundamental for photocatalysis due to their interaction with the reactive species (Figure 7).

$$TiO_2 + h\nu \rightarrow h^+ + e^-$$

$$h^+ + H_2O_{abs} \rightarrow H^+ + {}^{\bullet}OH$$

$$h^+ + {}^{-}OH_{abs} \rightarrow {}^{\bullet}OH$$

$$e^- + O_{2\ abs} \rightarrow {}^{\bullet}O_2^-$$

Scheme 1: Principal reactions of photogenerated electrons and holes with adsorbed species.[43]

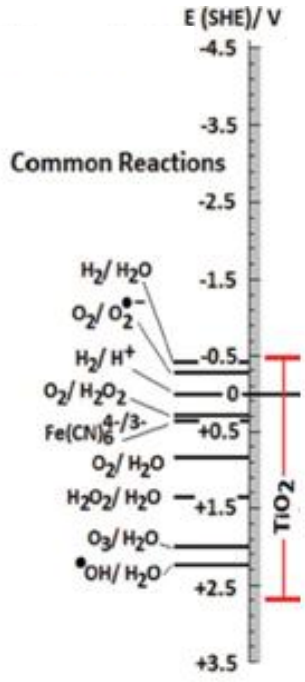

Figure 7: Titania bandgap compared to different redox couples.[84]

For the degradation of pollutants in waster also the pH of solution is important: the zero point charge (point where the electrical charge density on the surface is zero) for titania is about 6. At superior values the generation of the reactive ${}^{\bullet}OH$ radicals (E_{ox} = 2.1V), after light absorption, is easier and they can transform the organic molecules by hydrogen abstraction, oxidation or electrophilic attack.[122, 124] Generally the reaction starts with the hydroxyl attack leading to further oxidative degradation of the organic to mineralization. Even titanoxyl radicals enhance decomposition of molecules in solution.[86]

Titania is present in nature in different allotropic structures: the most common are anatase, rutile and brookite (Figure 8). Other five phases have been reported under high pressure (as TiO_2 II). Rutile is the only stable structure, anatase and brookite are metastable, so they tend to transform in rutile under harsh conditions or in the presence of dopants.[43] Brookite is the more difficult to synthesize, so it is the less studied and

exploited. From the photocatalytic aspect different polymorphs present different photocatalytic activity: the most active under UV irradiation is anatase, followed by rutile and the amorphous phase.[93] The main factor that allows a better photocatalitic activity for anatase is a higher density of localised states that slows the recombination of charge carriers enhancing the presence of surface adsorbed hydroxyl radicals. On the other hand, rutile presents a higher kinetic of electron-hole recombination, due to a larger grain size and a subsequent lower capacity of absorbing species compared to anatase.[43]

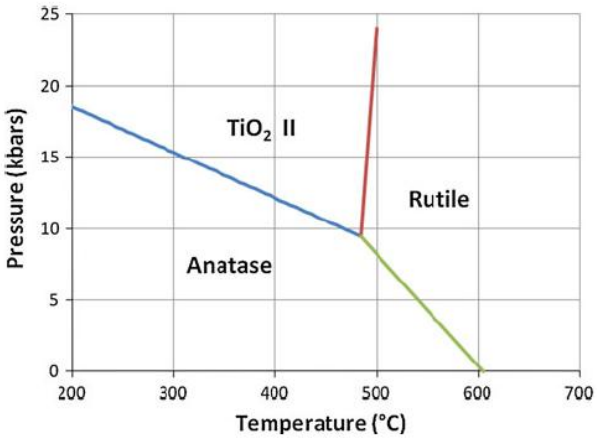

Figure 8: Pressure/temperature phase transition diagram of titania.[43]

The photocatalytic activity is also strictly correlated to the way of synthesis of the material because the electron-hole recombination is affected by the presence of impurities, the particle dimension and by the surface area. This leads to several reproducibility difficulties during the synthesis. To overcome this problem, commercial TiO_2 P25 from Degussa (about 80% anatase and 20% rutile), obtained by spray pyrolisis, has been taken as a standard material for its high photocatalytic activity and its synthetic reproducibility.[86]

Even using the same material, experimental data are not always reproducible between different research groups because of the huge number of variables in the reaction systems (light intensity, emission spectra distribution, configuration and geometry) and in the environment (moisture and impurities).[71] These problems are common in heterogeneous catalysis but, using light irradiation as a reagent, also its features have to be taken into account.[86]

The use of titania as a photocatalyst requires the excitation of the electrons by light with a wavelength equal to the band gap region, which is ~3.4eV for anatase,[107] ~3.3eV for

brookite[72] and ~3.0eV for rutile.[2] The bandgap energy falls in the UV region of the spectrum. On the other hand, solar radiation is the most attractive energy source for photocatalysis because it is free and renewable. Its emission is composed by a 5% of UV, harvesting infrared and visible respectively around 52% and 43%. Unfortunately the excitation of titania under solar light is not possible for the position of its bandgap. For that reason, research has been driven into bandgap tuning to enhance the visible light response of this semiconductor. That permits the utilization of a bigger fraction of the incoming radiation, expanding possible applications as a photocatalyst.[60]

Different strategies of visible-enhancement of titania bandgap have been developed: coupling with a narrow bandgap semiconductor, doping with metal or nonmetal ions, co-doping with foreign ions, surface sensitization with organic dyes or metal complexes, fluorination and noble metal deposition. Briefly the enhancements of the most applied doping systems are subsequently explained.

The use of another semiconductor, with a near and thermodynamically favorable bandgap to titania, can increase the lifetime of charge carriers and the activity by the interfacial charge transfer between the two solids.[95, 96] As reported coupling with SnO_2 favours the charge separation and so also the photocatalytic activity of titania.[48, 60, 126]

Metallic and nonmetallic elements have been widely studied but both presents pros and cons. The use of metal ions, that replaces titanium ions in the solid structure, is difficult to reproduce and the material is unstable, on the other side, using nitrogen or other nonmetallic ions the synthetic conditions are really harsh and it is really difficult to reproduce.[86]

Noble metal deposition is one of the most widely used techniques because the metal enhances the bandgap of titania and leads to a favourable surface structure with high quantum efficiency that speeds the rate of organics degradation in water.[60]

1.3.3. Metal nanoparticles in photocatalysis

Noble metal nanoparticles have found wide use in photocatalysis as part of sustainable and green processes. That is because they can transform the incoming solar energy into chemical energy available for reactions. Usually the application of those system is in heterogeneous catalysis, but some non-supported catalytic studies have been performed. For their peculiar properties and photocatalytic activity metal oxides are the most used supports (TiO_2, SiO_2 and ZrO_2) but other silver halides have been studied.[117] The main reason is that the metal particles capture the incoming radiation and transfer the charge carriers to the support enhancing surface reactions.[39]

This charge transfer on the semiconductor can be classified in metal doping techniques, even if in this case the metal nanoparticles are not substituting the ions in the solid framework. The metal in fact consist in a separate phase in surface contact with titania. Generally noble metals are used because they are chemically inert for photo oxidation.[86]

When metal nanoparticles are applied to catalysis, one of the most important features to keep under control is the particle dimension because, as reported above, physicochemical features change with the size and the shape of the particles. Considering also the interactions with the substrate, other characteristics are: dispersion of the metal on the surface (generally reported as a percentage) and loading (percentage of metal weight on the material).

These parameters are strongly dependent on the synthetic procedure applied to support nanoparticles.[86] The principal methods can be subdivided in: physical routes (sonochemistry, microwave irradiation, supercritical fluids and pulse laser ablation), physico-chemical routes (sonoelectrochemistry and flame pyrolisis) and chemical routes (impregnation, co-precipitation, deposition precipitation, microemulsion, photochemistry, electrochemical reduction and chemical vapour deposition).[118]

The interaction of the nanoparticles with the incoming light is a well known mechanism. Generally noble metal nanoparticles present two absorption bands: the first is originated from the intraband excitation of 6sp electrons and falls in the visible range (called Surface Plasmon Resonance band) and the second one, in the UV region, is the result of an interband transition from 5d to 6sp orbitals (as indicated for gold in Figure 9). These transitions are important in photocatalysis because allow the transfer of the excited electrons to electron acceptors leaving reactive holes on the nanoparticle. The positive

charges instead are able to remove electrons from adsorbed molecules and are more powerful oxidants if they are in the lower 5d band than in the 6sp. This leads to the possibility of using nanoparticles as catalysts under visible and UV irradiation.[117]

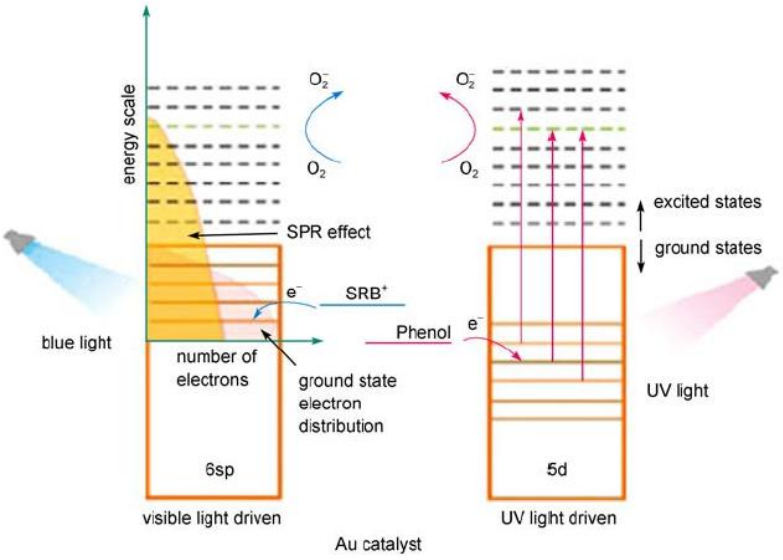

Figure 9: Proposed mechanism of UV-VIS reactivity of gold nanoparticles. On the left the degradation of a synthetic dye (SRB^+) under VIS irradiation and on the right the phenol decomposition under UV.[129]

Although this interesting energy conversion, the aim of finding commercial applications for supported metal nanoparticle catalysts is not always easy because the catalysts have to undergo specific features as stability and reusability. Furthermore, in the case of photocatalysis, these solids have to:

- Absorb the solar irradiated photons and generate electron-hole pairs by the metal nanoparticle
- Separate easily the charge carriers and transfer them to the semiconductor interface where reaction happen
- The semiconductor have to possess a suitable surface for thermodynamically favourable reactions (free energy of the products lower than the reagent one)
- The whole catalyst have to present a high catalytic activity with low activation barriers for the selected reaction.[64]

1.3.3.1. Surface Plasmon Resonance

Some metallic nanoparticles possess a band of absorption in the visible region called Surface Plasmon Resonance (SPR) or Localized Surface Plasmon Resonance (LSPR). This band is originated by the collective oscillation of valence electrons of the metal confined in a nanometric space when they interact with an electromagnetic field (Figure 10). It is responsible for the characteristic colour of the nanoparticles.

The principal point of interest in the SPR bands is that they have the possibility of concentrating the energy of the incoming radiation in the small surrounding of the nanoparticle, leading to the formation of a strong electric field in this portion of space. The surroundings of the plasmonic nanostructures are so called "hot spots" for their high surface energy density. The decay of this excitation can happen by radiative scattering for big plasmonic structures (>50nm) or by the formation of charge carriers that are then transferred to the surroundings for particles smaller than 30nm.[64]

Metals present electrons (d electrons for transition metals) free to move on the surface of the material with a mean free path around 50nm for gold and silver. That explains why, if particles are smaller than this size, resonance is only a surface phenomenon. When these free electrons interact with a radiation of wavelength much larger than their size, resonance will occur (Figure 10). That means that when the front of the radiation passes the metal particle, the electron density in the particle is polarized to the opposite side of the particle and oscillates in resonance with the light frequency as a standing oscillation. The conditions of this phenomenon are determined by absorption and scattering spectroscopy and it is strictly correlated to the type, shape and size of the metal, and the dielectric constant both of the metal and the surrounding molecules. When shape or size of a nanoparticle changes also its surface geometry is modified. This leads to a movement in the surface electrical density and changes as a consequence also the SPR band. For that reason the absorption and scattering properties will change depending on the different oscillation frequency of electrons and their cross sections. Also the media can affect the oscillation frequency of the surface electrons because, varying the dielectric constant, will change also the interactions within the superficial electrons of the particle and the molecules of solvent nearby. Not only the solvent is in contact with the nanoparticle surface, the ligand or other chemically bonded molecules can even change the electron density, causing a shift in the surface absorption maximum. This interaction is mostly used for nanoparticle application as sensitive sensors.[32]

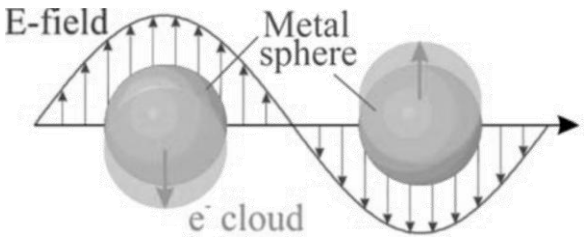

Figure 10: Interaction within the electromagnetic field and metallic nanoparticle electron cloud. [128]

These interactions between the electrons and the radiation were described quantitatively by the Mie,[74] the first who solved Maxwell's equation taking into account appropriate boundary conditions for spherical particles. In his theory the total extinction cross section (σ_{ext}), given by absorption and scattering, is the product of the overall electric and magnetic multipole oscillations. The equation can be reduced as Equation 1 (quasi-static or dipole approximation)[24] for nanoparticles smaller than the wavelength (λ) of the exciting light ($\lambda >> 2R$ and for gold $2R$<25nm[134] where R is the radius of the particle). That approximation is possible when it is considered that only the dipole absorption of the electron cloud contributes to the extinction cross section of the nanoparticle.

$$\sigma_{\text{ext}} = \frac{9V\epsilon_{\text{m}}^{3/2}}{c} \cdot \frac{\omega\epsilon_2(\omega)}{[\epsilon_1(\omega) + 2\epsilon_{\text{m}}]^2 + \epsilon_2(\omega 2)^2}$$

Equation 1: Mie equation for nanoparticles smaller than the incident light.[65]

Where V is the total volume of the spherical particles, c is the speed of light, ω is the angular frequency of the exciting radiation and ε_m is the dielectric constant of the medium (assuming that it is frequency independent). $\varepsilon_1(\omega)$ and $\varepsilon_2(\omega)$ are respectively the real and imaginary part of the dielectric function of the particle material [$\varepsilon(\omega) = \varepsilon_1(\omega) + i\varepsilon_2(\omega)$].[65] Resonance occurs for nanoparticles when $\varepsilon_1(\omega) \sim -2\varepsilon_m$ only if ε_2 is small or weakly dependent on ω. Instead the bandwidth and the peak height are approximately determined by $\varepsilon_2(\omega)$.[134]

This theory has the advantage of being simple and explains with good approximation experimental results, anyway it presents some problems in predicting the results for small nanoparticles.[65]

The dipole approximation reports that the dependence on the size is limited only to the variation of the total volume of particles and this doesn't comprehend the variation of the

individual radius. Despite this, it is experimentally observed that plasmon bandwidth is strongly dependent on the size of the nanoparticles. Also the position of the maximum can be susceptible to both blue and red-shift when the size of the particles decreases.[59] For nanoparticle diameters below 20nm quadrupole and other high-order terms become significant.[24] As a consequence Mie theory should be modified for small particles assuming that the dielectric function of the metal nanoparticle is directly dependent on the radius [$\varepsilon(\omega) = \varepsilon(\omega,R)$], leading to a size-dependent absorption cross section called intrinsic size effect.[65]

In some works,[1] Mie model is reported as Mie-Gans model. This correction is due to the fact that Mie theory is valid only for spherical particles but the nanoparticles in solution can have different structures or be aggregated in complex shapes. Gans theory permits the correction of the overall extinction spectrum of the previous reported model for spheroids, considering the global shape of aggregates and rod-like nanoparticles.[1] This combined theory is in accordance with the experimental results, because UV-VIS spectra of spheroidal nanoparticles present two characteristic absorption bands. The first one is in the same position of spherical nanoparticles and it is due to plasmon excitation along the shorter axis, the other band is red-shifted and generally more intense and corresponds to the excitation along the longer axis.[1, 54]

Surface plasmon band is not a common behavior for metal nanoparticles. A study performed by Creighton et al.[24] determined the position and shape of the SPR band for several metals both in water environment and in the vacuum. Only few of the colloidal metals show a prominent absorption in the UV-VIS range and the ones that do this are metals with free surface electrons as Li, Na, K, Rb, Cs, Mg and Ca. Ag presents also this band but shifted in the visible range. Furthermore, Cu is not considered because its absorption band is not very high even if it is in the visible range. Gold, for its well known nanosize properties, is not contemplated in this article.

SPR band can enhance the concentration of the charge carriers in a nearby semiconductor by three different methods: direct contact injection, near-field electromagnetic and scattering mechanisms when the two parts are at nanometric distance and they convey the electric field of the nearby particles. The most exploited in photocatalysis is the first one and the charge transfer is similar to dye sensitization of semiconductors (Figure 11).[64] The mechanism can be explained as follows: the incident visible photons are

absorbed by the SPR band of the nanoparticles and the produced electrons are subsequently transferred to the conduction band of the semiconductor.[40] In addition the size and shape tuning possibilities for the nanoparticles allow the capacity of taking advantage of the entire visible spectrum. This mechanism can demonstrate that the centers of reaction of the active species are at the three phase interface between metal, semiconductor and liquid.[64]

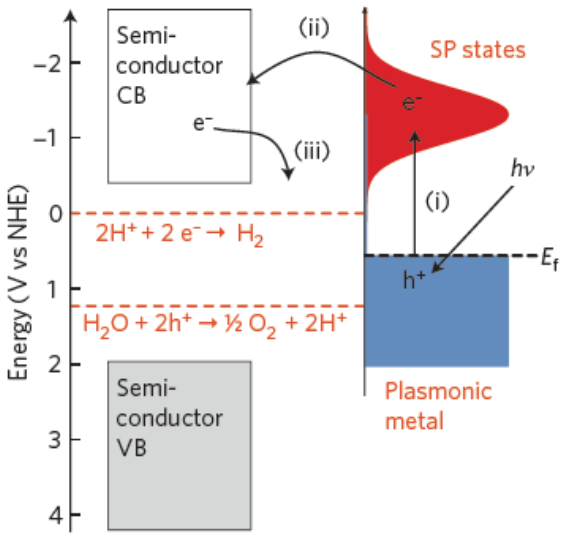

Figure 11: Proposed mechanism for plasmon induced charge transfer with approximated energy levels on the NHE scale. Semireactions are referred to water splitting photocatalysis. Energy transfers are: i) excitation from the Fermi level to surface plasmon (SP) states; ii) transfer to the nearby semiconductor; iii) activation of the surface reaction.[64]

The effective transfer of the photons from the metal to the semiconductor was demonstrated for gold modified titania. This shows a higher activity if the photon absorption band is wider, so it can interact with a bigger amount of incident photons,[58, 57] leading to size positive relationship between the SPR intensity and the rate of enhancement.[64]

Great importance has also the energy position of the bands involved. Generally the conduction band of the semiconductor is around -1.0 and 0V and the valence one between 2.0 and 3.5V respect to the NHE electrode (Figure 5). SPR energy instead is between 1.0 and 4.0V for the noble metals and their Fermi level is ca. at 0V (Figure 11). From these data it can be calculated the energy of the produced excited electrons. Due to the reported energy relations, only the negative charge carriers can be transferred from the metal to the semiconductor, being available for reactions. The holes remaining on the

metal not always have sufficient energy to perform reactions, in particular with big metal nanoparticles.[64]

The not complete explanation of the mechanisms involved and the possibility of application of these systems brought great developments in research in the last years in this field.[9, 78, 109, 116] A more accurate analysis on the most used metals will follow in the sequent paragraphs.

1.3.3.2. Gold nanoparticles

Between metallic nanoparticles supported on titania, gold has reached the highest attention[22, 47, 46] for photocatalysis and for heterogeneous catalytic oxidation.[11] This interest is primarily due on its late discovered activity, because gold was considered of no usefulness in catalysis before the 80s, the opposite as platinum and palladium. Pioneering work in this field was done by Haruta et al.[113] demonstrating that, despite gold bulk metal, its nanoparticles can be really active also at low temperatures. The same author proved also the dependency of its activity from the particle size, discovering that it disappears for particles bigger than 20nm.[44] For these reasons, gold supported catalysts have become the principal example of nanoscience with properties visible only in the nanometric dimension. Starting from low-temperature oxidation of carbon monoxide wide studies have been developed in aerobic oxidations and organic reactions with gold nanosized catalysts.[86]

The main feature that makes gold a photocatalyst is its SPR absorption around 560nm in the visible part of the spectrum and causes the peculiar red colour of gold colloidal solutions. The SPR band permits the excitation of gold nanoparticles and the transferring of electrons in the surrounding environment. In general the recombination of excited electrons is fast but it can be slowed down if the medium or other molecules can trap them. This is the case of the Au/TiO_2 catalysts, reaching high activity with small gold nanoparticles and low gold loading. The simultaneous presence of gold and titania is able to generate charge separation states with milder oxidation and reduction potentials (respectively positive gold and titania conduction band) acting as a photocatalyst.[86]

As reported in paragraph 1.3.2, titania plays a key role in this photocatalytic system: it is able on its own to absorb the photons in the UV range and generate the charge carriers

that migrate on the surface. These excited species can interact with the adsorbed molecules leading to the production of superoxide and other highly reactive radicals.[86] For that reason catalytic activity depends both on the metal and on the type of support. The most widely used in the case of gold are CeO_2, ZrO_2, Fe_2O_3 and TiO_2 because they posses high surface area.[30, 75] In particular Au/TiO_2 catalysts shows a good catalytic activity in different reaction as CO oxidation,[45] aniline oxidation,[41] benzylamine oxidation[4] and selective nitroaromatics hydrogenation[23]. [86]

1.3.3.3. Silver nanoparticles

Silver nanoparticles have developed great interest for their catalytic activity and also for their unique shape-dependent optical properties.[40] Wide studies have been performed on these nanoparticles applied as: sensors and antibacterial agents exploiting its surface enhanced raman scattering,[108] localized surface plasmon resonance[70] and metal-enhanced fluorescence.[94] These nanoparticles, as gold ones, consent the enhancement in the visible of titania absorption increasing the life of the charge carriers.[73, 99] In particular the presence of silver nanoparticles on titania can improve its bactericidal activity under UV light[7] and increase the absorption of oxygen on the surface.[8]

Gupta et al.[42] proposed a reaction mechanism for the charge transfer between silver nanoparticles and titania comparable to the one explained for gold. Under visible irradiation the metallic electrons of silver nanoparticles can be excited by the SPR effect from metal states to higher energy states. These electrons can then be injected in the conduction band of the support. In the case of silver, this transfer can also be favoured by the introduction of band-bending elements in the metal-semiconductor interfacial region between the space charge layer and the strong negative field induced by SPR. [110, 111]

A study performed by Grabowska et al. showed that under UV irradiation better performances are reached with high silver loadings on titania P25 (2% w/w), while using visible light the 1% w/w catalyst gave the best results. That demonstrates that the catalytic activity is not linearly correlated to the metal loading because increasing the quantity of metal leads to an increase in the particle dimension and semiconductor surface coverage.[40]

Furthermore, as reported by Christopher et al.,[19] silver SPR band can be tuned in different ranges of the visible spectrum by changing its size and shape. These peculiar properties together with its low cost make silver an interesting metal for photocatalytic applications.

1.3.3.4. Bimetallic nanoparticles

Alloys have been studied for aerobic oxidations but its application in photocatalysis is not so common. One of the most interesting features in alloying nanoparticles is that the UV-VIS absorption shows only one SPR band with a maximum differently shifted in relation to the metal ratios, this in the case if the two metal present a SPR band.[10, 88] In other cases a photocatalytic active metal is coupled to another metal that doesn't absorb light but accepts the electrons collected by the SPR band creating a not usual mechanism of reaction. This is the field explored by Tanaka et al.: gold nanoparticles are co-immobilized on titania surface with a metal co-catalyst (Ir, Cu, Ag, Rh, Ru, Pd and Pt) and it is demonstrated that gold acts as an electron donor for the second metal through the titania electron states.[106]

In the case of gold catalysis it is reported that alloys exhibit a higher activity, in particular for AuPt,[97] AuPd,[53] and AuAg[17] alloys. Regarding the photocatalytic activity of this metal AuCu[100] and AuAg[13] alloys have attracted high attention because they exploit cheaper metal than gold itself. One of the biggest problems with these alloys is the loss of activity of the second metal during the reaction, especially in the case of copper, because O_2 oxidizes its surface and eliminates alloying effects. Sugano et al.[100] studied the aerobic oxidation of 2-propanol and proposed a mechanism to explain the favourable redox interactions between the two metals. The collective oscillation of the electrons on the surface gold atoms irradiated by visible light is able to reduce the oxidized Cu atoms maintaining the alloying effect.

In regard to silver alloys, Barakat et al.[9] demonstrated a higher activity for photocatalytic degradation of pollutants in water solutions using AgPt nanoparticles supported on titania. Furthermore AgCu alloy has been studied for its absorption properties,[10, 18, 88] but difficulties in stabilizing the oxidation state of those two metals prevented this alloy to find application in photocatalytic reactions.

1.4. Biomass upgrade by supported metal nanoparticles

Several catalytic methods have been developed to obtain valuable chemicals from biomass accordingly to its peculiar characteristics and low reactivity (section 1.1.1). In recent years supported metal nanoparticles have been applied in sugar degradation reaching significant results in selective catalytic oxidation reactions, previously performed only via biochemical routes. The obtained products, belonging to the aldonic acid family and its derivatives, are valuable chemicals for pharmaceutical, cosmetics, alimentary and detergent industries with the additional property of being highly biodegradable and biocompatible. Some examples of commercial selective oxidation derivatives are: gluconic acid used for cleaning rust from metals, gluconolactone exploited as free radicals scavenger in solar creams against UV skin ageing and lactobionic acid applied as medical solvent for organ preservation.[76]

Different metals have been tested for these catalytic oxidation reactions; in particular in the study performed by Mirescu et al.[76] Au, Pd and Pt supported on TiO_2 and Al_2O_3 were investigated. Gold presented the highest activity and the best selectivity in the formation of aldonic acids from monosaccharides and disaccharides. Moreover the experimental parameters for the oxidation of glucose to gluconic acid with gold catalyst supported on carbon were optimized by Biella et al.,[11] in particular regarding the pH range and amount of base required.

Photocatalysis application to biomass degradation is a new research field. Even if metal supported catalysts have been applied to alcohol oxidation,[22, 30] the complex polyol structure of sugars have not been studied in depth.

Some applications of pure titania in UV photodegradation of cellulose are reported in literature in the enhancement of alkali degradation of complex biomass[79] and applied to the selective oxidation of glucose to gluconic acid.[20] Furthermore Fan et al.[35] reported the conversion of cellulose to HMF catalyzed by UV irradiated titania enhancing the dissolution of the dimer with a high concentration of zinc chloride, that creates a water-soluble complex accelerating the degradation reaction.

2. MATERIALS AND METHODS

2.1. Chemicals

All chemicals were used as purchased without further purification.

Metal salts: Gold (III) chloride trihydrate 99.9% (Sigma-Aldrich), Silver nitrate >99.0% (Sigma-Aldrich).

Supports: Titanium (IV) Oxide Aeroxide P25 (Acros Organics), Titanium (IV) oxide anatase (Sigma-Aldrich), Titanium (IV) oxide rutile 99.99% (Sigma-Aldrich).

HPLC calibration standards: D-(+)-Maltose monohydrate >99.0% (BioUltra), D-(-)-Fructose >99%, D-(+)-Cellobiose ≥99%, D-(+)-Glucose ≥99.5% (GC), Furfural 99%, D-Sorbitol ≥99.5% (BioUltra) and D-Gluconic acid sodium salt >99% were purchased from Sigma-Aldrich.
Xylitol 99%, D-Mannitol 99% and 5-Hydroxymethyl-2-furaldehyde ≥98% were purchased from AlfaAesar.

Other chemicals: $NaBH_4$ (Sigma-Aldrich), Poly (vinyl alcohol) M_n ~9000-10000 (Sigma-Aldrich), Poly (ethylene glycol)-*block*-poly (propylene glycol)-*block*-poly (ethylene glycol) M_n ~5800 (Sigma-Aldrich), H_2SO_4 >95% (Fischer Chemicals).

Solvents: Ultrapure water (purification system Millipore MILLI-DI resistivity >1MΩ×cm at 25°C, UK).

2.2. Instruments

2.2.1. Synthesis of catalysts and activity tests

Vacuum oven (Mod. OV-11, Fischer Scientific, UK), equipped with a vacuum pump was used to dry WI catalysts. Catalysts filtration was operated in a all-glass filter holder (Millipore, UK) with nylon filters 0.2µm, diameter 47mm (Whatman). WI catalysts were calcined in a 1100°C ashing furnace (Mod. AAF-1100, Carbolite, UK) equipped with a temperature control (Mod. 2416 Carbolite, UK).

Reactions were run in a Photoreactor (Mod. LZC-4, Luzchem Research Inc. ON, CAN) equipped with 14 fluorescent visible or UVB lamps arranged 6 at the top and 4 on each side; the lamps were 12" long. The temperature controller was set at 25˚C for the whole reaction and the temperature was kept constant with a computer controlled fan. The emission spectra of the VIS set of lamps is reported in Figure 12 and in Figure 13 for UVB lamps. The illuminance of the two emission sources was detected by a luxmeter provided with the photoreactor as indicated in Table 1.

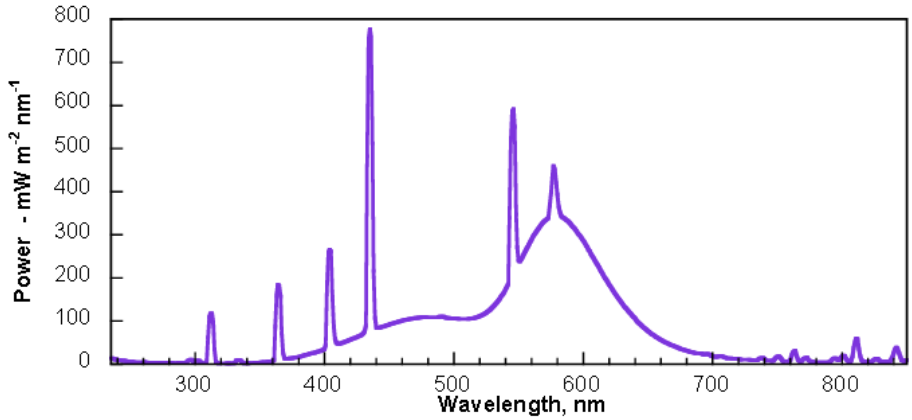

Region	Range, nm	Dose mWm^{-2}	% energy
UVA	316-400	1754	3.34
UVB	281-315	670.0	1.28
UVC	235-280	269.0	0.51
Visible	401-700	47837	91.16
NIR	701-850	1945	3.71

Figure 12: Emission spectrum of the VIS Luzchem lamps measured in the range 235-850nm at 25°C. Resolved peaks at 312, 365, 405, 438, 546, 576, 581(broad) and 811nm. The table shows the energy distribution at the target expressed as a percentage of the total energy in the monitored range. Data from Luzchem Exposure Standards (www.luzchem.com).

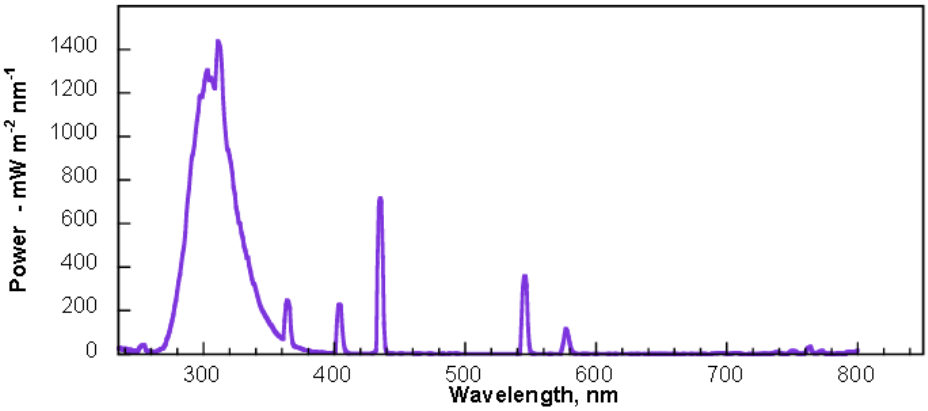

Region	Range, nm	Dose mWm^{-2}	% energy
UVA	316-400	20986	32.04
UVB	281-315	35337	53.94
UVC	235-280	2049	3.13
Visible	401-700	6693	10.22
NIR	701-850	443.0	0.68

Figure 13: Emission spectrum of the UVB Luzchem lamps measured in the range 235-850nm at 25°C. Resolved peaks at 313, 351(broad), 365 and 406nm. The table shows the energy distribution at the target expressed as a percentage of the total energy in the monitored range. Data from Luzchem Exposure Standards (www.luzchem.com).

Table 1: Illuminance of the Luzchem photoreactor sets of lamps detected by the luxmeter provided with the reactor.

Set of lamps	Illuminance (lx)
VIS	19900
UVB	84

Universal Arc Lamp Housing Family (Mod. 66902, Newport, UK) equipped with a Xe lamp with nominal power 300W was used to test the enhancement in the visible of activity of titania, the irradiance spectrum of the lamp is reported from the manual in Figure 14. The lamp was provided with a distilled water liquid filter (Newport, UK) with circulating water moved by a peristaltic pump (speed 60rpm, Mod. 505S, Watson-Marlow, USA). The transmittance spectrum of the liquid filter is in Figure 15. This filter was not enough to remove the IR radiation so an additional Hot Mirror glass filter (Mod. 20HMS-0, Newport, UK) was put with transmittance indicated in Figure 16. Moreover, for some experiments, a coloured glass filter was inserted (Mod. FSQ-GG420, Newport, UK) with a cut-off value of 420nm to maintain only the visible part of the emission spectrum. Transmittance is reported in Figure 17. The filters were positioned in the reported order in the direction of the beam. The irradiation power of the lamp was

detected by a radiometer (Mod. PMA2100, Solar Light, USA) exposed to the source for five minutes with a frequency of measurements of 60Hz and is indicated in Table 2.

The reaction vial was positioned at a distance of ca. 10cm from the filters on a stirring plate. The shade of the fumed cupboard was covered with tinfoil and kept closed during reaction.

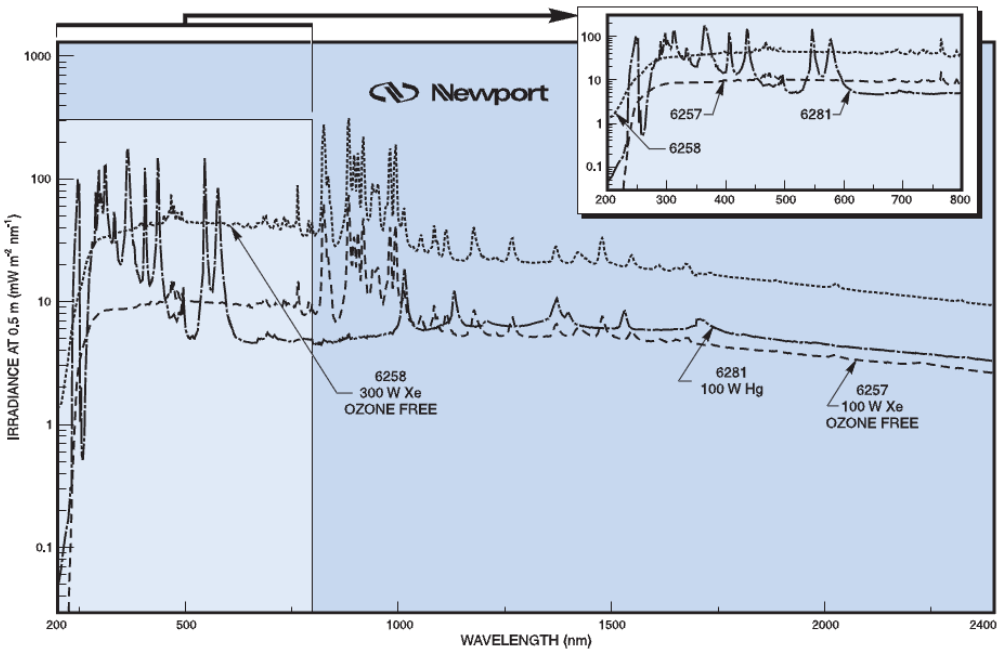

Figure 14: Irradiance spectrum of 300W Xe lamp (dotted line). Vertical axis is in logarithmic scale. Data from www.newport.com

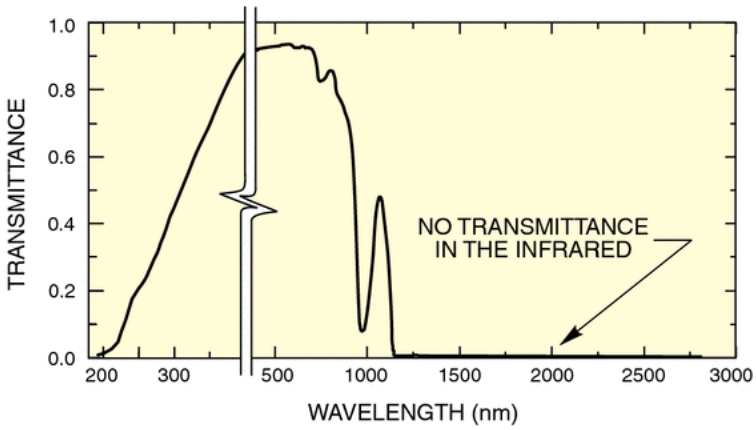

Figure 15: Transmittance spectrum of the distilled water liquid filter. Data from www.newport.com

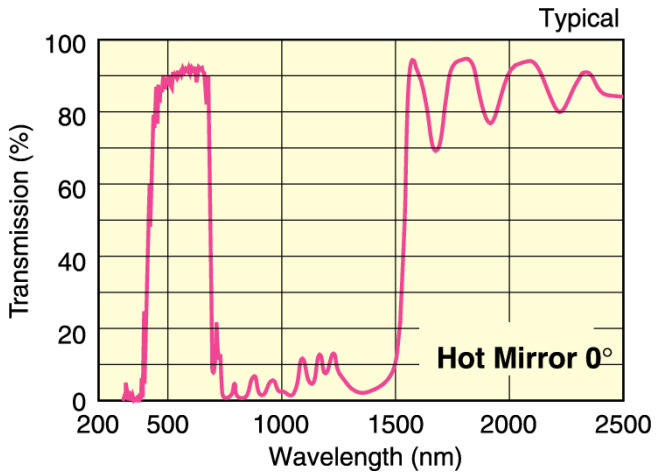

Figure 16: Transmittance spectrum of the hot mirror filter. 0° indicates that the filter is positioned perpendicularly to the direction of the beam. Data from www.newport.com

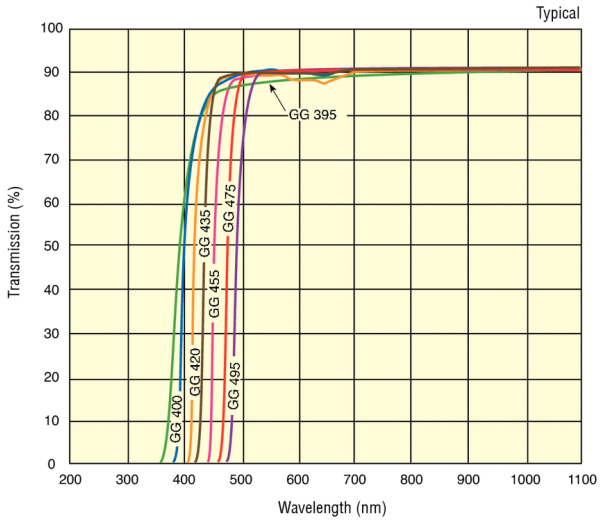

Figure 17: Transmittance spectrum of the coloured glass filter Mod.GG420. Data from www.newport.com

Table 2: Energy and irradiance of 300W Oriel lamp with different filters.

Filters	**Energy emitted by the source in 5min (KJ/m^2)**	**Maximum irradiance of the source in 5min (W/m^2)**
liquid water filter	4337.2	14458
liquid water filter + hot mirror	1663.3	5544
liquid water filter + hot mirror + cut off 420nm	1250.2	4167

2.2.2. Products analysis by HPLC

Sugars are highly polar molecules and for this reason, the common C_{18} reverse-phase columns are not suitable for this analysis, because the molecules would just coelute and thus no separation would occur. To achieve a good level of separation it is necessary to have a polar environment made by the stationary phase, able to interact with the sugars and by the polar eluent phase tuned to maximize the interactions occurring between the analytes and the stationary phase.

There are several options available on the market for the sugar analysis and the vast majority of them are based on two different columns:

- DIOL column: in which the silica particles are coated with aliphatic chains with terminal OH groups
- AMINO column: in which the silica particles are coated with aliphatic chains with terminal NH_2 groups

Both these columns have in common the presence of highly polar terminal groups that are able to interact in several ways with the analytes. In the literature these two types of column are widely applied in the separation of sugars, and sugar alcohols.

After having performed a literature background, several methods have been found in the separation of the degradation products of cellulose. Unfortunately, it is not possible to compare the performances of each method because the chromatograms are not often present in the supporting information of the articles (Table 3).

Table 3: Principal methods for the determination of cellulose degradation products.

Method	Column	Eluent Phase	Detector	Flow rate (ml/min)	Temperature (K)	Ref.
1	Aminex HPX-87H (9 µm, 300×7.8 mm)	H_2SO_4 0.5 mM	RI	0.7	323	[63]
2	Transgenomic™ CARBONSep CHO-620 (10 µm, 6.5 × 300 mm)	H_2O	RI	0.5	338	[27]
3	Nucleogel OA HY (300 × 7.8 mm, 10 µm)	H_2SO_4 0.5 mM	RI + UV-VIS (254nm)	0.5	353	[90]
4	Varian Metacarb 67C column (300 x 6.5 mm)	H_2O	RI	-	-	[37]
5	C_{18} (4.6 x 250mm)	CH_3OH/H_2O (77/23)	UV-VIS (284nm)	0.8	-	[34]

Different columns and experimental conditions had been tested to tune and obtain the best performing analysis set-up. The utilized HPLC (Mod. 1200 Santa Clara, Agilent, USA) was equipped with an inline degasser, a quaternary pump, an autosampler and a column switch. The selected detectors were: a variable wavelength UV-VIS (VWD) and a refractive index one (RID); the analytical column was an Aminex HPX-87H 300mm×7.8mm, 9 µm particle size (Bio-Rad CA, USA). The system was controlled by the Agilent Chemstation software running on a desktop computer.
The mobile phase of the instrument was 25mM sulphuric acid in ultrapure water. The run conditions for this experimental set-up were a flow rate of 0.65ml/min with the column heated at 60°C, RID temperature at 50°C and injection volume: 10µL.

The analyses of the standard samples confirmed that two independent detectors were required to analyse the samples coming from the degradation of biomass and sugars in general. In fact, the RI is a universal detection system based on the different refractive index between the mobile phase and the analyte, and for this reason it is extremely versatile and it is characterized by high sensitivity. On the other hand, this means that it is really sensitive to multiple parameters, such as temperature, and eluent phase composition to name but a few. It is clear how there is a price to pay for such high sensitivity and flexibility of this detection system, and it is also clear how it is necessary to couple the RI with another detector to be able to analyse different samples by exploiting different properties. That is the main reason why the application of just one

detection system is not sufficient due to the possible presence of matrix effects in real samples. The application of a series of two independent detection systems allowed us to check the presence with the VWD detector of the dehydration products such as HMF, levulinic acid, formic acid, and other compounds which absorb in the visible spectrum, whilst the sugars and sugar alcohols were analysed with the RID detector.

Products have been identified and their concentrations have been determinate by calibration curves. The injection of each standard solution was repeated 3 times and the values for the retention times (t_r) were obtained by averaging the 15 retention times collected for each sample. As it can be seen in Table 4, the instrument had a linear response in the concentration range considered, and the linearity between the concentration and the signal is confirmed by the linear regression coefficient R^2 which is greater than 0.99 for each of the molecules considered.
In addition, another useful parameter is the capacity factor (k) defined as follows:

$$k = \frac{t_r - t_m}{t_m}$$

Equation 2: Calculation of k factor in chromatography.

In which t_r is the retention time for the analyte and t_m is the retention time of the mobile phase. This parameter basically defines the quality of the separation at given conditions for the analytes considered. Usually, to achieve a decent chromatographic separation values of k between 1 and 5 are required. In our case it can be noted how the values of k were generally lower than 1. These are the typical values reported in the literature for the separation of sugars and sugar alcohols achieved with the Aminex column.

Despite the generally low capacity factor, the relative standard deviation (%RSD) was generally less than 1% over 3 replicate injections based on the peak area, thus indicating a high reproducibility level of the measurements in the range considered.

As a rule no yields were reported under the intercept value of the calibration curves during the analysis of HPLC chromatograms.

Table 4: HPLC calibration curves.

Standard	Retention time (min)	Range (mmol/L)	Detection system	Equation	R^2	k
Cellobiose	7.08	0.2-50	RID	y=47358x-4659	1.0000	0.39
Maltose	7.21	0.2-51	RID	y=48269x-18087	0.9990	0.41
Gluconic acid	8.59	0.1-20	RID	y=19850x-26	0.9994	0.68
Glucose	8.61	0.01-50	RID	y=24906x+884	1.0000	0.69
Fructose	9.28	0.1-50	RID	y=24847x-9893	0.9996	0.82
Mannitol	9.56	0.1-40	RID	y=26314x+878	0.9990	0.87
Sorbitol	9.69	0.1-40	RID	y=26095x+5788	0.9993	0.90
Xylitol	10.57	0.1-40	RID	y=21369x-3061	0.9983	1.07
HMF	27.80	0.01-10	UV-VIS	y=21003-2751	0.9981	4.45
Furfural	42.53	0.01-2	UV-VIS	y=12437x+43	0.9990	7.34

Characterisation of the oxidation products was performed with a Mass Spectrometer Micromass LCT (Waters, USA) by the Central Analysis service of Liverpool University. The instrument was set in the ionisation mode ES+ with cone voltage of 40V, the sample was dissolved in methanol and injected with a syringe pump.

2.2.3. Catalysts characterisation

UV-VIS absorbance analyses were performed in 10.0mm quartz cuvette in the range 200-820nm (Instrument Mod. Evolution 220, Thermo Scientific, UK). Instrument settings were: bandwidth 2nm, integration time 0.01s, data interval 0.20nm and scan speed 1200nm. Baseline was obtained with distilled water.

UV-VIS solid reflectance spectra were done in the range 200-800nm (Instrument Mod. UV-2550, Shimadzu, USA). Instrument settings were: sampling interval 0.5nm, slit 5nm and barium sulphate was used as a reference. The catalyst powder was put in a quartz sample holder. Reflectance data were transformed with Kubelka-Munk function for scattered light (Equation 3). The assumption of this law is that the particle distribution is random and the dimension is much smaller than the thickness of the layer. The theory does not consider any regular reflection of the light on the sample. This function is related to the extinction factor (ε) in transmission spectroscopy and it is proportional to the concentration (as Lambert-Beer law) for dilute species. The function, as absorbance, depends on the wavelength (λ).

$$F(R_\infty)_\lambda = \frac{(1-R_\infty)^2}{2R_\infty} = \frac{k}{s} \propto \frac{\varepsilon * c}{s}$$

Equation 3: Kubelka-Munk function.

In the equation R_∞ is the absolute Reflectance of the sample but it is usually substituted with R'_∞ which is the reflectance relative to a standard ($BaSO_4$ for UV-VIS range); *k* is the absorption factor, *s* is the scattering factor and *c* is the concentration of the sample.

XRD instrument (Mod. D8 Advance, Bruker, USA) was equipped with a Cu-kα_1 source of radiation and a Ge monochromator in reflection mode. Scans were done for 2h in the range 2θ: 10-80. Catalyst powders were loaded on zero background silica wafers.

FTIR analyses were done in the range 6000-400cm^{-1} with a Bruker instrument (Mod. HTS-XT Tensor 27, USA).

ICP analyses were performed in the Central Analysis service of Liverpool University with an instrument ICP-OES-SoP, Spectro Ciros CCD.

Nanoparticle TEM images were obtained with a JEM-1010 (Jeol Ltd, JPN) instrument operated at 100kV. The samples were prepared by depositing 10μL of the supported particles suspended in hexane (1mg/1ml hexane) onto a carbon-coated copper grid (300mesh) and subsequently dried at room temperature. Analyses were performed from the Photochemistry reactivity group of Prof. J. Perèz-Prieto at the Instituto de Ciencia Molecular (ICMOL) of Valencia.

2.3. Synthetic methods

2.3.1. Preparation of supported catalysts by wetness impregnation

This method is widely used for catalyst preparation. In the synthesis followed as a guideline[67] concentrated aqueous solution of metal salts were prepared. The support was then suspended in the minimum amount of water (2-4ml) in a vial under magnetic stirring and the metal salts solution were added. The solvent was slowly evaporated under stirring at 80°C until it became a paste, dried at 110°C overnight in a vacuum oven, calcined at 200 or 400°C for 3h (ramp 20°C/min) and grinded.

Metal loadings were calculated as weight percent of total metal on the support as in Equation 4.

$$\%\frac{w}{w} = \frac{m_{metal}(g)}{m_{support}(g)} \times 100$$

Equation 4: Calculation of metal loading of a supported catalyst.

The monometallic catalysts synthesized with this method are listed in Table 5 and the bimetallic one in Table 6. The content of each metal in the bimetallic catalysts was calculated as indicated in Equation 5.

$$\%\, Au = \frac{n_{gold}(mol)}{n_{total\ metal}(mol)} \times 100$$

Equation 5: Calculation of content of each metal in the bimetallic catalysts.

Table 5: Monometallic catalysts synthesized by WI method.

Catalyst	Metal	Metal loading (% w/w)	Calcination temperature (°C)
0.5-Ag/TiO_2-C200	Silver	0.5	200
1-Ag/TiO_2-C200	Silver	1	200
2.5-Ag/TiO2-C200	Silver	2.5	200
5-Ag/TiO_2-C200	Silver	1	200
1-Ag/TiO_2-C400	Silver	1	400
1-Au/TiO_2-C200	Gold	1	200
1-Au/TiO_2-C400	Gold	1	400

Table 6: Bimetallic catalysts synthesized by WI method.

Catalyst	Metal	Content of Au (% mol)	Content of Ag (% mol)	Total metal loading (% w/w)	Calcination temperature (°C)
1-$Au_{95}Ag_5/TiO_2$-C200	Gold and silver	95	5	1	200
1-$Au_{85}Ag_{15}/TiO_2$-C200	Gold and silver	85	15	1	200
1-$Au_{50}Ag_{50}/TiO_2$-C200	Gold and silver	50	50	1	200
1-$Au_{15}Ag_{85}/TiO_2$-C200	Gold and silver	15	85	1	200
1-Au_5Ag_{95}/TiO_2-C200	Gold and silver	5	95	1	200
1-$Au_{95}Ag_5/TiO_2$-C400	Gold and silver	95	5	1	400
1-$Au_{85}Ag_{15}/TiO_2$-C400	Gold and silver	85	15	1	400
1-$Au_{50}Ag_{50}/TiO_2$-C400	Gold and silver	50	50	1	400
1-$Au_{15}Ag_{85}/TiO_2$-C400	Gold and silver	15	85	1	400
1-Au_5Ag_{95}/TiO_2-C400	Gold and silver	5	95	1	400

2.3.2. Preparation of supported catalysts with preformed metal nanoparticles

Method 1

Following the work published by bin Saiman et al.[12] a gold colloidal solution was prepared. The appropriate quantity of chloroauric acid was dissolved under stirring in a round bottom flask with a small amount of water (10ml). A PVA 1M water solution was prepared and added to the metal solution to reach PVA/metal 1.2 w/w ratio. A fresh $NaBH_4$ 0.1M water solution was then prepared and transferred into the flask ($NaBH_4$/metal ratio 5mol/mol). The as obtained solution was stirred for 30min. The desired amount of titania was than suspended in 20ml of water and acidified to pH 1 with sulphuric acid, it was then added to the metal solution using other 20ml of water to wash the glassware. After 2h of stirring the solution was then filtrated and washed with distilled water until a neutral pH value was obtained. The solid was dried overnight at RT. The powders were then collected from the filter and refluxed with 50ml of water at 80°C for 2h to remove the excess of ligand and reducing agent,[68] the obtained solid was than filtered, washed with water, dried at RT and grinded.

Metal loadings are calculated as previously reported in Equation 4. The reported method was used to synthesize the catalyst reported in Table 7.

Table 7: Catalyst synthesized by colloidal Method 1.

Catalyst	Metal	Metal loading (% w/w)
1-Au/TiO2-PVA	Gold	1

Method 2

Colloidal monometallic and bimetallic catalyst were synthesized as reported by Huang et al.[52] Aqueous solutions of $AgNO_3$ (1.5 mM), $HAuCl_4$ (1.5 mM), P123, and $NaBH_4$ (1g/L) were prepared. The molar ratio between P123 and the total quantity of metal in solution was 5 or 10. An appropriate amount of $AgNO_3$ aqueous solution was added to 25ml of an homogeneous solution of P123 and water and stirred vigorously for 5min. $HAuCl_4$ solution was then added. Immediately after that, 15ml of the $NaBH_4$ solution were slowly dropped (within 15min) into the stirring mixture. The volume was then adjusted to 100ml with distilled water and the solution stirred for 60min.

The as obtained colloids were supported on titania following the same procedure reported in Method 1.[68] Total metal loadings are calculated as in Equation 4 and the molar ratio between gold (or silver) and the total metal is expressed as in Equation 5.

The monometallic catalyst synthesized with this method are listed in Table 8, the bimetallic ones in Table 9.

Table 8: Monometallic catalysts synthesized by colloidal Method 2.

Catalyst	Metal	P123/metal ratio (mol/mol)	Metal loading (% w/w)
1-Au/TiO2-P123	Gold	5	1
1-Ag/TiO2-P123-5	Silver	5	1
1-Ag/TiO2-P123-10	Silver	10	1

Table 9: Bimetallic catalyst synthesized by colloidal Method 2.

Catalyst	Metal	P123/metal ratio (mol/mol)	Content of Au (% mol)	Content of Ag (% mol)	Total metal loading (% w/w)
1-$Au_{95}Ag_5/TiO_2$	Gold and silver	5	95	5	1
1-$Au_{85}Ag_{15}/TiO_2$	Gold and silver	5	85	15	1
1-$Au_{50}Ag_{50}/TiO_2$	Gold and silver	5	50	50	1
1-$Au_{15}Ag_{85}/TiO_2$	Gold and silver	5	15	85	1
1-Au_5Ag_{95}/TiO_2	Gold and silver	5	5	95	1

2.3.3. Photocatalytic reactions

Different cellobiose solutions of concentration 2.80×10^{-3}mol were prepared. The solid was solubilised by sonication for 3min until the solution was crystal clear in a volumetric flask. Each catalyst was tested weighting 40mg of the powder in a 14ml vial and adding every time 10ml of cellobiose solution. After the addition of the disaccharide, the vials were covered with tinfoil to prevent surrounding light reaching the suspension and were put quickly in the irradiation system. Rubber septa were used to cap the vials to avoid the evaporation of the mixture throughout reaction. Needles were insert in the septa for withdrawals during the reactions.

Pre-screening reactions were done to test the activity of the catalysts and optimize the synthetic parameters. Five vials was put stirring along a line in the centre of Luzchem photoreactor to consent the same irradiation for all the samples for 13h. Temperature controller was set at 25°C. Then the reactions were repeated with the catalysts presenting the best activity with only one vial each time positioned in the centre of the system to guarantee the best stirring and exposure to the lamps.

When the lamp setup was used, the vial was put on a stirring plate at 500rpm. No temperature controller was needed because a temperature/time calibration of the system was done and the vial was maintained at 26°C for all the reaction time.

Both the radiation sources were preheated at least for 30min before put the vial and start the reaction.

Samples were taken every 2h or at the end of the reaction time, centrifuged for 5min at 13400rpm to remove any suspended catalyst particles and then analyzed with HPLC following the method reported in paragraph 2.2.1.

2.3.4. Dark reactions

Reactions performed without irradiation followed the same procedure reported in section 2.3.3 and the radiation source was kept turned off.

2.3.5. Thermal reactions

The preparation of the reaction mixture was the same as paragraph 2.3.3 and the solution was put in smoked 16ml vials. These reactions were performed on a stirring plate in a preheated oil bath kept at 70°C by a thermocouple control. Up to 5 vials were covered with tinfoil, capped with rubber septa and put stirring immerged in the same oil bath for 6h. Each vial was provided with two needles: a long one in the suspension and a short one to avoid spills of the solution during withdrawals.

Samples were taken every 2h and at the end of reaction, centrifuged for 5min at 13400rpm to remove any suspended catalyst particles and then analyzed with HPLC following the method reported in section 2.2.1.

3. RESULTS AND DISCUSSION

3.1. Identification of the products of reaction

The research field in biomass transformation has obtained increasing attention in these years due to the growth in price and decrease in availability of fossil fuels.[91, 114] Studies in catalytic depolymerisation and transformation of lignocellulose are still complex due to the structural features of this polymer.[114] For this reason cellobiose is used as a molecular model of biomass structures in catalytic works to understand which type of reactions are promoted by the selected catalysts. On the other hand, titania and supported metal nanoparticles are widely used in photocatalysis[9, 22, 86] but its application in the field of biomass is not studied in depth: only a few papers are applying photoactivated titania to biomass under UV irradiation.[20, 79] To the best of our knowledge no papers have been published about the hydrolysis of biomass with photocatalysis, in particular using visible light.

The aim of our study was to explore the photocatalytic activity of titania and supported metal nanoparticles towards the hydrolysis and depolymerisation of cellobiose under UV and visible light irradiation. That means that it was expected to break the β-1,4-glycosidic bond generating two glucose molecules from the sugar dimer (Scheme 2). Surprisingly only a small amount of cellobiose was hydrolysed to monomers (under visible light irradiation a maximum of 5% glucose yield for titania anatase after 10h) with cellobiose conversions up to 36% (for *1-*$Au_{50}Ag_{50}/TiO_2$ catalyst). It was found that the main product of reaction was not glucose but it was observed the presence of other two significant peaks during HPLC analyses of reaction. Our efforts have then been devoted to the identification of those products and the final hypothesis was that they were the result of a selective oxidation process in analogy to the results reported in literature for reactions applied to the photo-oxidation of alcohols.[29, 55, 120]

The presence of other sugar monomers, sugar alcohols, dimers (as maltose) and dehydratation products (as HMF and furfural) was also investigated, but they were not detected with our catalysts.

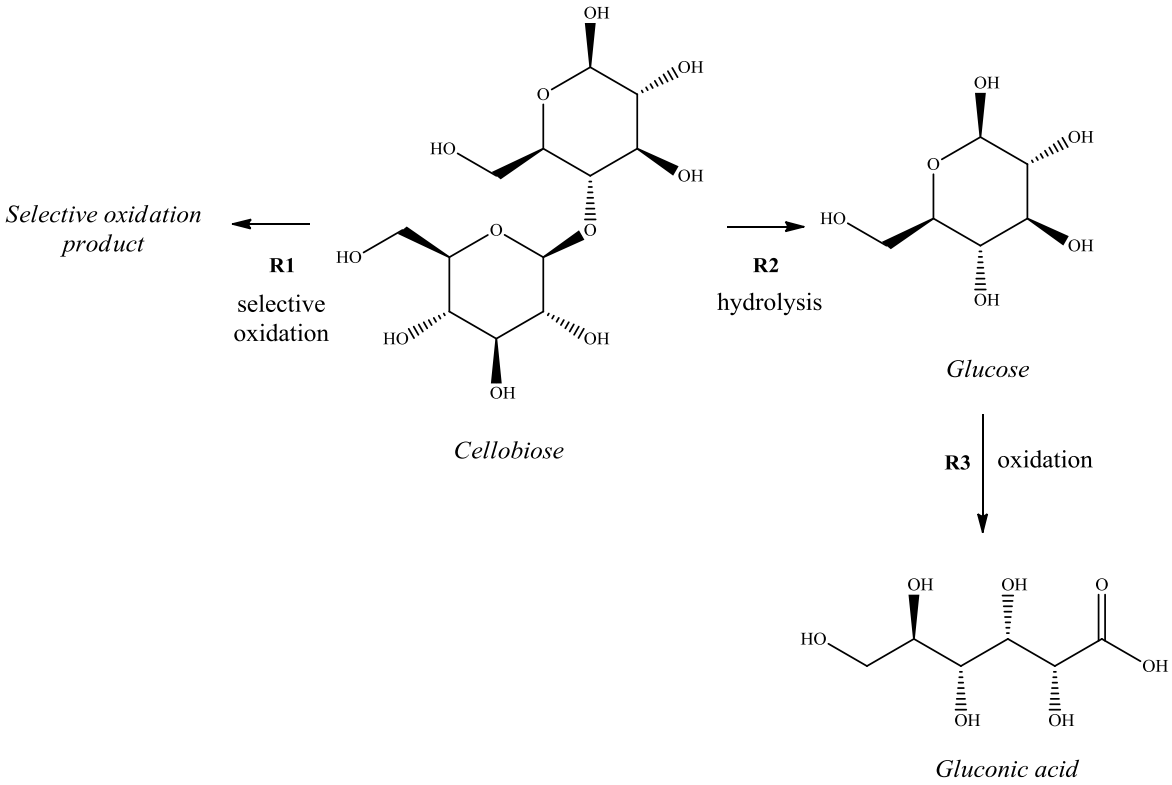

Scheme 2: Products of reaction detected by HPLC calibration curves.

The analysis of the reaction was carried out by HPLC and the concentrations and retention times of the expected products of hydrolysis were detected with calibration curves (section 2.2.2). The RID and VWD HPLC chromatograms of reaction presented several peaks but only the ones important for catalysis were analyzed, generally taking in consideration only peaks with area greater than 1000 units. The HPLC chromatograms, and consequently the distribution of products, was found to be the same both with reactions performed only with the support (TiO_2) and with catalysts prepared with different metal nanoparticles.

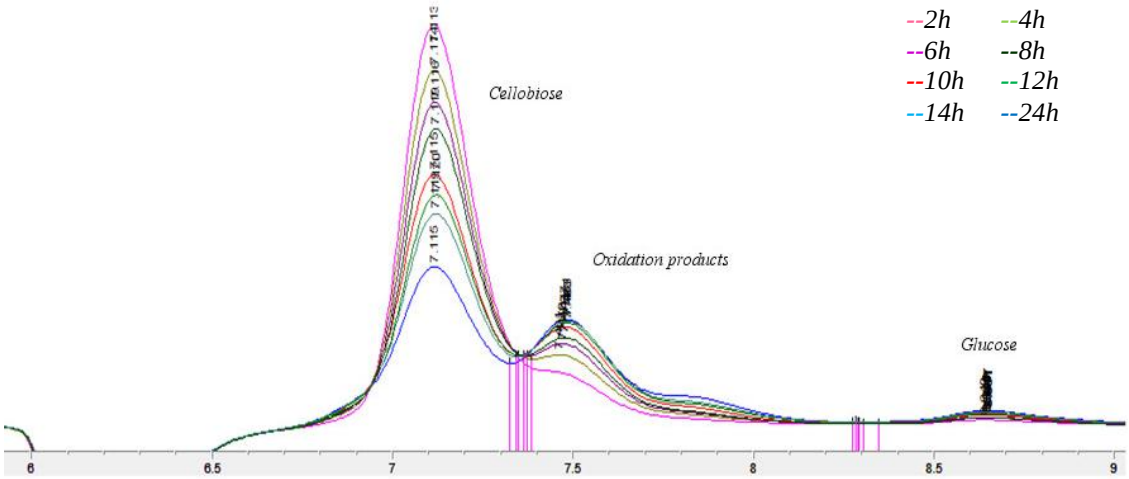

Figure 18: Characteristic trend of HPLC analysis with RID detector. Peak at RT 7.1min is cellobiose, the peaks at 7.5 and 7.8min are the selective oxidation products and glucose is the peak at 8.6min. Test performed with 1-Ag/TiO2-P123-5 catalyst in the Luzchem photoreactor, withdrawals after 2, 4, 6, 8, 10, 12, 14 and 24h of reaction.

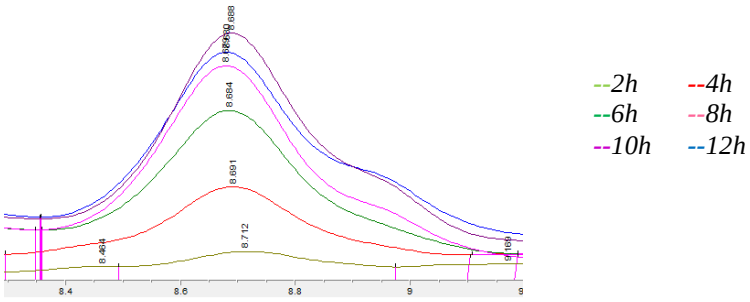

Figure 19: Characteristic trend of HPLC analysis with RID detector for glucose (RT 8.6min). The shoulder of the peak is gluconic acid. Test performed with anatase in the Luzchem photoreactor, withdrawals done after 2, 4, 6, 8, 10 and 12h of reaction.

A characteristic trend of HPLC analysis in different reaction times is represented in Figure 18. The first peak appearing is cellobiose (RT 7.1min) and it decreases during the reaction. The second known chemical is glucose that comes out at 8.6min. The principal products of reaction are indicated by the peaks appearing at 7.5 and 7.8min and increase during the reaction. In particular, the first peak is present already after 2h and the second one emerges later, suggesting a successive transformation of the first product. A zoom on glucose peak is reported in Figure 19. It can be seen that only after 6-8h of reaction a shoulder can be detected on the peak indicating that a second product is being eluted nearby glucose. This is the effect of a consecutive reaction for the production of gluconic acid. The two peaks are not separable because the RT obtained by calibration is around 8.6min for both the products, but the effective presence of the oxidation product was confirmed by a peak appearing in HPLC UV detector (λ=210nm)[11] which is proper of gluconic acid because glucose doesn't absorb in this region (Appendix, section 5.2).

The selective oxidation and hydrolysis reactions (*R1* and *R2* Scheme 2) develop as two parallel reactions. This could be deducted from the rate of increase in products concentration (Figure 18): in fact during the course of reaction both the glucose and the oxidation product peaks increase. Moreover, either the products are present from the first analysis after 2h, indicating that the two reactions happen simultaneously.

As the main reaction expected was hydrolysis, none of the analyzed calibration curves matched with the retention times of the main product of reaction. The fact that both the peaks in the chromatograms are appearing nearby cellobiose suggested that they can have a similar chemical structure, leading to comparable retention times. Furthermore, the observed oxidation of glucose to gluconic acid could indicate that the same reaction may happen also to cellobiose generating cellobionic acid by the oxidation of the equilibrium open form (Scheme 3). The presence of the second peak can potentially be explained by a secondary oxidation on cellobionic acid of a primary or secondary alcohol of the molecule. Some hypotheses of secondary oxidation are reported in appendix (section 5.1). Furthermore, another explanation of the presence of the second peak could be the dehydratation of cellobionic acid to the lactone form when it comes in contact with the acid eluent of the HPLC and it loses a molecule of water.

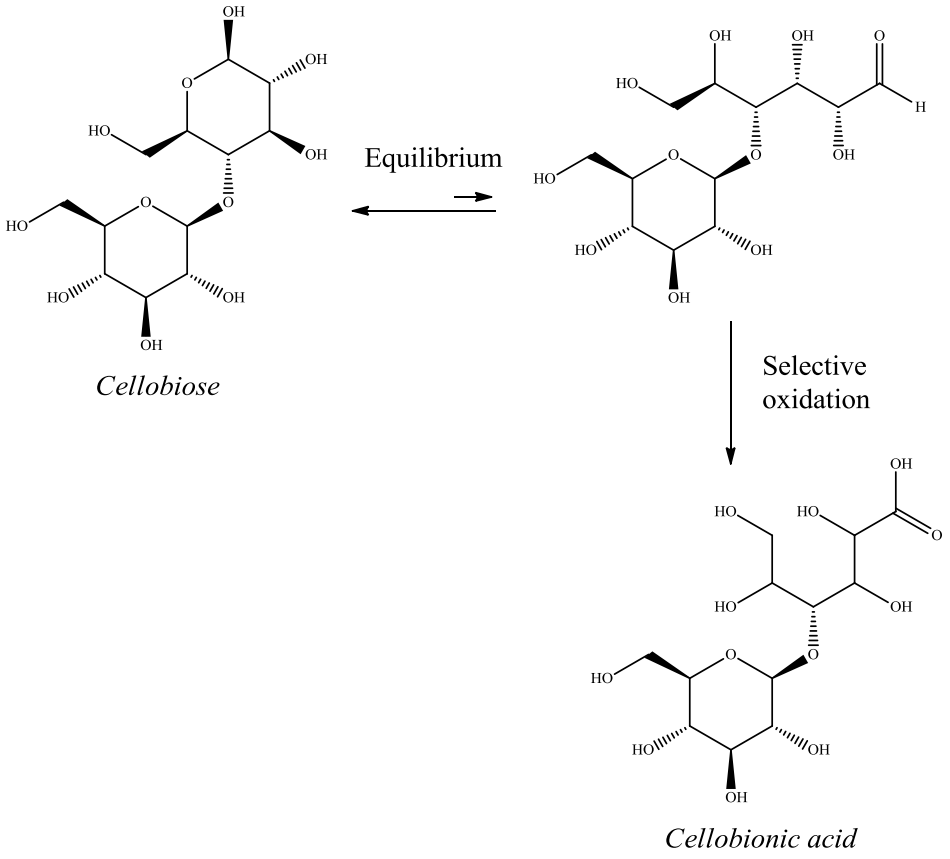

Scheme 3: Possible selective oxidation product from cellobiose.

Unfortunately no commercial samples are available for the supposed products, so it was not possible to confirm their HPLC retention time as no standards were purchasable. To overcome this problem reaction samples were submitted to mass spectroscopy (ESI^+) to try to identify the products by their fragmentation. Similar molecular weights and overlapping of the fragments didn't allow the exact identification but supported the presence in the reaction mixture of the products reported. Possible fragmentations pattern are reported in the appendix, section 5.1. Studies are still in development for the identification of the reaction products.

Due to characterisation problems an exact quantification of the oxidation products was not possible and further tests have to be performed to confirm definitely the hypothesis reported. The activity studies on the catalysts are then reported as cellobiose conversion, considering that: as the conversion of cellobiose increases, the area of the two main peaks of reaction increases proportionally. A comparison between the different catalysts is even possible on the selective oxidation reaction by analyzing the areas of the peaks of the oxidated products. Besides glucose yield is reported because it was the first aim of the research and, even if it is always really low, its concentration increases during the

reaction. Gluconic acid instead, although it was detected by calibration, was not quantifiable for the low amount generated.

The role played by light in this reaction is fundamental because the semiconductor is activated only in the presence of irradiation. This statement is justified by tests performed for all the catalysts synthesized both with and without light in the same experimental conditions (sections 2.3.3 and 2.3.4). All the reactions in the dark showed a cellobiose conversion lower than 5% after 13h, so the catalysts can be defined as not active if not exposed to a light source of irradiation. Experimental data can be found in appendix 5.3.

The identical distribution of products obtained with pure titania and supported metal nanoparticles suggests that titania is the active part of the system towards the oxidation and dehydratation of cellobiose. A possible explanation of the mechanism, which is in accordance with the obtained data, can be found in the literature.[40, 60, 86] In these papers it is indicated that metal nanoparticles are not catalysts themselves but operate as electron acceptors and act as dopants in the visible range for the semiconductor bandgap. Moreover, this excess of charge on titania is donated to the water and to the oxygen adsorbed onto the titania surface generating highly reactive radicals that oxidize the reagents in solution. Therefore, it could be titania that acts as a catalyst towards the oxidation of cellobiose and the metal nanoparticles act as antennas to transfer the electrons to its conduction band (Figure 20).

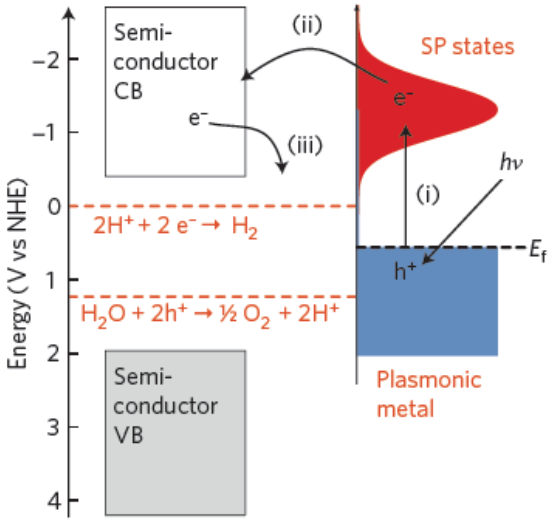

Figure 20: Proposed mechanism for plasmon induced charge transfer with approximated energy levels on the NHE scale. Semireactions are referred to water splitting photocatalysis. Energy transfers are: i) excitation from the Fermi level (E_f) to surface plasmon (SP) states; ii) transfer to the nearby semiconductor; iii) activation of the surface reaction.[64]

Furthermore, biomass is susceptible to hydrolysis in superheated water in the absence of catalysts, but this process becomes significant only under hydrothermal conditions (T>190°C). As regards our reaction, the contribute of water to the hydrolysis of cellobiose was first evaluated by analyzing only cellobiose in water under light irradiation. During this experiment no products were detected after 6h of reaction confirming that cellobiose hydrolysis and oxidation are negligible at RT and are enhanced by light irradiation only in the presence of catalysts. Secondly the temperature effect was evaluated with the catalysts with metallic nanoparticles and with the pure titania P25 in tests performed at 70°C in an oil bath in the dark (section 2.3.5). The maximum cellobiose conversion obtained in these tests was 6% after 6h and the product peaks were too small to be analyzed (more data in appendix 5.3) confirming the negligibility of reactions on cellobiose without light irradiation.

3.2. Role of titania

Titania has different crystalline structures: rutile, anatase, brookite and an amorphous phase. Only the first two have industrial applications because the third has a lower natural abundance and it is more difficult to synthesize than the others.[25] The difference between the phases is due to the relative position and coordination of titanium and oxygen atoms in the material lattice. Rutile and anatase present a tetragonal structure respectively in the spatial group of $P4_2/mnm–D^{14}_{4h}$ for rutile and $I4_1/amd–D^{19}_{4h}$ for anatase. Brookite instead has an orthorhombic structure of spatial group $Pbca\text{-}D^{15}_{2h}$. The Miller lattice indexes for the three phases are $a = b = 4.59$Å, $c = 2.96$Å for rutile, $a = b = 3.78$Å, $c = 9.51$Å for anatase and $a = 9.16$Å, $b = 5.43$Å, $c = 5.13$Å for brookite[62] (Figure 21).

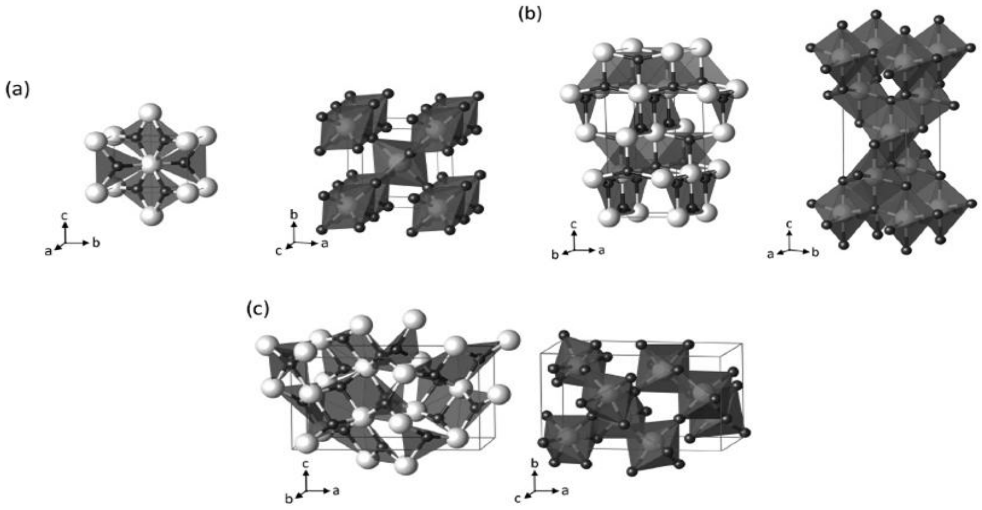

Figure 21: Representation of the crystalline structures of (a)rutile, (b)anatase and (c)brookite as reported by Landmann et al.[62] For each phase is indicated the Ti_3O building block on the left and the TiO_6 polyhedra on the right. Ti atoms are white and O atoms are black.

The different position of the atoms in the structure causes different electronic properties in the semiconductor and so the band gap slightly differs from a phase to another. The value is around ca. 3.4eV for anatase[107], 3.3eV for brookite[72] and 3.0eV for rutile[2] and the excitation falls in the UV region of the spectra.

It is widely proved that titania is catalytically active in the UV region[60, 86, 96] especially in the degradation of pollutants in water.[28, 124] Generally anatase possess higher activity than rutile[86] because it has a higher density of localised states within its bandgap which slows recombination of charge carriers and enhances the production of surface adsorbed hydroxyl radicals. Instead rutile presents a higher kinetic of electron-hole recombination

and it is due to a larger grain size and a subsequent lower capacity of absorbing species compared to anatase.[43] Despite this general trend, catalytic activity is also strictly correlated to the synthesis of these oxides[85] because the presence of impurities, the particle dimension and the surface area can affect the lifetime of charge carriers. Furthermore, it was found that rutile and anatase can present different selectivity in the same reaction, as reported by Augugliaro and Kimura et al..[6, 55]

The activity of the different phases of titania was evaluated towards the reaction of hydrolysis of cellobiose in the Luzchem photoreactor under UV and VIS irradiation.

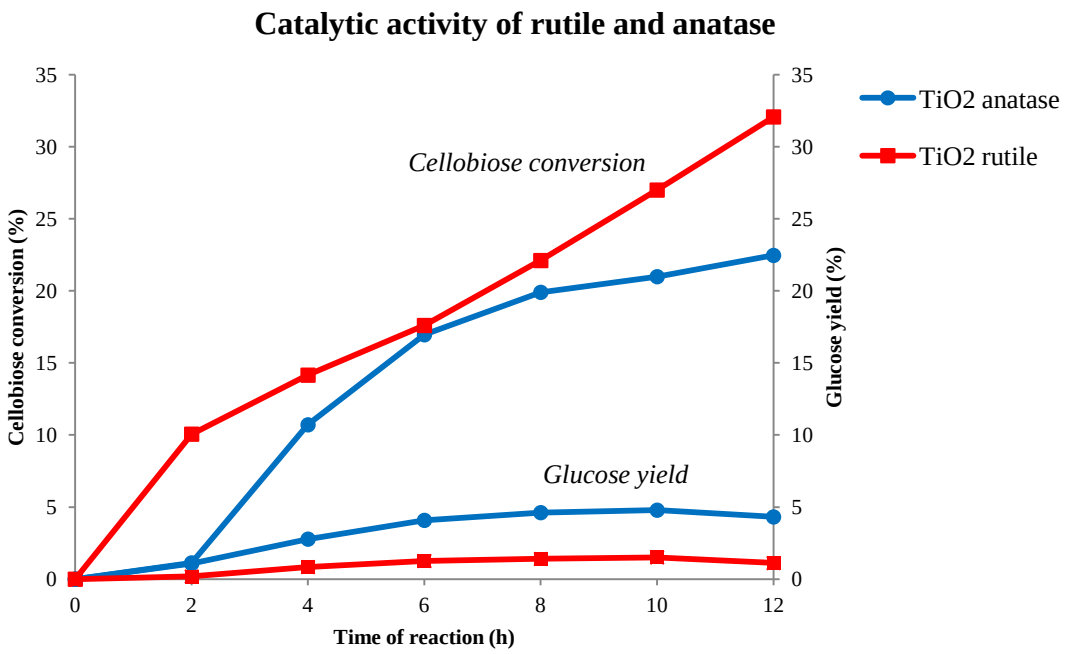

Figure 22: Catalytic performances of TiO_2 rutile and anatase under visible light irradiation. Reactions preformed in the Luzchem photoreactor for 12h.

Table 10: Catalytic data of TiO_2 anatase and rutile in the Luzchem photoreactor under visible light irradiation. The decrease in glucose yield is due to the production of gluconic acid. No yields are reported for the selective oxidation products because quantification was not possible.

Catalyst	Time of reaction (h)	Cellobiose conversion (%)	Peak area oxidation product (7.5min)	Peak area oxidation product (7.8min)	Glucose yield (%)
TiO_2 anatase	2	1	0	392	1
TiO_2 anatase	4	11	4731	938	3
TiO_2 anatase	6	17	5235	954	4
TiO_2 anatase	8	20	5807	1691	5
TiO_2 anatase	10	21	6995	1965	5
TiO_2 anatase	12	22	6564	2096	4
TiO_2 rutile	2	10	9648	403	0
TiO_2 rutile	4	14	13641	1406	1
TiO_2 rutile	6	18	17040	1950	1
TiO_2 rutile	8	22	21500	2063	1
TiO_2 rutile	10	27	24864	2592	2
TiO_2 rutile	12	32	28089	2698	1

In the visible tests rutile presents a higher catalytic activity than anatase, reaching a cellobiose conversion of 32%, compared to the 22% of anatase after 12h. (Figure 22). Furthermore, both the solid show the oxidation product as principal product of reaction (Table 10). The activity of titania under visible irradiation is due to the emission spectrum of the visible lamps because, as a simulation of the solar spectrum, it presents 5% of UV radiation with peaks at 312, 365 and 405nm that directly activate the titania for the production of radicals (emission spectrum of the visible set of lamps can be found in section 2.2.1).

The difference in activity between anatase and rutile can be explained in relation to the bandgap of the two crystalline structures. In fact, the bandgap position for a semiconductor can be determined experimentally from its solid UV-VIS spectrum by extrapolation of the rising part of the plot (cut-off value) with the horizontal axis of the graph.[82] This relation is also expressed by the mathematical Equation 6:

$$E = \frac{h \times c}{\lambda} = \frac{6.626 \times 10^{-15} \times 3 \times 10^{8}}{\lambda}$$

Equation 6: Relation between the energy bandgap (E) and the cut-off wavelength (λ).

where E is the bandgap energy (eV), h is the Planck constant (J×s), c is the speed of light (m/s) and λ is the cut-off wavelength in the UV-VIS spectrum (m).[50] The λ calculated

from the above reported bandgaps is respectively 414nm for rutile and 365nm for anatase. This determines that rutile absorbs more energy than anatase because its cut-off value comprehends the three peaks of emission in the UV of the visible set of lamps. On the other hand, anatase only covers the energy given by the emission peaks at 312 and 365nm (emission spectrum in section 2.2.1).

The conversion trend of the two solids is also different because anatase reaches a steady value of conversion after 8h, instead the conversion for rutile increases linearly for the whole period of reaction considered. This can be explained by differences in absorption and poisoning of the active sites of the structures, but further post-reaction analyses have to be performed to confirm this assumption.

Another difference in the catalytic activity of the two titania structures is related to selective oxidation products and glucose yield. As can be seen from Table 10 and from the HPLC chromatograms reported (Figure 23), anatase has a higher glucose yield and lower oxidation product yield than rutile revealing a higher affinity for the hydrolysis reaction than for the selective oxidation one. This difference between the two phases can be due to the structures of the solids that absorbs differently the reagents, as reported in literature by diffuse reflectance spectroscopy studies and quasi-fermi level measurements,[5, 6] leading to alternative behaviours.

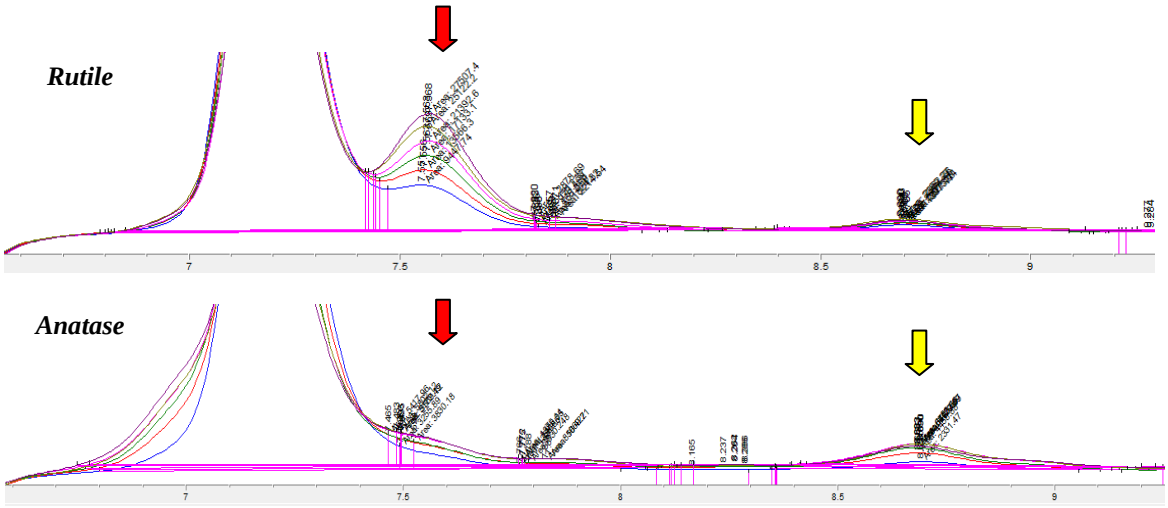

Figure 23: HPLC chromatograms with RID detector. Different lines represent the product distribution after 2, 4, 6, 8, 10 and 12h of reaction performed with anatase and rutile under visible light irradiation. Peak at RT 7.1min is cellobiose, the peaks at 7.5 and 7.8min are the selective oxidation products(--) and glucose(--) is the peak at 8.6min.

The analysis of the crystalline structures of titania towards the reaction of hydrolysis and selective oxidation of cellobiose was completed examining within the different supports also Degussa P25, about 80% anatase and 20% rutile. That was done because Degussa P25 is reported in the literature[86] as a high-activity catalyst and a reference material for photocatalysis[98] because its synthesis is obtained by spray pyrolisis and it is highly reproducible.[86] The solids were tested under UV and visible light irradiation to find the one with the highest activity for the supportation of nanoparticles.

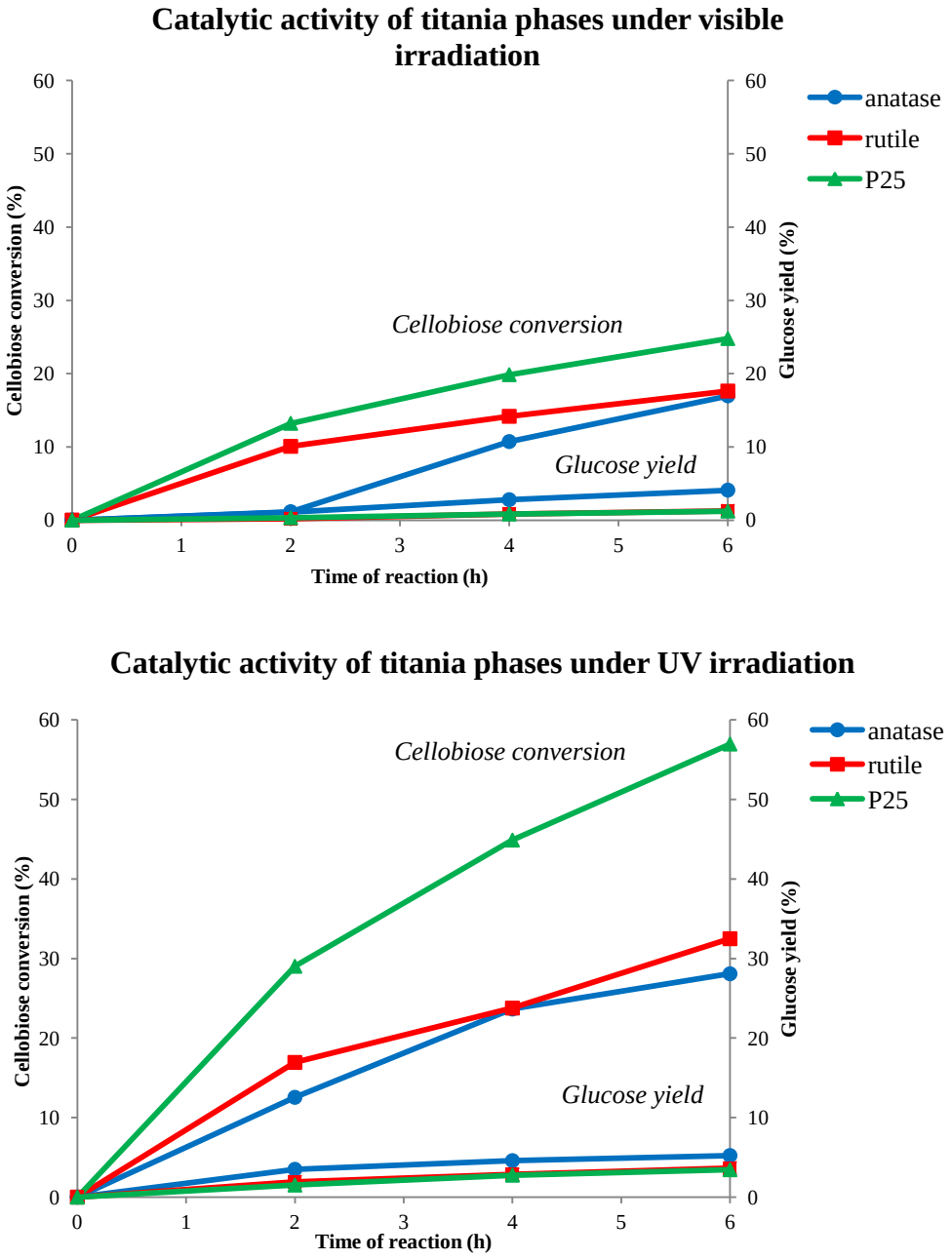

Figure 24: Catalytic performances of titania P25, rutile and anatase under visible and UVB irradiation. Reaction performed in the Luzchem photoreactor for 6h.

Table 11: Catalytic data of TiO_2 P25, anatase and rutile in the Luzchem photoreactor under UV irradiation.

Catalyst	Time of reaction (h)	Cellobiose conversion (%)	Peak area oxidation product (7.5min)	Peak area oxidation product (7.8min)	Glucose yield (%)
TiO_2 P25 (UV)	2	29	20181	4004	2
TiO_2 P25 (UV)	4	45	25798	7370	3
TiO_2 P25 (UV)	6	57	27730	8334	3
TiO_2 rutile (UV)	2	17	13964	1650	2
TiO_2 rutile (UV)	4	24	18006	2026	3
TiO_2 rutile (UV)	6	32	22700	2704	4
TiO_2 anatase (UV)	2	13	-	539	3
TiO_2 anatase (UV)	4	24	6639	1517	5
TiO_2 anatase (UV)	6	28	7076	2013	5

As reported in Figure 24 and Table 11 the differences in activity reported for the visible irradiation between rutile and anatase are maintained also under UV light. As expected, centring the irradiation to lower wavelength (UVB), a higher activity for all the samples is obtained because more energy is given to the semiconductor bandgap. Furthermore, the reported data indicate Degussa P25 as the most active support towards the reaction of selective oxidation of cellobiose, even if anatase remains the best one for the hydrolysis reaction.

Therefore, the high catalytic activity and its importance in photocatalysis justifies the choice of using titania P25 as a support for the synthesized catalysts in this study.

3.3. Effect of the metal nanoparticles

In the literature[39, 86] is reported that the presence of metal nanoparticles on the surface enhances the light absorption in the visible range for titania and other semiconductors. Supported metal nanoparticles can be prepared via different techniques[118] such as impregnation, deposition, precipitation and immobilization. This last has great advantages due to the potential high control in morphology and homogeneity of the nanoparticles as compared with simple metal salt impregnation method. The metal nanoparticles act as an electron acceptor when the frequency of excitation source is close to their SPR band. These electrons are then transferred to the titania conduction band and they are responsible for the generation of highly reactive species as hydroxyl and hydroperoxyl radicals.[40, 60, 86]

The aim of supporting gold and silver nanoparticles on the titania P25 was to analyze the enhancement on the reaction compared with the pure titania if exposed to a light source with a radiation profile comparable with the solar spectrum. The catalyst *1-Au/TiO2-P123* (1% w/w metal loading, P123 triblock copolymer as a ligand) was selected as a reference because it showed the highest conversion between the monometallic catalysts synthesized.

The Oriel Xe lamp 300W system was used to analyze the differences between the support and the synthesized catalysts because it gives the possibility of removing part of the emission spectrum with the use of selected filters. Two tests were performed: the first one (***A***) with the lamp equipped with a hot mirror filter to remove the IR radiation to prevent the heating of the reaction mixture, and with a coloured filter with a cut-off value of 420nm to avoid the UV excitation of titania. The second one (***B***) maintaining only the hot mirror filter on the lamp to increase the irradiation power (power values can be found in section 2.2.1). This last was done to analyze the differences between the absence and presence of metal nanopartiches when a more powerful radiation reaches the reaction, compared to the previous used photoreactor.

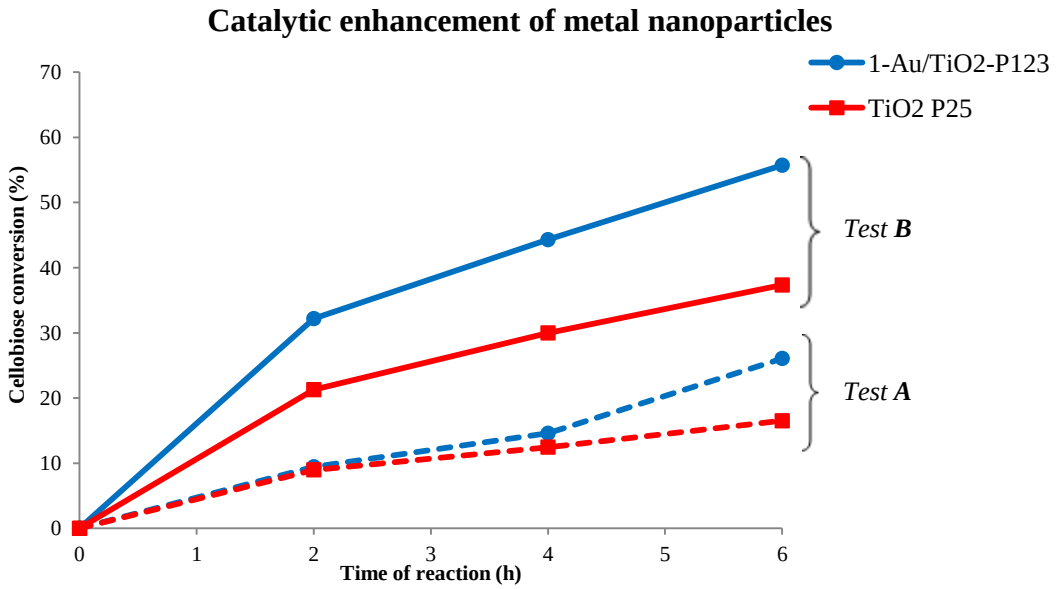

Figure 25: Catalytic performances of 1-Au/TiO2-P123 catalyst compared to titania P25. Tests performed with Oriel Xe lamp 300W for 6h. Test A with hot mirror and cut-off filter (420nm), Test B with only hot mirror filter.

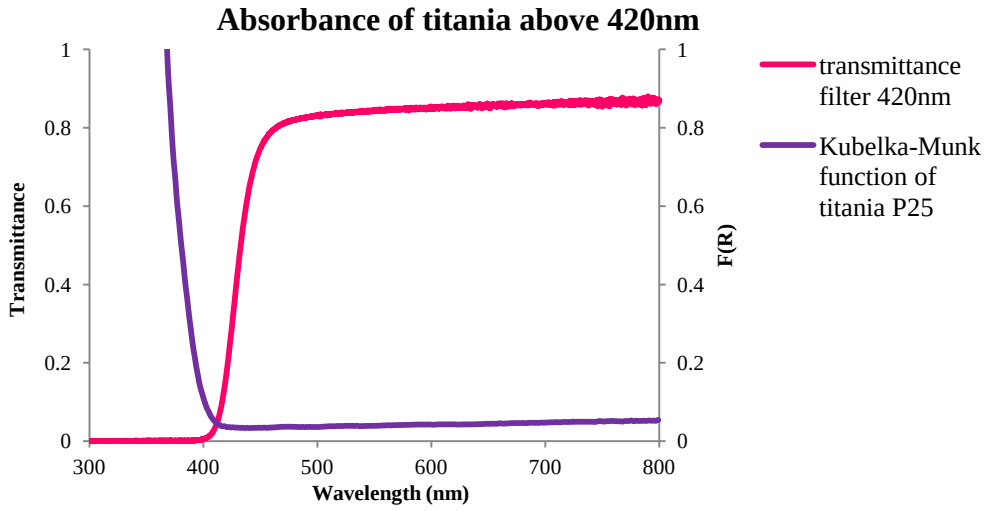

Figure 26: Overlap between the transmittance value of the cut-off filter and the Kubelka-Munk function of titania P25.

As reported for titania structures, also the addition of metal nanoparticles leads to the same products distribution in HPLC chromatograms, indicating a higher yield for the selective oxidation reaction than for the hydrolysis one. In test ***A*** the gold catalyst reached a cellobiose conversion of 26% after 6h compared to the 16% conversion of titania P25 (Figure 25). This suggests that the presence of the nanoparticles is enhancing the activity of the catalyst under visible light irradiation. Even though the presence of the cut-off filter removes almost completely the UV part of the emission spectrum, titania presents activity because there is a little overlap between the absorbance of titania

expressed by the Kubelka–Munk function and the transmittance spectrum of the filter, as indicated in Figure 26.

Test ***B*** increases the trend reported in the first test (Figure 25) because it was achieved a cellobiose conversion of 56% for the gold catalyst compared to the 37% of the titania P25. The performed tests confirmed the enhancement of activity acted by the nanoparticles towards titania P25 in the visible range for the reaction performed.

As a comparison the catalyst and the support were tested under UV irradiation in the Luzchem photoreactor (Figure 27).

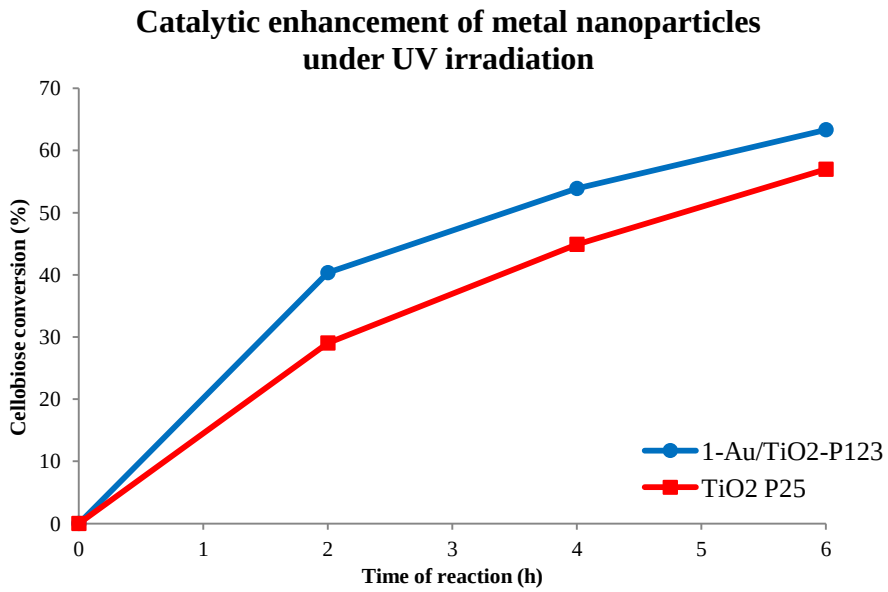

Figure 27: Catalytic performance of 1-Au/TiO2-P123 catalyst and titania P25. Tests performed in the Luzchem photoreactor under UVB irradiation for 6h.

Even in this case a little enhancement of activity was found after 6h (5% more than titania P25). In this set of reaction the active part of the catalyst is titania, because it is directly activated by UV irradiation, so the observed improvement of the presence of metal nanoparticles can be attribute to the presence of a 10% visible radiation emitted from the UV lamps near to the SPR position of the gold (peaks at 436 and 545nm as reported in the emission spectrum in section 2.2.1; gold SPR band ca. 540nm).

These data reported that the presence of metal nanoparticles on titania surface is enhancing the harvesting of electron in the visible and so increasing catalytic activity of titania towards the analyzed reaction.

3.4. Optimization of the metal containing catalysts

Different catalysts were tested on cellobiose; gold and silver were chosen as metals and loaded on titania P25 because they both present SPR band and are widely used in photocatalysis. The alloying effect between those two metal was also evaluated in the performed reaction. All the catalysts were tested in the Luzchem photoreactor under visible irradiation for different times. Pre-screening tests were done for 13h with 5 vials in the reactor to check the activity of the catalysts and optimize the synthetic parameters, then the most active ones were tested for 6h with one vial in the centre of the chamber to improve the stirring and reach the best conversion values.

The catalysts were synthesized using two different methods: either by wetness impregnation or using the sol method to preform the nanoparticles before supportation. The literature reports the impregnation as the simplest and quickest method to synthesize metal nanoparticles.[3, 130] That is because the metal salt solution is added directly onto the support and the nanoparticles are formed by calcination. On the other hand, this advantage is balanced with a not uniform particle size distribution and a not controllable dispersion of the nanoparticles on the surface. The sol method, instead, allows a greater control over the synthetic parameters because the nanoparticles are formed in a colloidal suspension of stabilizing agent and subsequently immobilized on the titania. This process is more complex and requires a longer synthetic time but it is possible to characterise the nanoparticles before the supportation by UV-VIS spectrophotometry.

For the reasons explained above in our research wetness impregnation method was used only as a screening technique to evaluate the catalytic activity of the metal in the reaction, and a greater attention was dedicated to the synthesis and characterization of the preformed nanoparticles with the colloidal method.

The catalysts were named *n*-Au_xAg_y/TiO_2-*m* where *n* is the metal loading on the support (% w/w), *x* and *y* are the percentage molar ratios respective of gold and silver and *m* is an indication of the calcination temperature (*C*) for WI samples or the stabilizing agent for sols (*P123* or *PVA*).

3.4.1. Monometallic catalysts

3.4.1.1. Silver and gold catalysts prepared by wetness impregnation

As a first step the optimum metal loading on titania surface was determined. Four silver catalysts were synthesized with different metal loadings in the range 0.5-5% w/w and calcined at 200°C. Their cellobiose conversion was evaluated with pre-screening tests for 13h and reported in Figure 28.

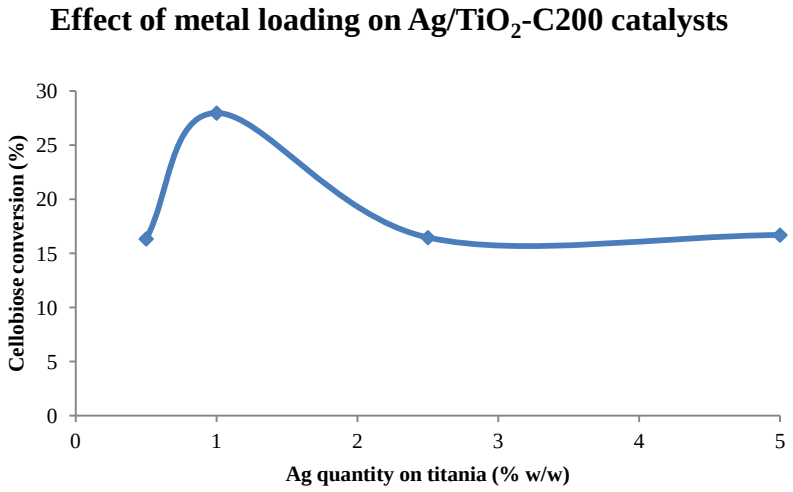

Figure 28: Catalytic tests of determination of the optimum metal loading for Ag/TiO_2-C200 catalysts with loadings 0.5, 1, 2.5 and 5% w/w. Pre-screening tests performed in the Luzchem photoreactor under visible light irradiation for 13h.

The highest conversion (26%) was reached by the *1-Ag/TiO_2-C200* catalyst within the different loadings tested. Therefore for the performed reaction the obtained data are comparable with the one reported in the literature.[40, 98] In fact it is indicated for the reactions of phenol degradation and water splitting an optimum loading of 1% w/w that allows the best ratio between catalytic activity of the metal and light/nanoparticle interaction. This can be explained for the fact that using a lower percentage of the metal the electrons produced and transferred to titania are not enough to enhance the activity of the support. On the other hand, increasing the quantity of metal nanoparticles loaded can cause, as reported in literature,[86] an increase in the particle dimension due to sintering effects and a variation of its shape. This leads to the observed decrease in activity because a minor number of atoms are available on the surface to act as antennas for the incident light. It has to be noted also that the loadings analyzed (up to 5% w/w) are decreasing only in a small amount the available surface area of the titania for reaction because the supported nanoparticles are not enough to cover completely the surface and

to prevent the absorption of water and oxygen responsible for the generation of reactive radicals.

Another pre-screening test was performed to evaluate the effect of the calcination temperature. In fact, the synthesis followed reports a calcination temperature of 400°C.[67] This parameter was compared with the catalytic activity of the silver samples calcined at 200°C, and it was observed that the catalyst *1-Ag/TiO_2-C400* presented a cellobiose conversion of 24% after 13h of reaction, with a value lower than the 28% obtained with the *1-Ag/TiO_2-C200* sample (Table 12). This small difference in activity can be explained by the partial sintering of the particles when calcined at higher temperatures.[16, 68, 98]

Table 12: Effect of the calcination temperature on the 1-Ag/TiO_2-C catalysts activity. Pre-screening tests performed for 13h.

Catalyst	Cellobiose conversion (%)	Peak area oxidation product (7.5min)	Peak area oxidation product (7.8min)	Glucose yield (%)
1-Ag/TiO_2-C200	28	25069	2924	1
1-Ag/TiO_2-C400	24	19790	2376	0

One of the most important features of the synthesized catalysts is the presence of the SPR band that allows the enhancement of activity compared to pure titania. The wide particle size distribution in the WI samples can be demonstrated by UV-VIS solid spectroscopy, as reported in Figure 29.

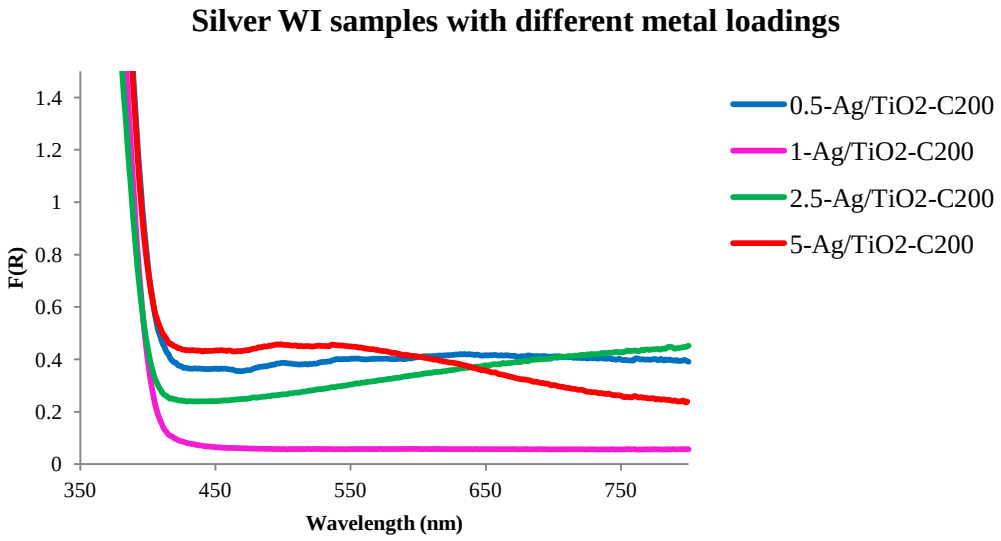

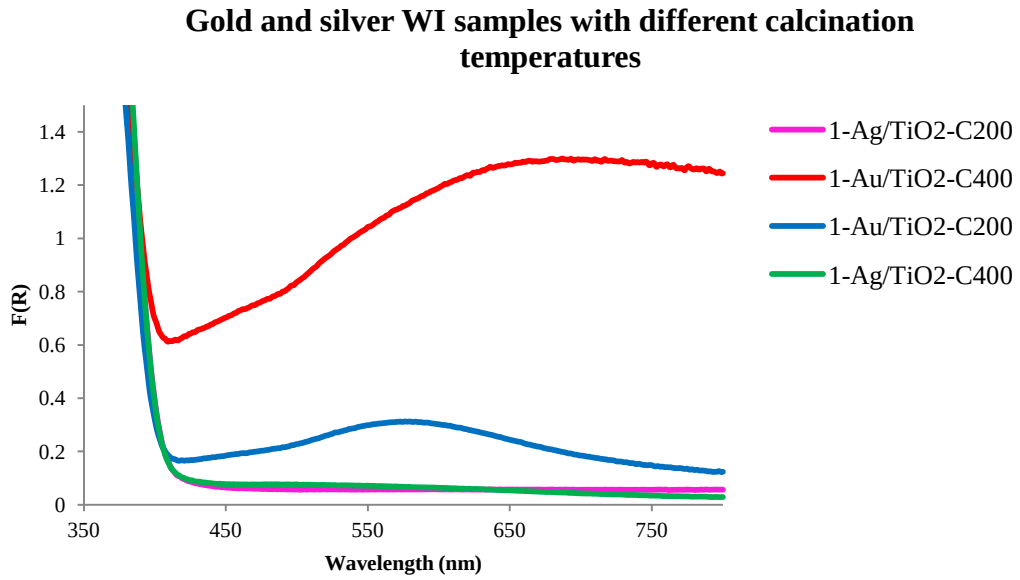

Figure 29: Solid UV-VIS spectra of gold and silver WI samples with different metal loadings and calcined at different temperatures. The vertical axis value is reported as a result of Kubelka-Munk function of reflectance.

From the curves it can be clearly seen that none of the silver samples present a clear SPR band in the range 400-600nm. This can be due both to the distribution but also to the nature of silver nanoparticles that are easily oxidized in air. On the other hand, the gold nanoparticles are more stable than the silver ones and exhibit a clear but weak band around 550nm for the sample calcined at 200°C and a more broad band red-shifted for the sample calcined at 400°C. The shift and the broadening of the gold SPR band is an indication that the dimension of nanoparticles is affected by the calcination temperature leading to bigger particles for higher temperatures.

Activity of the wetness impregnation monometallic catalysts

Despite the UV-VIS analysis, the presence of the nanoparticles is confirmed by the catalytic activity of the sample (Table 13 and Figure 30). Furthermore, oxidized silver atoms in the nanoparticles don't affect catalytic activity because they can be reduced by irradiated light, as reported in the widely applied photoreduction method.[51, 119]

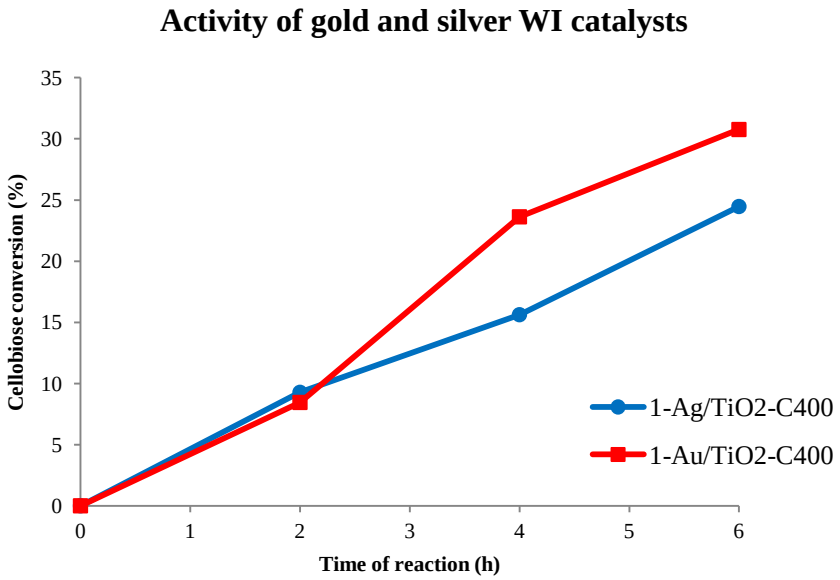

Figure 30: Catalytic performances of 1-Au/TiO_2-C400 and 1-Ag/TiO_2-C400 catalysts. Tests performed in the Luzchem photoreactor under visible light irradiation for 6h.

Table 13: Catalytic data of 1-Au/TiO_2-C400 and 1-Ag/TiO_2-C400 catalysts.

Catalyst	Time of reaction (h)	Cellobiose conversion (%)	Peak area oxidation product (7.5min)	Peak area oxidation product (7.8min)	Glucose yield (%)
1-Ag/TiO_2-C400	2	9	8952	-	0
1-Ag/TiO_2-C400	4	16	15427	-	0
1-Ag/TiO_2-C400	6	24	23245	2067	0
1-Au/TiO_2-C400	2	8	12679	-	1
1-Au/TiO_2-C400	4	24	18091	1373	2
1-Au/TiO_2-C400	6	31	22904	2427	2

The gold catalysts showed a higher cellobiose conversion and a higher product yield than the silver one suggesting that gold is a better metal for the reaction of selective oxidation and of hydrolysis of cellobiose.

3.4.1.2. Monometallic catalysts prepared with preformed nanoparticles

The sol-method or colloidal method is widely used in catalysis[3] because, as previously reported, it allows to tune each of the different steps of reaction and to analyze the nanoparticles before immobilization. For the synthesis of the colloidal catalysts two methods were chosen. The first one, named Method 1, is reported by Saiman et al.[12] and utilizes PVA as a stabilizing agent with a ratio PVA/metal=1.2 w/w. Method 2 instead uses P123, a triblock copolymer, as a ligand following the synthesis of Huang et al.[52] (section 2.3.2).

Characterisation of sols

The first indication of the formation of the stabilized nanoparticles by reduction of the metal salt with sodium borohydride was the change in colour. In fact, the gold solution quickly turned from yellow to wine red and the silver one from transparent to green/gray. To confirm the presence and formation of the nanoparticles, the obtained colloidal solution were analyzed by UV-VIS spectrophotometry to visualize the characteristic presence of the SPR band of gold and silver (Figure 31). The bands were found respectively at 526 and 389nm, in the same range as literature data.[33, 86]

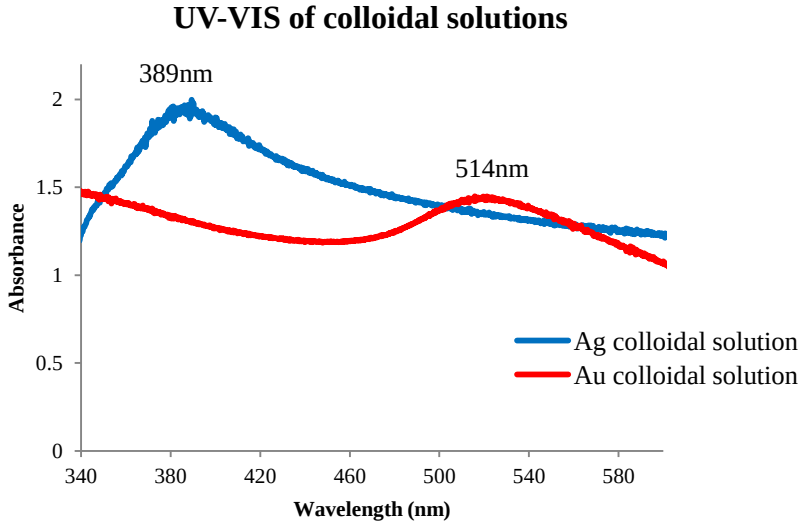

Figure 31: UV-VIS spectra of colloidal solutions of gold and silver prepared with the Method 2.

Colloidal solution have a limited stability despite the presence of the stabilizing agent. In fact the nanoparticles tend to collapse or to be oxidized by the oxygen in the air. In order to avoid any changes in the synthesized solutions, the sols were supported as soon as they were synthesized but a small aliquot was kept to monitor the temporal stability of the

nanoparticles. The colloids were stored at 4°C and in the dark for 6 weeks and were analyzed regularly.

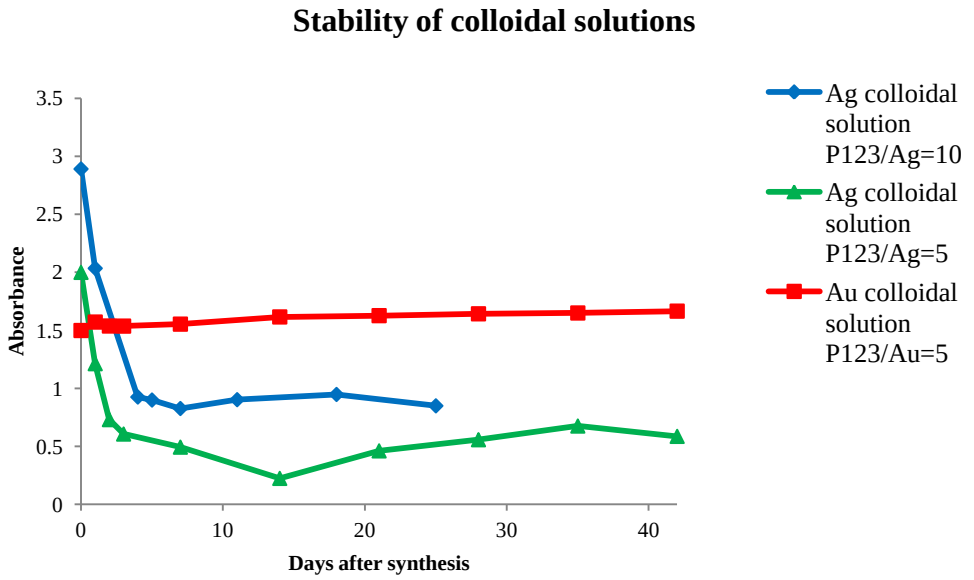

Figure 32: Analysis of the stability of colloidal solutions of gold and silver synthesized with Method 2 with different ratios of stabilizing agent (P123).

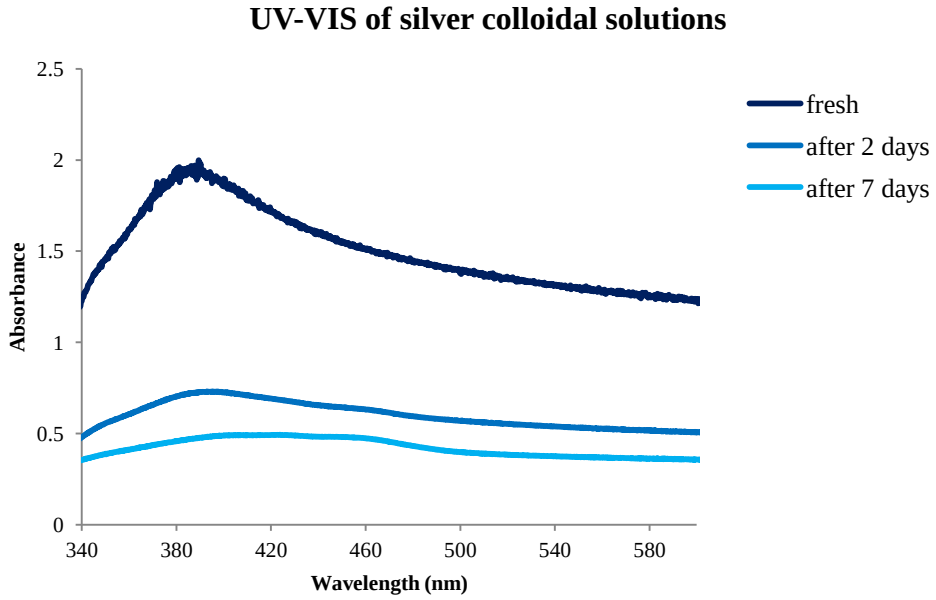

Figure 33: UV-VIS spectra of the silver colloidal solutions within a week (P123/Ag=5).

As reported in Figure 32 the gold solution was stable for the whole time because gold nanoparticles do not oxidize easily. Silver nanoparticles instead precipitated after few days as silver oxide, this was confirmed by the change in the UV-VIS spectra (Figure 33) and also from the colour of the solution that became clearer with a grey precipitate at the

bottom. In order to enhance the stability of these silver nanoparticles the quantity of stabilizing agent was increased from a starting ratio P123/Ag of 5 to a value of 10 because a bigger quantity of ligand permits a better stabilization of the reduced particles in solution. The same approach was applied with the new catalyst as the absorbance values appeared different changing the ratio because with more stabilizing agent the solution was more opaque (higher scattering). Because no improvement was observed in the stability, the monitoring of the sol was stopped after 4 weeks.

Effect of the type of stabilizing agent on gold based catalysts

The gold colloidal catalyst were synthesized following the two different methods reported (section 2.3.2). The synthesized catalysts were first characterized by UV-VIS solid spectroscopy and TEM and then tested in the performed reaction. The use of different procedures allowed us to select the best synthetic pathway and stabilizing agent for the synthesized catalysts.

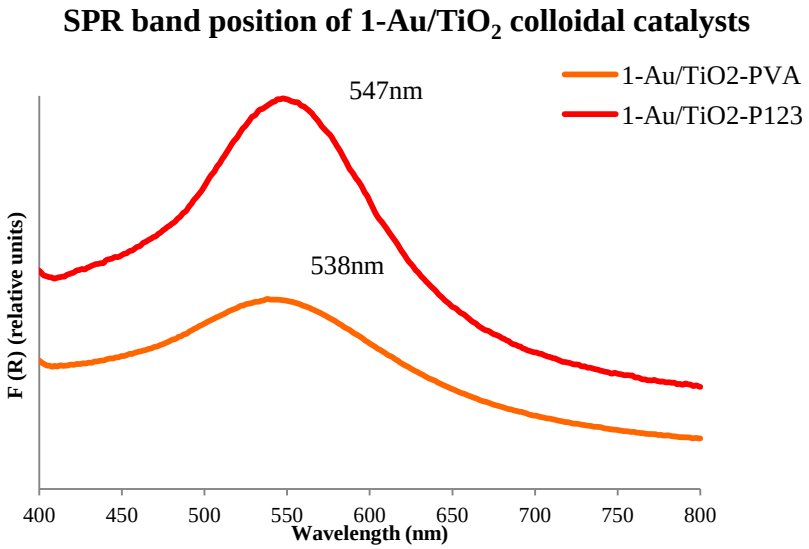

Figure 34: Solid UV-VIS spectra of 1-Au/TiO_2 samples with different stabilizing agents. The vertical axis value is reported as a result of Kubelka-Munk function of reflectance.

The UV-VIS analysis on solids (Figure 34) confirms the presence of gold nanoparticles with a SPR band in the same position for both the methods but the maxima of the peak suggest a different particle size dimension in the two samples. Instead the broaden shape of the peak and the absorbance value can be related to the different dielectric environment created by the residual ligands. As reported by Ghosh et al.[38] longer chains

surfactants should shift the maximum of absorption to longer wavelength and create a thicker layer that increases the plasmon band intensity. This is valid supposing a not complete removal of the stabilizing agent from the nanoparticles shell.

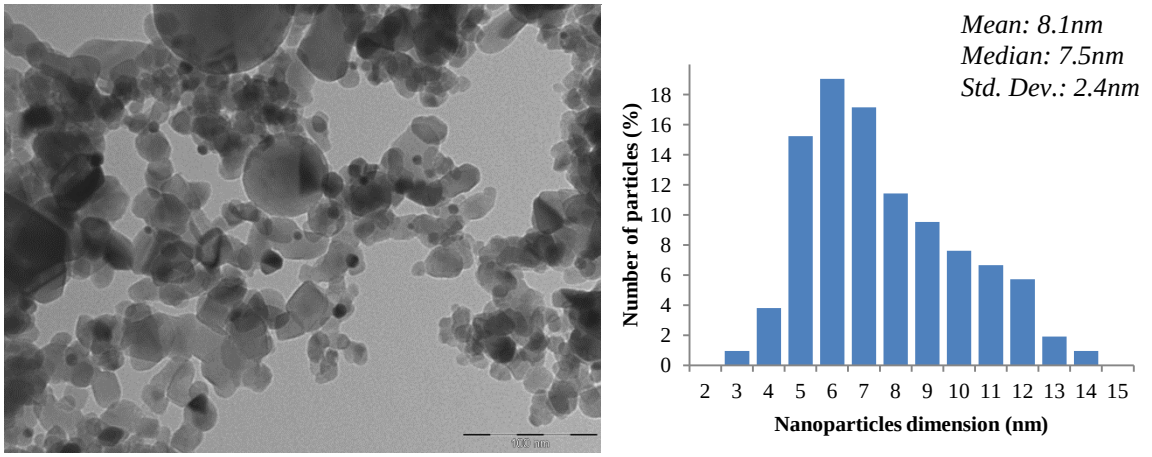

Figure 35: TEM image of 1-Au/TiO_2-P123 catalyst (scale 100nm) on the left and dispersion of nanoparticles dimension on the right (ca. 100 particles analyzed).

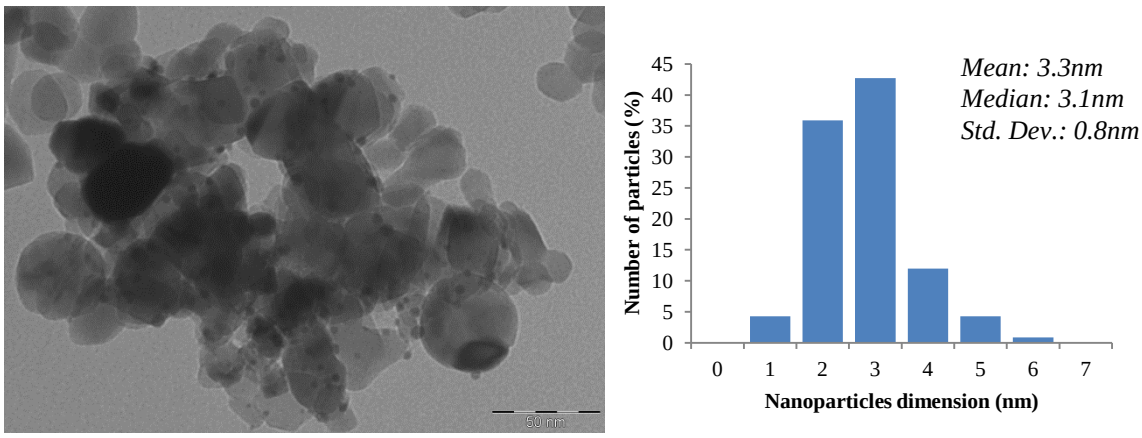

Figure 36: TEM image of 1-Au/TiO_2-PVA catalyst (scale 50nm) on the left and dispersion of nanoparticles dimension on the right (ca. 100 particles analyzed).

TEM images of the two synthesized catalysts reported in Figure 35 and 36 underline that the synthesis described with the Method 1, leads to a dimension of nanoparticles of ca. 3nm, that is much smaller than the one obtained with Method 2 with a distribution centred at 6nm (histograms in Figure 35 and 36). This is a consequence of the different preparation method, because both the nanoparticle dimension and size distribution depend upon the type of stabilizing agent, the stirring speed, the methodology followed for the addition and the strength of the reducing agent. Furthermore, Method 1 synthesis requires the use of a larger quantity of ligand than Method 2 thus, the availability of a larger number of polymer molecules in solution can lead to the formation of smaller

metal nanoparticles. Also the shape of the gaussian distribution is different and broader for the *1-Au/TiO$_2$-P123* sample. The tailing in the curve of dispersion in the case of this sample could be a consequence of the incomplete removal of ligand that leads to bigger particles because, even if they were treated under reflux for the same time, the different polarity and structure of the two polymers can require different times for the complete removal.

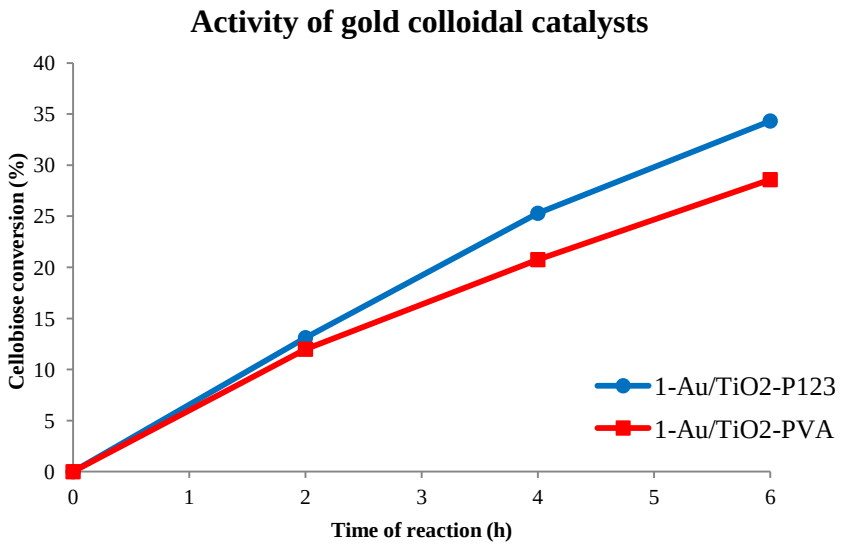

Figure 37: Catalytic performances of the different 1-Au/TiO$_2$ catalysts. Reaction performed in the Luzchem photoreactor under visible light irradiation for 6h.

Table 14: Catalytic data of 1-Au/TiO$_2$ colloidal catalysts.

Catalyst	Time of reaction (h)	Cellobiose conversion (%)	Peak area oxidation product (7.5min)	Peak area oxidation product (7.8min)	Glucose yield (%)
1-Au/TiO$_2$-PVA	2	12	10359	840	0
1-Au/TiO$_2$-PVA	4	21	18029	1661	0
1-Au/TiO$_2$-PVA	6	29	23938	2060	0
1-Au/TiO$_2$-P123	2	13	13061	1193	0
1-Au/TiO$_2$-P123	4	25	21112	2263	1
1-Au/TiO$_2$-P123	6	34	27024	3217	1

In relation to the catalytic activity of the two gold samples it can be seen from Figure 37 and Table 14 that *1-Au/TiO$_2$-P123* catalyst after 6h presents a cellobiose conversion of 34%, higher than the 29% of *1-Au/TiO$_2$-PVA* indicating that Method 2 is better for the reaction performed. This highlights that for the selective oxidation of cellobiose it seems

not necessary a really small dimension of the particles and a strict control on the morphology.

Effect of the quantity of stabilizing agent on silver based catalysts

Another parameter that influences the catalytic activity of the catalysts is the quantity of the stabilizing agent. With the aim of increasing the stability of silver nanoparticles, the quantity of P123 was raised from 5 to 10 molar ratio; subsequently the samples were treated under reflux with water for 2h at 80°C.

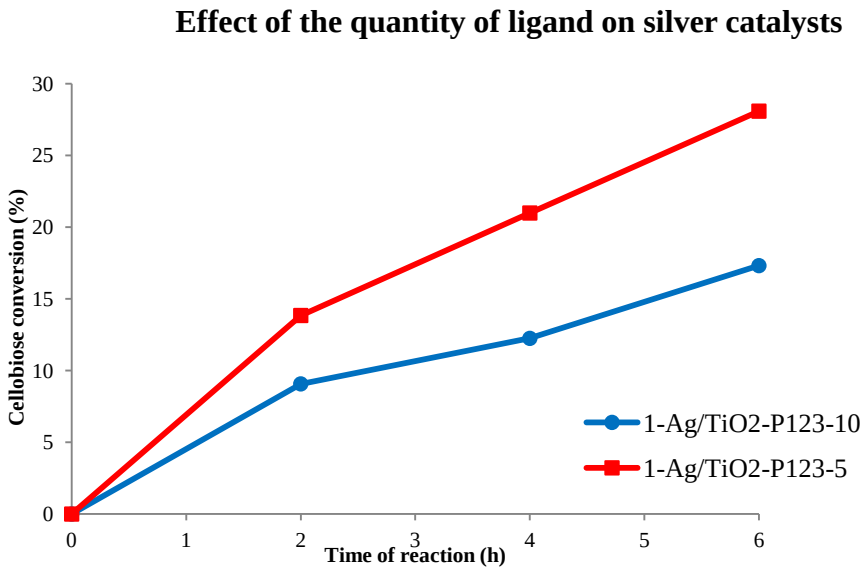

Figure 38: Catalytic performances of 1-Ag/TiO_2 catalysts synthesized with a P123/Ag molar ratio of 5 and 10. Reaction performed in the Luzchem photoreactor under visible light irradiation for 6h.

Catalytic data report the highest activity for the sample with the lower polymer quantity. This is because with the same reflux time the ligand was not completely removed causing a lower cellobiose conversion for the sample with a metal to polymer ratio of 10 (Figure 38).

To examine the effect of the removal of ligand on the catalytic activity the *1-Ag/TiO_2-P123-10* catalyst was treated under reflux for different periods of time, characterised by IR spectroscopy and tested under the same conditions as the other catalysts.

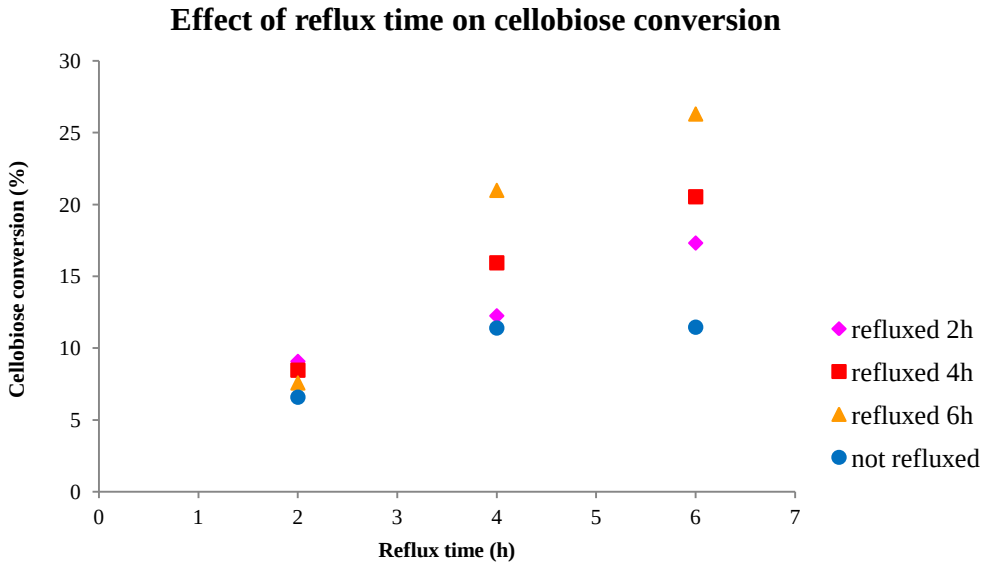

Figure 39: Evaluation of the catalytic activity after 6h for 1-Ag/TiO_2-P123-10 catalysts refluxed for 0, 2, 4 and 6h. Reaction performed in the Luzchem photoreactor under visible light irradiation.

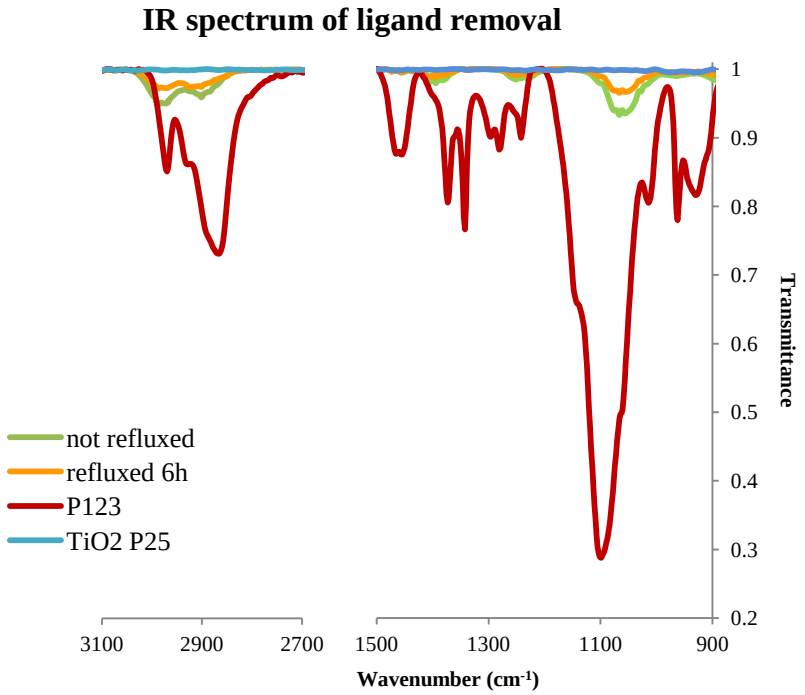

Figure 40: IR spectroscopy of TiO_2 P25, P123, 1-Ag/TiO_2-P123-10 refluxed for 6h and not refluxed. The characteristic bands of the polymer are reported: 1100cm^{-1}stretching C-O-C, 2980cm^{-1} stretching CH_3, 2922cm^{-1} stretching CH_2 and 2851cm^{-1} stretching CH.

The data in Figure 39 show that when the ligand quantity is increased from 5 to 10 molar ratio a proportional increase in the reflux time is necessary to remove the stabilizing agent. In fact, only the cellobiose conversion at higher reflux time (6h) is comparable

with the results obtained with the *1-Ag/TiO_2-P123-5* catalyst with a lower surfactant ratio.

The effective removal of the ligand by reflux was also checked by IR spectroscopy. In Figure 40 are highlighted the characteristic bands of the triblock copolymer (P123: C-O-C stretching 1100cm^{-1}; CH_3, CH_2, CH stretching 2980, 2922, 2851cm^{-1} respectively). These peaks are more visible in the not refluxed catalyst than in the sample refluxed for 6h. Moreover, in the fingerprint region at 400-960cm^{-1} are present the stretching modes of Ti-O bonds, visible in both the catalysts.[103]

Determination of the quantity of metal immobilized

The synthesis and supportation of sols requires two collection steps of the solid catalyst by filtration: the first after the immobilization on titania, the second one after the removal of excess reagents. During the filtration it is possible to have some leaching of metal or of the nanoparticles in the liquid phases. The presence of metal nanoparticles was checked by UV-VIS analysis and the not reduced metal in solution was analyzed by Inductively Coupled Plasma (ICP).

Table 15: ICP leaching results for the different steps of the reaction.

Sample name	P123 quantity	Step of reaction	Time of reflux (h)	Molar ratio Ag lost/Ag tot (%)	Molar ratio Au lost/Au tot (%)
1-Au/TiO_2-P123	5	support	-	-	0.52
1-Au/TiO_2-P123	5	reflux	2	-	-
1-Ag/TiO_2-P123-5	5	support	-	0.06	-
1-Ag/TiO_2-P123-5	5	reflux	2	4.52	-
1-Ag/TiO_2-P123-10	10	support	-	0.20	-
1-Ag/TiO_2-P123-10	10	reflux	2	0.43	-
1-Ag/TiO_2-P123-10	10	reflux	4	0.25	-
1-Ag/TiO_2-P123-10	10	reflux	6	0.16	-

No gold or silver nanoparticles of catalytic size were detected. Therefore, it can be assumed that the metal detected by ICP is coming from the unreduced reagent or oxidized nanoparticles. The results of the ICP analyses (Table 15) present really small leaching values for the supportation step as ligand in solution prevents the release of the metal. On the other hand, the reflux step causes a high loss of metal in particular for the

silver catalyst with a P123/Ag ratio of 5. Furthermore, by increasing the quantity of stabilizing agent, the leaching is lower and its value is inversely proportional to the reflux time. This indicates that the highest quantity of metal is lost at the beginning of the reflux step.

The metal immobilized and its crystalline phase can be detected by X-Ray Powder Diffractometry on the crystalline phase of titania. Samples were acquired on zero-background sample holders in the 2θ range 10-80. As a blank comparison a spectrum of the titania P25 was analyzed.

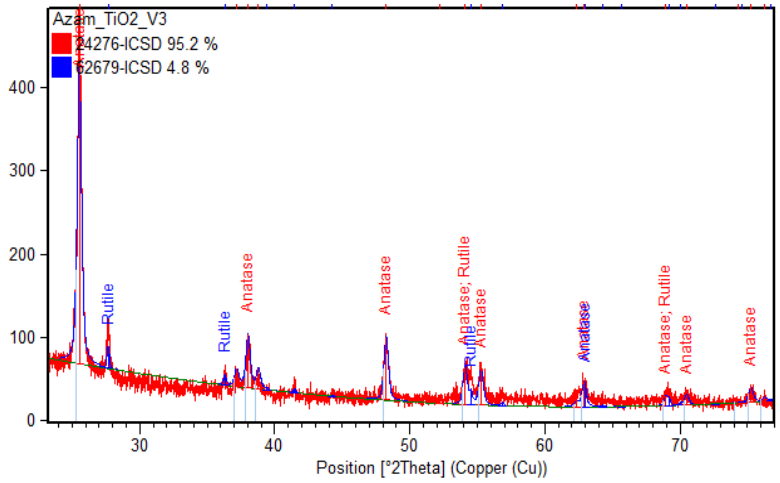

Figure 41: P-XRD spectra of titania P25 as purchased. The result of overlap with ICSD database is reported for anatase (--) and rutile (--).

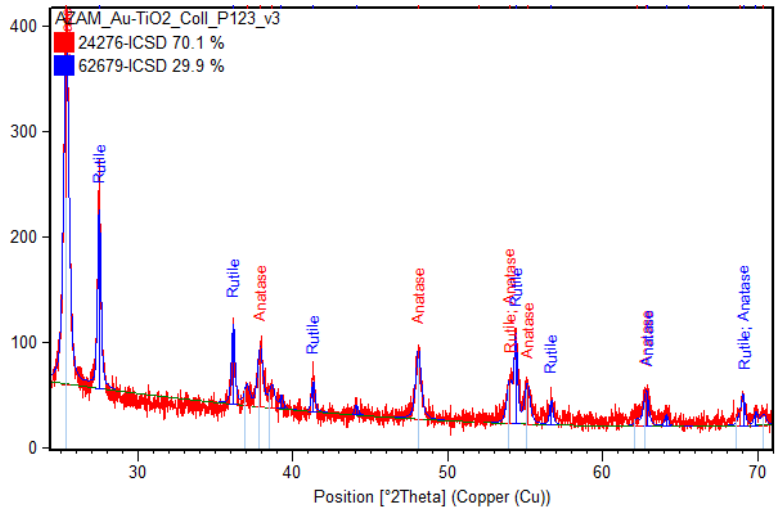

Figure 42: P-XRD spectra of 1-Au/TiO_2-P123 catalyst. The result of overlap with ICSD database is reported for anatase (--) and rutile (--).

In Figure 41 can be observed for titania P25 the overlap with anatase and rutile spectra from ICSD database (RSC, UK). The spectrum recorded for *1-Au/TiO_2-P123* catalyst is instead reported in Figure 42. The gold nanoparticles are not detectable in the range analyzed because the peaks are too small respect the titania peaks; this is due to the low percentage of metal loaded.[121] Furthermore, an increase in rutile percentage in the structure of the titania P25 is revealed and it is probably due to the reflux treatment at 80°C of the catalyst, because rutile is the most thermodynamically stable structure.[43] Other spectra of gold and silver catalysts were obtained but no differences were highlighted from the results above reported determining the impossibility of detecting gold and silver nanoparticles by P-XRD analyses with the applied procedure.

3.4.1.3. Activity of the monometallic catalysts

Monometallic gold and silver catalysts were synthesized following WI and sol method and they were both tested for the performed reaction. A comparison between the two synthetic methods can be found in Figure 43 and Figure 44 for each of the a analyzed metals.

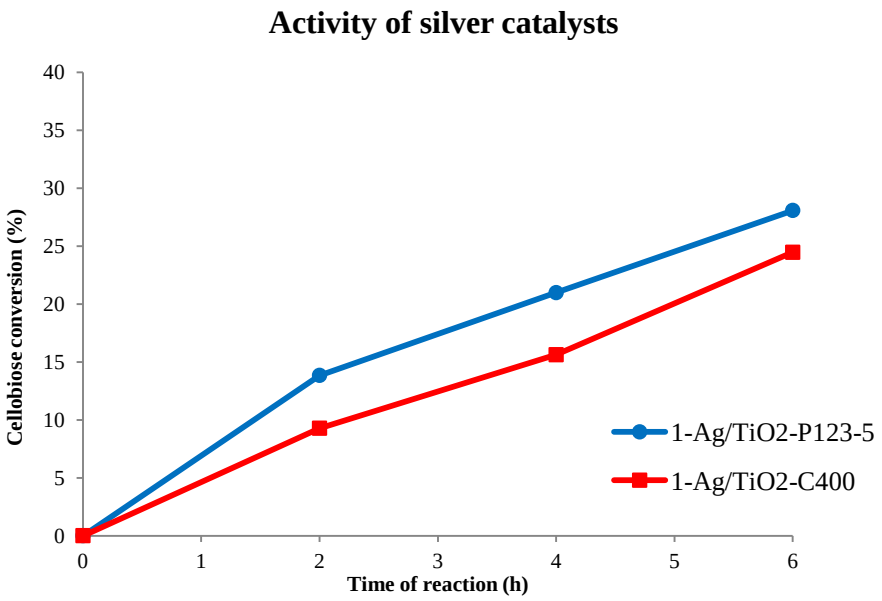

Figure 43: Catalytic performances of 1-Ag/TiO_2 catalysts. Colloidal sample (1-Ag/TiO_2-P123-5) and WI sample (1-Ag/TiO_2-C400). Tests performed in the Luzchem photoreactor under visible light irradiation for 6h.

Table 16: Catalytic data of 1-Ag/TiO_2 catalysts.

Catalyst	Time of reaction (h)	Cellobiose conversion (%)	Peak area oxidation product (7.5min)	Peak area oxidation product (7.8min)	Glucose yield (%)
1-Ag/TiO_2-C400	2	9	8952	-	0
1-Ag/TiO_2-C400	4	16	15427	-	0
1-Ag/TiO_2-C400	6	24	23245	2067	0
1-Ag/TiO_2-P123-5	2	14	12931	-	1
1-Ag/TiO_2-P123-5	4	21	16909	1504	1
1-Ag/TiO_2-P123-5	6	28	19784	2234	2

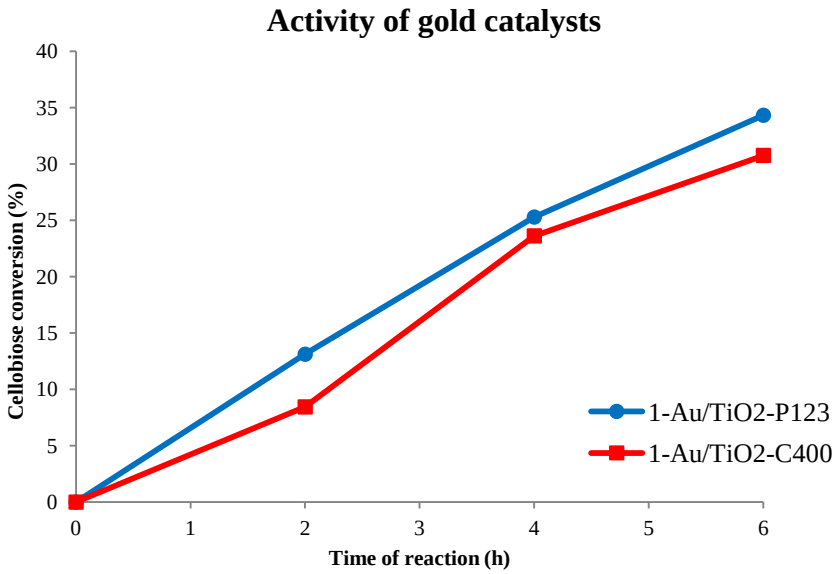

Figure 44: Catalytic performances of 1-Au/TiO_2 catalysts. Colloidal sample (1-Au/TiO_2-P123) and WI sample (1-Au/TiO_2-C400). Tests performed in the Luzchem photoreactor under visible light irradiation for 6h.

Table 17: Catalytic data of 1-Au/TiO_2 catalysts.

Catalyst	Time of reaction (h)	Cellobiose conversion (%)	Peak area oxidation product (7.5min)	Peak area oxidation product (7.8min)	Glucose yield (%)
1-Au/TiO_2-C400	2	8	12679	-	1
1-Au/TiO_2-C400	4	24	18091	1373	2
1-Au/TiO_2-C400	6	31	22904	2427	2
1-Au/TiO_2-P123	2	13	13061	1193	0
1-Au/TiO_2-P123	4	25	21112	2263	1
1-Au/TiO_2-P123	6	34	27024	3217	1

The change in preparation method leads to differences in the activity, specifically the preformed nanoparticles catalysts present always a slightly higher activity than the WI ones. As reported in Figure 43 and Table 16 for silver catalysts is reached a cellobiose conversion of 28% after 6h of reaction for the colloidal sample, compared to 25% of the WI sample. For the gold system, instead, the colloidal catalyst reaches a conversion of 34% and 31% for the WI (Figure 44 and Table 17).

For this reason, and for the better characterisation performable, gold and silver monometallic catalysts, synthesized by colloidal immobilization with P123 as stabilizing agent were demonstrated promising catalysts for the reaction of selective oxidation of cellobiose and not for the reaction of hydrolysis, due to the low amount of glucose produced.

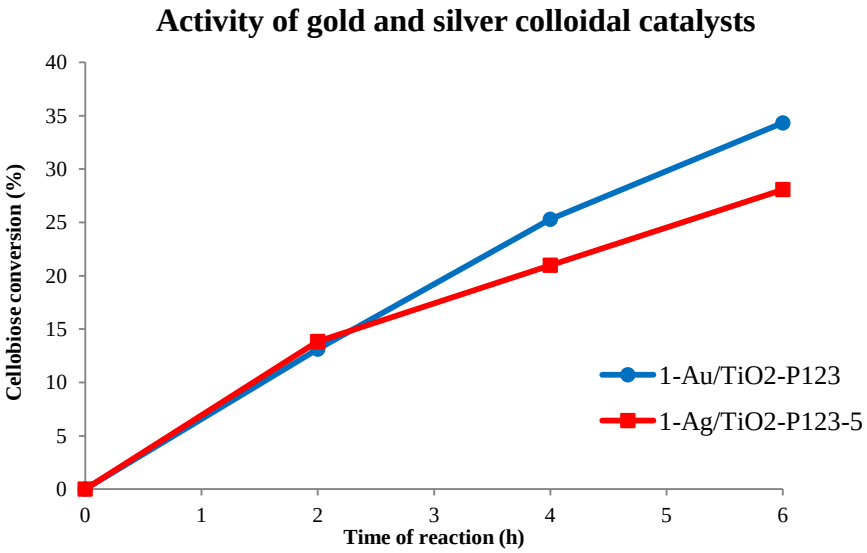

Figure 45: Catalytic performances of 1-Ag/TiO2-P123-5 and 1-Au/TiO2-P123 catalysts. Reaction performed in the Luzchem photoreactor under visible light irradiation for 6h.

A comparison of the catalytic activity of the two metal in the colloidal catalyst (Figure 45) presents a conversion after 6h of reaction of 34% for gold and 28% for silver indicating that, as for WI catalysts, *1-Au/TiO$_2$-P123* catalyst is more active than *1-Ag/TiO$_2$-P123-5*.

In the literature it can be found several application for gold nanoparticles in photocatalysis due to their stability and high activity in hydrogen production, dye decoloration, phenol decomposition and carboxylic acid degradation.[22, 86] On the other hand, silver is less commonly used, despite the reported activity in photodegradation of organics as methyl orange[39] and phenol[40]. However silver has several advantages over the use of gold for photocatalysts: first of all it is cheaper, it has potential application in biology for its antibacterial properties and its surface properties are easily tailorable (its plasmon resonance can be tuned to any wavelength in the visible spectrum[33]).[39, 40] To try to maintain the highly tunable silver properties and the better catalytic results obtained in this reaction for gold it was chosen to try an alloy of those two metal nanoparticles, maintaining the total metal loading on titania P25 at 1% w/w.

3.4.2. Bimetallic catalysts

Gold and silver bimetallic catalysts were synthesized on titania both with preformed nanoparticles and with the WI method and named as *1-Au_xAg_y/TiO_2* catalysts. The total metal loading on the titania was kept constant but the percentage molar ratio between the two metals (x and y) was varied to analyze the effect on the catalytic activity of the presence of silver in the alloy. The ratios synthesized are reported in Table 18.

*Table 18: List of catalysts synthesized with WI method and sol method. (*samples analyzed previously reported as a reference).*

Catalyst	Content of Au (% mol)	Content of Ag (% mol)
1-Au/TiO_2*	100	0
1-$Au_{95}Ag_5/TiO_2$	95	5
1-$Au_{85}Ag_{15}/TiO_2$	85	15
1-$Au_{50}Ag_{50}/TiO_2$	50	50
1-$Au_{15}Ag_{85}/TiO_2$	15	85
1-Au_5Ag_{95}/TiO_2	5	95
1-Ag/TiO_2*	0	100

3.4.2.1. Bimetallic catalysts prepared by wetness impregnation

WI catalysts were synthesized following the same method as the monometallic ones. The calcination temperature was chosen at 400°C, instead at 200°C, because of the not homogeneity of the samples calcined at 200°C, suggesting a not complete reduction. In comparison the samples calcined at 400°C for 3h presented a uniform colour as an indication of a complete reduction (colour comparison in Figure 46).

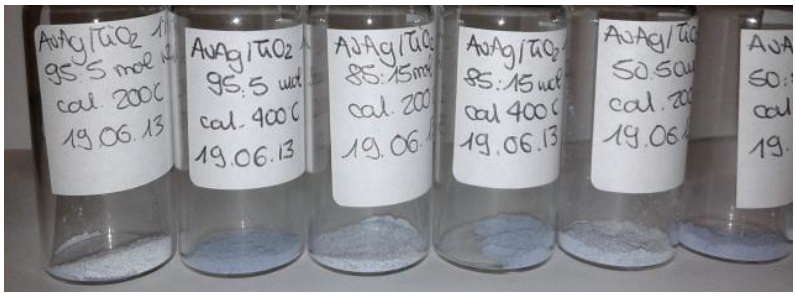

Figure 46: Differences in homogeneity of 1-AuAg/TiO2-C200 and 1-AuAg/TiO2-C400 catalysts.

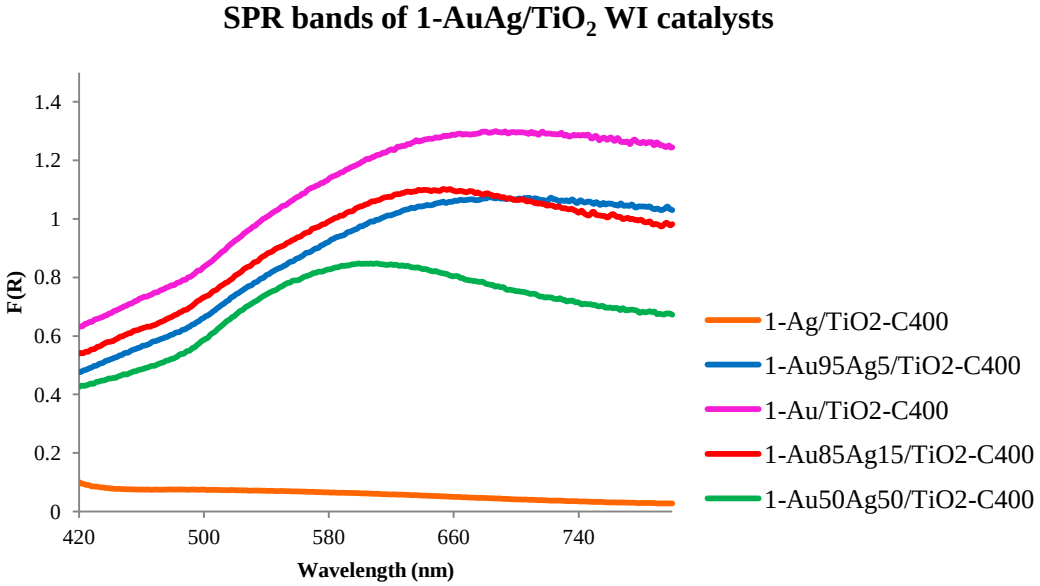

Figure 47: Solid UV-VIS spectra of 1-AuAg/TiO_2-C400 samples. The vertical axis value is reported as a result of Kubelka-Munk function of reflectance.

Solid UV-VIS spectra were recorded to analyze the presence of the SPR band of the metals but, as reported for WI monometallic catalysts, the bands appear really broad and not characteristic of the alloy (Figure 47). The height of the curve is dependent on the colour of the catalyst, in fact the catalysts with a higher ratio of gold are violet and present a higher Kubelka-Munk value whereas, instead when Ag is the dominant metal in the alloy the catalyst have pale colours that result in high reflectance values.

3.4.2.2. Bimetallic catalysts prepared with preformed nanoparticles

Bimetallic sol catalysts were synthesized following Method 2 with a P123/metal molar ratio of 5, on the base of the analyses performed with monometallic samples.

The formation of nanoparticles was proved by the change in colour of the sols after reduction (Figure 48). Gold was wine-red, and with the increase of the silver percentage in the solution the colour became more red, the catalysts with a substantial quantity of silver were brown and silver was green-gray. Furthermore, the reduction was confirmed by UV-VIS spectrophotometry (Figure 49).

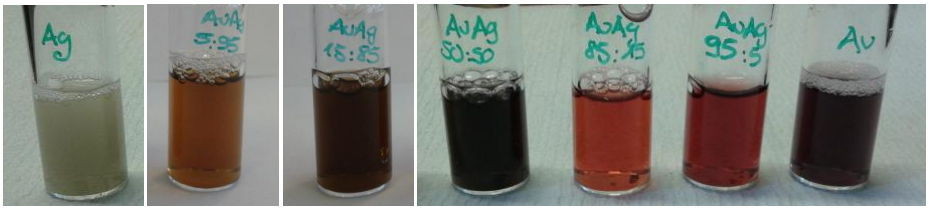

Figure 48: Colour of the sols before immobilization on titania. From left to right: Ag, Au_5Ag_{95}, $Au_{15}Ag_{85}$, $Au_{50}Ag_{50}$, $Au_{85}Ag_{15}$, $Au_{95}Ag_5$ and Au colloids.

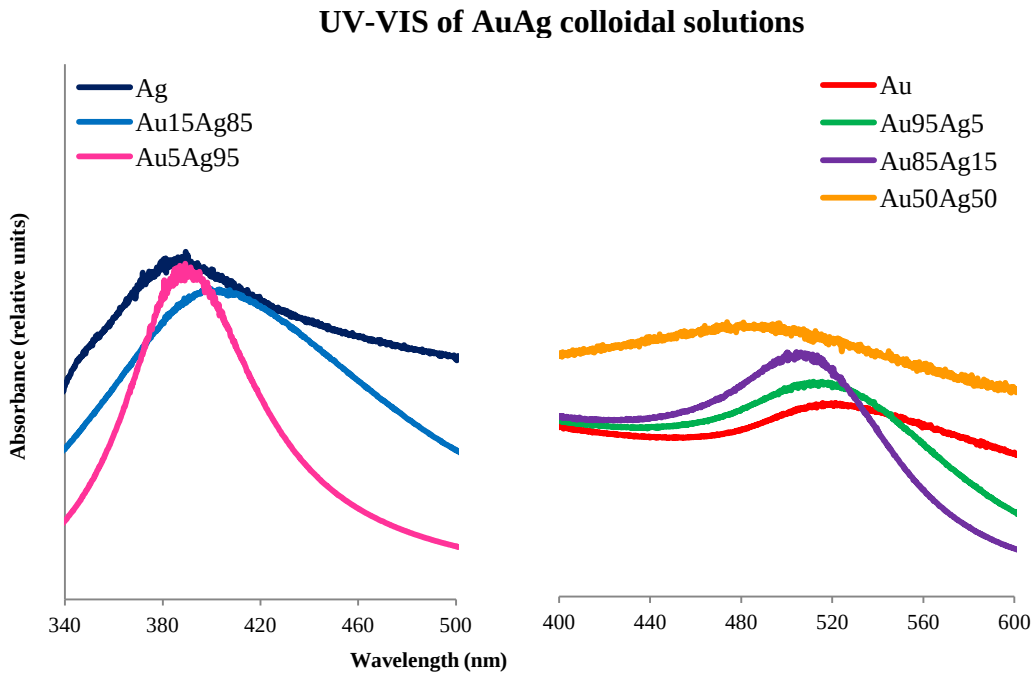

Figure 49: UV-VIS spectra of colloidal solution of 1-AuAg/TiO_2 catalysts with different metal ratios.

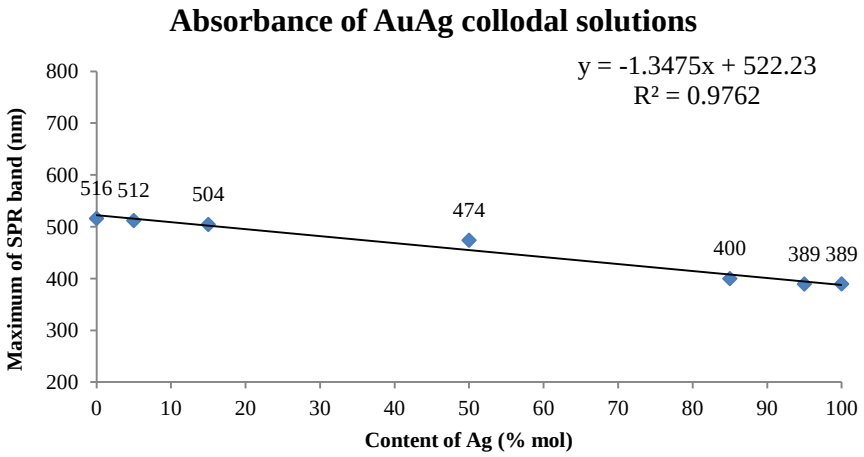

Figure 50: Linear relation between the percentage of the two metals and the maximum of the SPR band in UV-VIS spectra.

The formation of nanoparticles containing the two metals was suggested by the presence of a single SPR band (Figure 49) characteristic of alloys, as reported in the literature.[52] Furthermore, the position of the maximum of the band appears linearly dependent to the ratio of the two metals as represented in Figure 50.

As for the monometallic sol catalysts, the solution was first supported on titania than collected and refluxed for 2h at 80°C to remove the stabilizing agent. The liquid solutions were analyzed with ICP and UV-VIS, detecting no nanoparticles of the analyzed dimension in the solution for the absence of the SPR band. The ICP results reported in Table 19 indicate that when the silver percentage is increased in the catalysts, the metal leaching is higher as well and, as for the monometallic catalysts, the reflux step is the most problematic in the reaction for the loss of silver.

Table 19: ICP leaching results for the different steps of the reaction.

Catalyst	Step of reaction	Molar ratio Ag lost/Ag tot (%)	Molar ratio Au lost/Au tot (%)
1-$Au_{95}Ag_5/TiO_2$	support	-	0.43
1-$Au_{95}Ag_5/TiO_2$	reflux	-	-
1-$Au_{85}Ag_{15}/TiO_2$	support	-	-
1-$Au_{85}Ag_{15}/TiO_2$	reflux	-	-
1-$Au_{50}Ag_{50}/TiO_2$	support	-	-
1-$Au_{50}Ag_{50}/TiO_2$	reflux	0.91	-
1-$Au_{15}Ag_{85}/TiO_2$	support	0.04	-
1-$Au_{15}Ag_{85}/TiO_2$	reflux	1.73	-
1-Au_5Ag_{95}/TiO_2	support	0.06	-
1-Au_5Ag_{95}/TiO_2	reflux	8.52	-

The determination of the position of the SPR band in the immobilized catalyst was performed with solid UV-VIS spectrophotometry, as for the previously reported samples.

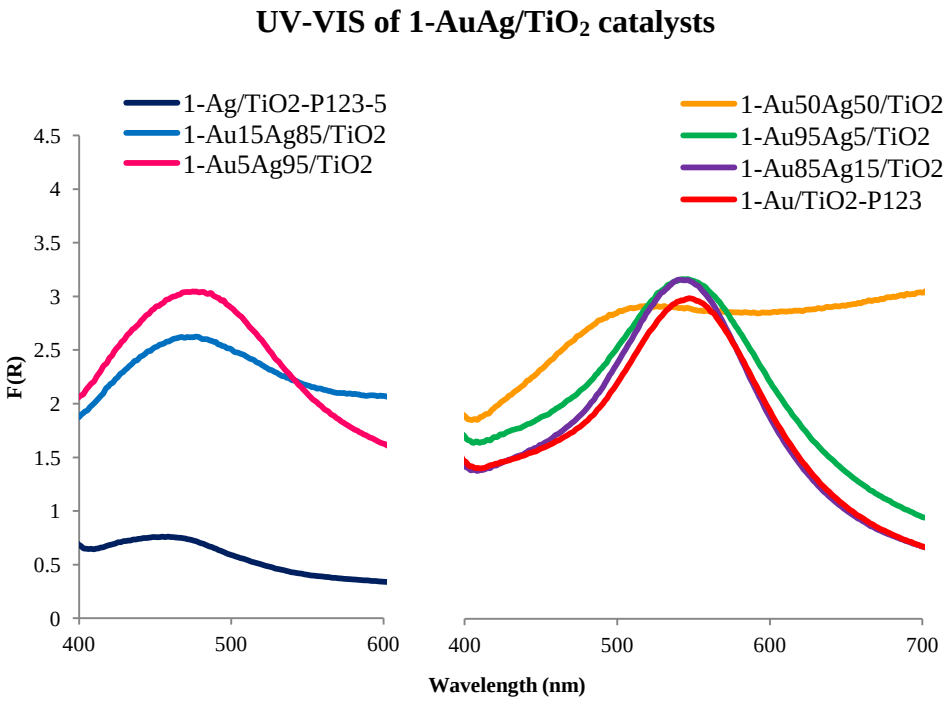

Figure 51: Solid UV-VIS spectra of 1-AuAg/TiO_2 samples. The vertical axis value is reported as a result of Kubelka-Munk function of reflectance.

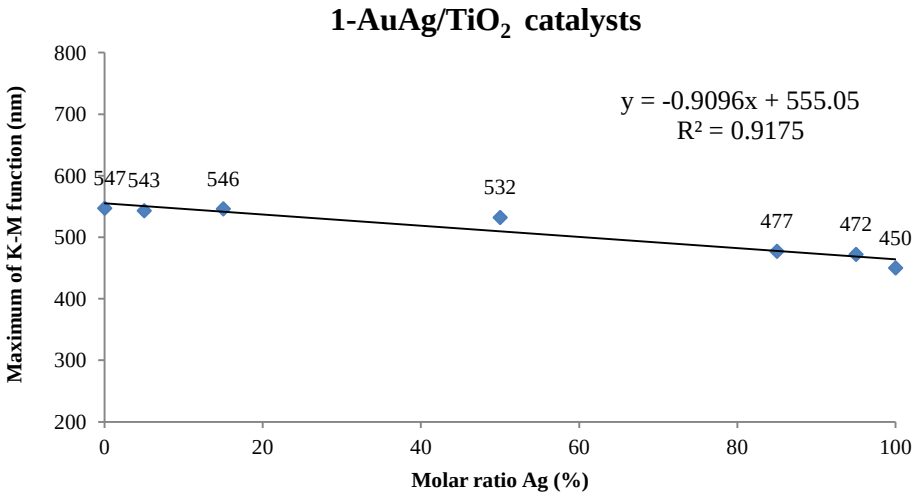

Figure 52: Linear relation between the percentage of the two metals and the maximum of the Kubelka-Munk function in UV-VIS solid spectra.

Differently from the WI bimetallic samples, with preformed nanoparticles the SPR band is clearly visible (Figure 51) and, as in the case of the above reported UV-VIS of colloidal solutions, its position is linearly related to the quantity of the metals in the alloy (Figure 52).

It can be observed that the maxima of the SPR band are red-shifted from the analyses on sols. This is explained by the interactions between the nanoparticles and titania surface and the partial sintering of the nanoparticles during the reflux step of synthesis, because it is performed at 80°C.[98] Furthermore, reflection value is different for different ratios because the reflection, and so the Kubelka-Munk function, depends on the colour of the catalysts (Figure 53).

Figure 53: Colour of the 1-AuAg/TiO_2 catalysts with different metal ratios.

Moreover, the shape of the curve in solid UV-VIS analyses changes with the ratio of the two metals. In particular *1-$Au_{50}Ag_{50}/TiO_2$* catalyst has a broader SPR band than the others. This is also explained by TEM measurement: the gaussian distribution of dimension of this catalyst is broader (Figure 54) than the *1-$Au_{85}Ag_{15}/TiO_2$* catalyst one,

used as comparison (Figure 55). Also, the mean dimension of the particles is different, centred to 9nm for the first one and ca. 4nm for the second one.

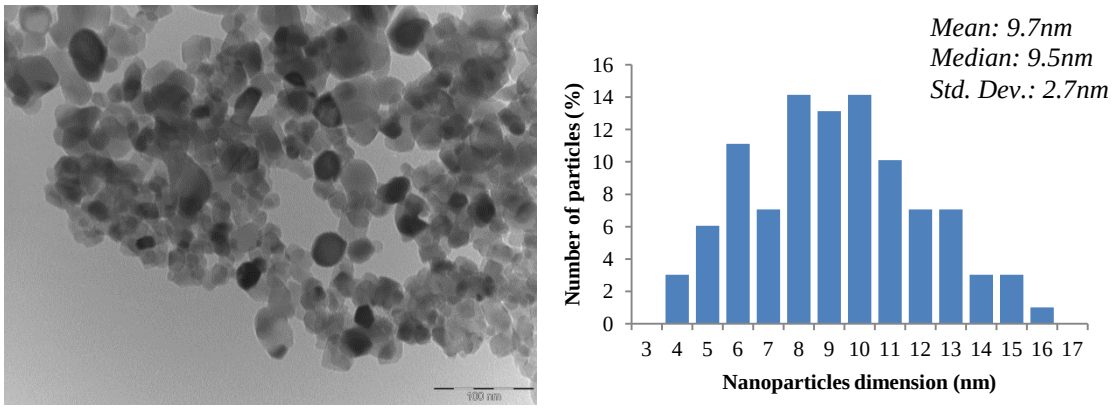

Figure 54: TEM image of 1-$Au_{50}Ag_{50}/TiO_2$ catalyst (scale 100nm) on the left and dispersion of nanoparticles dimension on the right (ca. 100 particles analyzed).

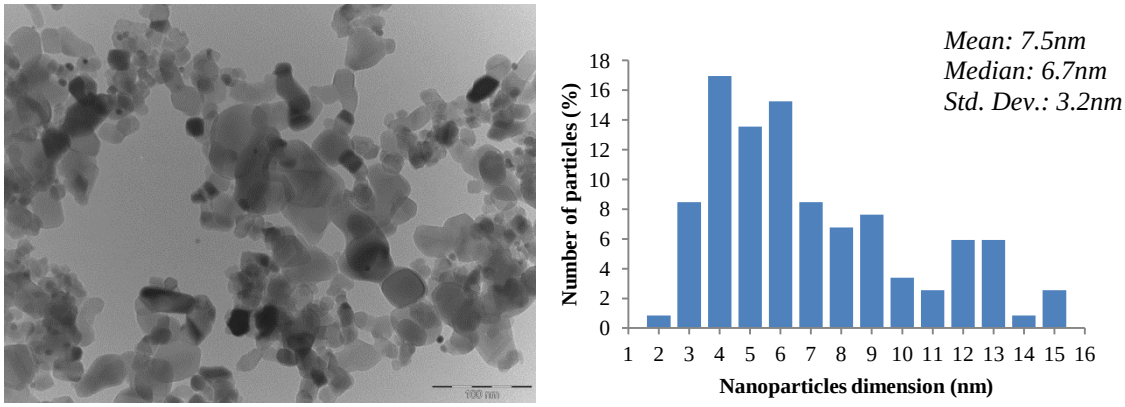

Figure 55: TEM image of 1-$Au_{85}Ag_{15}/TiO_2$ catalyst (scale 100nm) on the left and dispersion of nanoparticles dimension on the right (ca. 100 particles analyzed).

An important point that is underlined by Figure 50 and Figure 52 is that the position of the absorbance maximum of SPR changes with the ratio of the two metals. That means that the absorption value in the visible changes for different alloys. This can be a great advantage in tuning the light absorption properties of these catalysts only by changing the ratio of the two metals in an alloy in the range of wavelength desired, as was the initial purpose using silver nanoparticles. In relation to the performed reaction the conversion and yield values can also be increased in future studies exploiting a physical mixture of catalysts that absorb in different regions of the visible spectrum thus increasing the efficiency of irradiation to electron transfer to titania bandgap.

3.4.2.3. Activity of the bimetallic catalysts

As reported for the monometallic catalysts, the activity of the preformed nanoparticles sample is higher than the WI. As a confirm of this, an example of the activity of the bimetallic catalysts is reported in Figure 56 and Table 20 for the *1-$Au_{50}Ag_{50}/TiO_2$* catalyst.

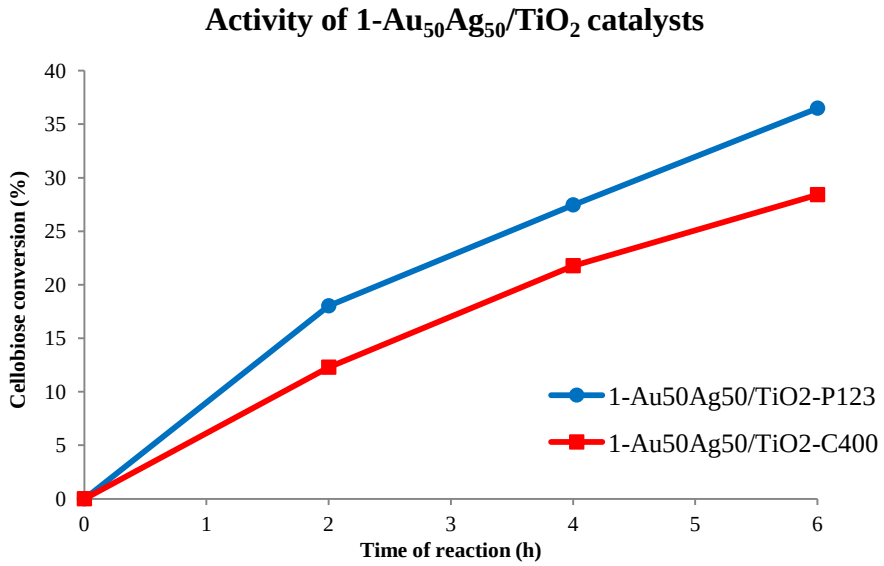

Figure 56: Catalytic performances of 1-$Au_{50}Ag_{50}/TiO_2$-C400 and 1-$Au_{50}Ag_{50}/TiO_2$ catalysts. Tests performed in the Luzchem photoreactor under visible light irradiation for 6h.

Table 20: Catalytic data of 1-$Au_{50}Ag_{50}/TiO_2$-C400 and 1-$Au_{50}Ag_{50}/TiO_2$ catalysts.

Catalyst	Time of reaction (h)	Cellobiose conversion (%)	Peak area oxidation product (7.5min)	Peak area oxidation product (7.8min)	Glucose yield (%)
1-$Au_{50}Ag_{50}/TiO_2$	2	18	17553	1444	0
1-$Au_{50}Ag_{50}/TiO_2$	4	27	25463	2504	1
1-$Au_{50}Ag_{50}/TiO_2$	6	36	29922	3568	1
1-$Au_{50}Ag_{50}/TiO_2$-C400	2	12	12442	-	0
1-$Au_{50}Ag_{50}/TiO_2$-C400	4	22	19686	1723	1
1-$Au_{50}Ag_{50}/TiO_2$-C400	6	28	23860	2214	1

The synthesized catalysts with preformed metal nanoparticles were tested in the same conditions under visible irradiation in the Luzchem photoreactor. Their cellobiose conversion during the reaction is reported in Figure 57.

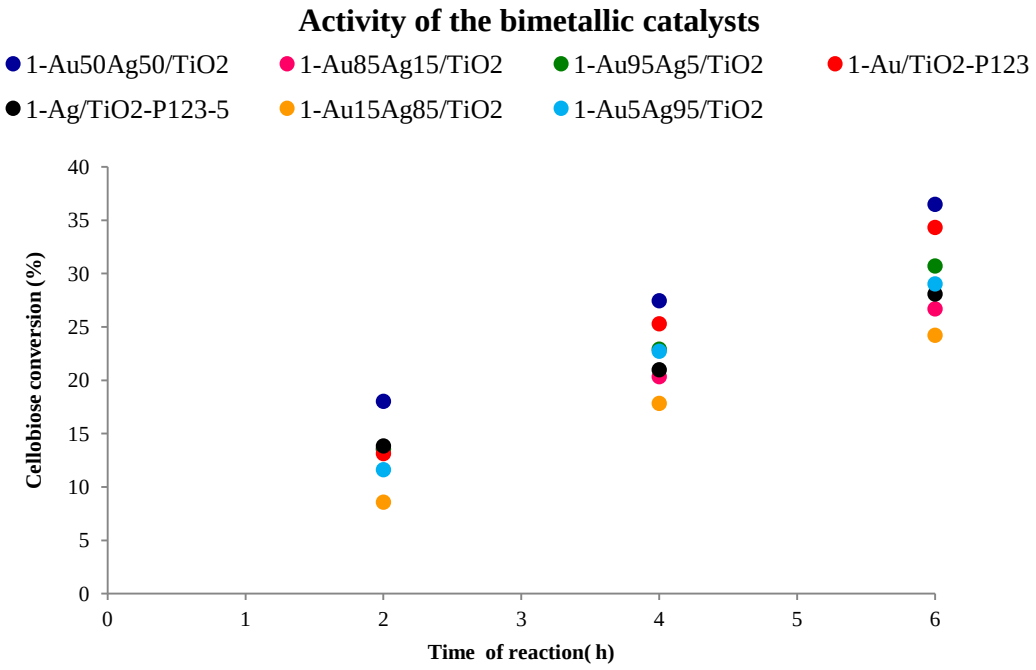

Figure 57: Catalytic performances of 1-AuAg/TiO_2 catalysts with different metal ratios. Reactions performed in the Luzchem photoreactor under visible light irradiation for 6h.

Table 21: Catalytic data for 1-AuAg/TiO_2 catalysts.

Catalyst	Time of reaction (h)	Cellobiose conversion (%)	Peak area oxidation product (7.5min)	Peak area oxidation product (7.8min)	Glucose yield (%)
1-Au/TiO_2-P123	2	13	13061	1193	0
1-Au/TiO_2-P123	4	25	21112	2263	1
1-Au/TiO_2-P123	6	34	27024	3217	1
1-$Au_{95}Ag_5$/TiO_2	2	14	12346	747	0
1-$Au_{95}Ag_5$/TiO_2	4	23	20535	1881	0
1-$Au_{95}Ag_5$/TiO_2	6	31	27309	2993	1
1-$Au_{85}Ag_{15}$/TiO_2	2	14	10532	1001	0
1-$Au_{85}Ag_{15}$/TiO_2	4	20	17086	1838	1
1-$Au_{85}Ag_{15}$/TiO_2	6	27	21090	3081	1
1-$Au_{50}Ag_{50}$/TiO_2	2	18	17553	1444	0
1-$Au_{50}Ag_{50}$/TiO_2	4	27	25463	2504	1
1-$Au_{50}Ag_{50}$/TiO_2	6	36	29922	3568	1
1-$Au_{15}Ag_{85}$/TiO_2	2	9	9956	923	0
1-$Au_{15}Ag_{85}$/TiO_2	4	18	16536	1276	1
1-$Au_{15}Ag_{85}$/TiO_2	6	24	21680	1498	1
1-Au_5Ag_{95}/TiO_2	2	12	12914	-	0
1-Au_5Ag_{95}/TiO_2	4	23	19811	1399	1
1-Au_5Ag_{95}/TiO_2	6	29	23682	2467	1
1-Ag/TiO_2-P123-5	2	14	12931	-	1
1-Ag/TiO_2-P123-5	4	21	16909	1504	1
1-Ag/TiO_2-P123-5	6	28	19784	2234	2

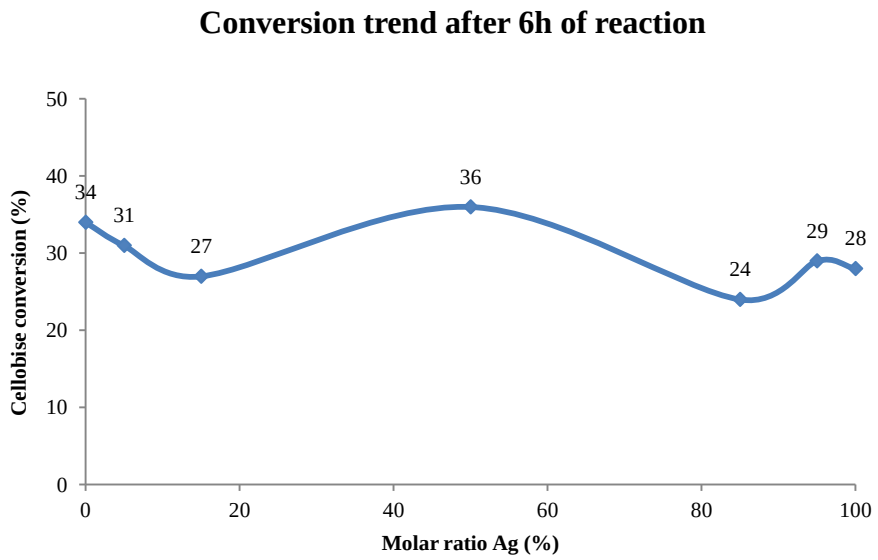

Figure 58: Conversion trend for 1-AuAg/TiO_2 catalysts after 6h of reaction under visible light irradiation in the Luzchem photoreactor.

From the data (Figure 57 and Table 21) the *1-$Au_{50}Ag_{50}/TiO_2$* catalyst appeared as the most active reaching a conversion of 36% after 6h, slightly higher than *1-Au/TiO_2-P123* catalyst which showed a conversion of 34%. The conversion trend reported in Figure 58 indicates that when a small amount of silver is added to a catalyst principally composed of gold it acts like a poison causing a decrease in the activity. The same symmetrical trend can be seen for large amounts of silver and small of gold. The *1-$Au_{50}Ag_{50}/TiO_2$* catalyst, instead, presents a small increase in the conversion value compared with the monometallic catalysts, and the other bimetallic catalysts tested in this study.

To conclude, it can be considered that within the catalysts prepared with preformed nanoparticles *1-$Au_{50}Ag_{50}/TiO_2$* is an interesting example of the advantages of alloying two metals compared with the traditional gold catalyst, but further characterisation has to be done to explain in detail the reaction mechanism and the link between the activity values and the catalyst features.

3.5. Future work

The reported data are exploring a new field of research in applying photocatalysis, and in particular metal nanoparticles, on titania for the upgrade of biomass into valuable chemicals. For that reason the study reported in this work is not complete and fully analyzed in all its aspects. In particular, due to the difficulties met in finding an unexpected oxidation reaction instead of an hydrolysis one, the characterisation of the product have to be completed to reach its quantification. Also the differences between the activity of the different phases of titania have to be elaborated and supported with surface absorption studies. Furthermore, the catalysts have to be characterised more in depth and tested on different sugar substrates to confirm their catalytic activity in selective oxidation reactions.

On the other hand, the yield obtained for the analyzed reaction can be increased applying the simultaneous use of more than one of the synthesized alloyed catalysts to cover a wider range of the visible emission by overlap of neighbouring SPR bands. This could enhance the absorption of photons thus the electrons transferred to titania.

Moreover, other “cheap” metals can be explored, such as copper, both on its own and in alloy to try to reach good activities exploiting metals not common in catalysis.

4. CONCLUSIONS

Titania and supported metal nanoparticles were explored as catalysts in the hydrolysis of cellobiose under visible and UV irradiation. Surprisingly the most important product of reaction was not found to be glucose but it was supposed to be the result of a selective oxidation process. This hypothesis is supported by the similar oxidation of glucose to gluconic acid observed in our reaction and reported in the literature,[20] as cellobiose is build up of two glucose molecules. The main product supposed is cellobionic acid, derived by the oxidation of the equilibrium reducing group of cellobiose. Further transformation can than occur to this product explaining the presence of the second peak. Although the complete characterisation of the main product was not possible, due to similar molecular weights of the proposed chemicals and their not commercial availability, mass spectroscopy analyses (ESI^+) supported the presence in the reaction mixture of the supposed products.

Photocatalytic experiments were first of all performed with titania analyzing its different crystalline structures to find the most active form and subsequently with immobilized nanoparticles. The catalytic tests were performed in a Luzchem photoreactor equipped with 14 fluorescent visible lamps.

Titania is a well known active catalyst under UV irradiation,[60] but its application on biomass upgrading is not studied in depth. In particular, for the performed reaction, the rutile phase was found to be more active than anatase both as cellobiose conversion and in the production of oxidation products. That is because the reported problems in characterisation of the oxidation products didn't allow its quantification but a comparison between the catalysts was possible by comparing the area of the peaks in the HPLC chromatograms. On the other hand anatase had a higher yield than rutile in the hydrolysis reaction as reported in (Figure 59).

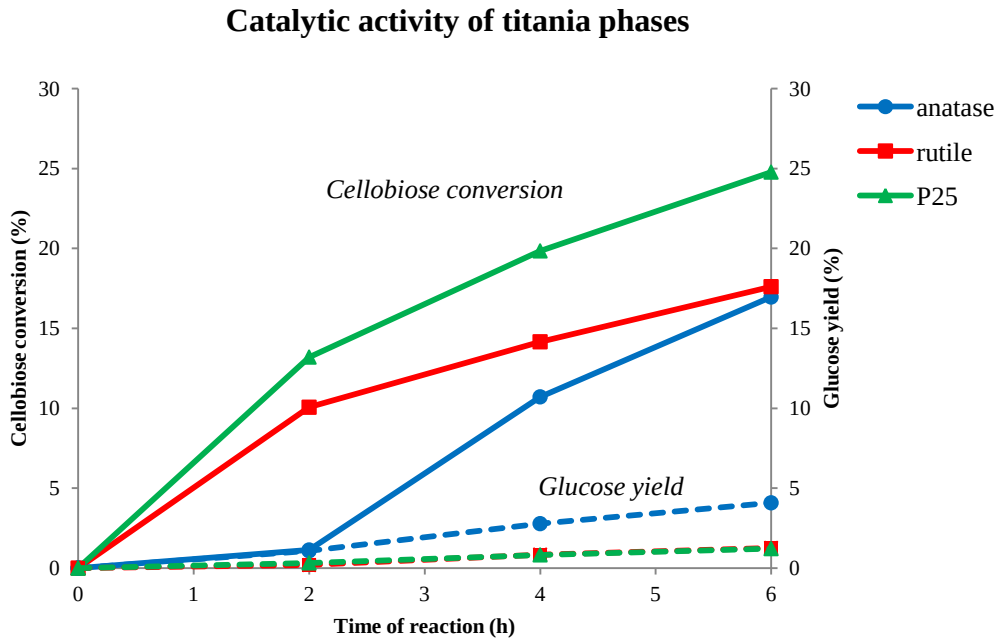

Figure 59: Catalytic performances of rutile and anatase under visible irradiation.

In comparison titania Degussa P25, about 80% anatase and 20% rutile, possessed the highest cellobiose conversion between all the other phases. For this reason, and for the fact that it is considered a standard material in photocatalysis,[86] titania P25 was chosen as a support for the synthesized nanoparticles.

The effective enhancement of activity of titania in the visible range by doping with metal nanoparticles was verified using a 300W Xe lamp, because it is a more powerful system than the Luzchem photoreactor and it permits the use of filters. The activity of pure titania P25 was compared to *1-Au/TiO_2-P123* selected as a reference between all the synthesized catalysts.

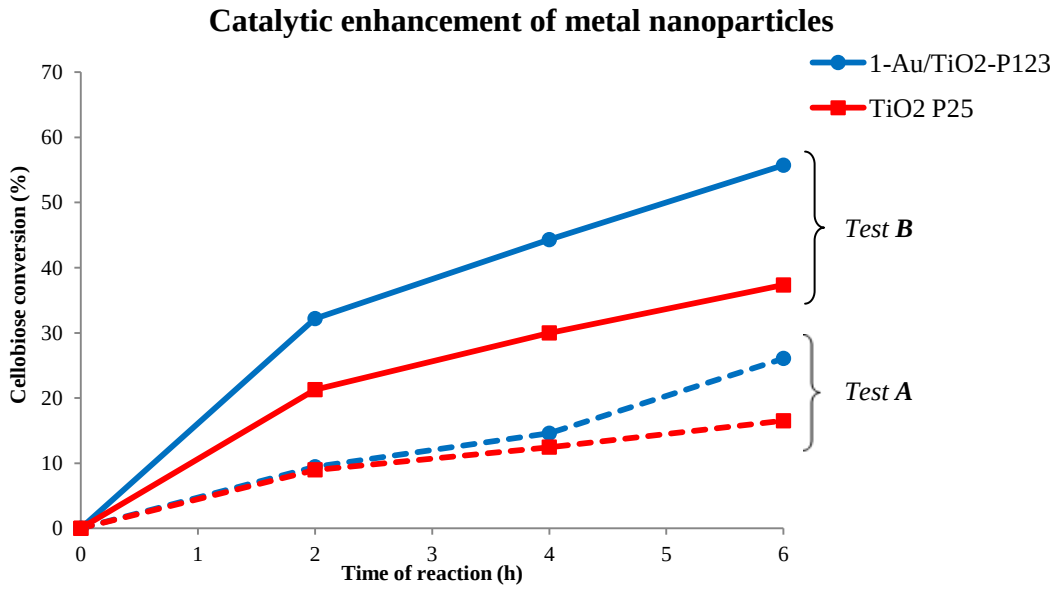

Figure 60: Catalytic performances of 1-Au/TiO2-P123 catalyst compared to titania P25. Tests performed with Oriel 300W Xe lamp for 6h. Test A with hot mirror and cut-off filter (420nm), Test B with only hot mirror filter.

The first test (Test ***A*** Figure 60) was performed with a cut-off filter at 420nm, that means removing the UV part of irradiation of the system to avoid in part the direct excitation of titania. After 6h of reaction the catalyst presented an enhancement of conversion of 10% compared to titania P25. The second test (Test ***B***) was instead done without cut-off filter thus irradiating the reaction with a higher power than the photoreactor. In this case an increase in conversion of the 20% was obtained confirming the trend reported in Test ***A***.

Furthermore the same distribution of products, detected by HPLC, was found for all the experiments performed with pure titania and titania-supported nanoparticles. This suggests that titania is the active part of the system towards the oxidation and dehydratation of cellobiose. A possible explanation of the mechanism, in accordance with the obtained data, can be found in the literature.[40, 60, 86] In these papers it is indicated that metal nanoparticles are not catalysts themselves but operate as electron acceptors in the visible range for the semiconductor bandgap. Moreover, this excess of charge on titania is donated to the water and to the oxygen adsorbed onto the titania surface (O_2, H_20) generating highly reactive radicals that oxidize the reagents in solution. Therefore, it could be titania that acts as a catalyst towards the oxidation of cellobiose and the metal nanoparticles behave like antennas that transfer the electrons to its conduction band.

Several catalysts were synthesized with gold and silver nanoparticles on titania P25 and they were tested in the Luzchem photoreactor under visible irradiation for 6h. The metal loading onto titania was kept to 1% w/w because it was found to be the best ratio for catalytic activity. The metal nanoparticles were synthesized by impregnation of the metal salt directly on the support and with immobilisation of sols. The first method allowed a quick screening of the metals and features of the catalyst, the second one was used for a better characterisation of the nanoparticles before and after immobilisation.

Moreover two pathways were followed to synthesize monometallic gold sols: the first using poly(vinyl alcohol) as a stabilizing agent (PVA)[12] and the other one with a triblock copolymer (P123).[52] Different results in activity were found for the catalysts and higher values were presented for the P123 synthesis. The two synthesized catalysts were observed to have different particle size dimension with smaller particles for *1-Au/TiO_2-PVA* catalyst, as indicated by TEM characterisation. Also the amount and the removal of stabilizing agent was examined, with the aim of increasing the stability of silver sols, but a bigger quantity of ligand was found to be not positive for the activity of the catalyst.

Within monometallic gold and silver catalysts the samples prepared by immobilization of sols were more active than the WI method, as reported in Figure 61 and Figure 62, in fact they achieved a higher conversion and oxidation product yield. Furthermore the best values were achieved by gold catalysts with both the methods, in particular for *1-Au/TiO_2-P123* catalyst.

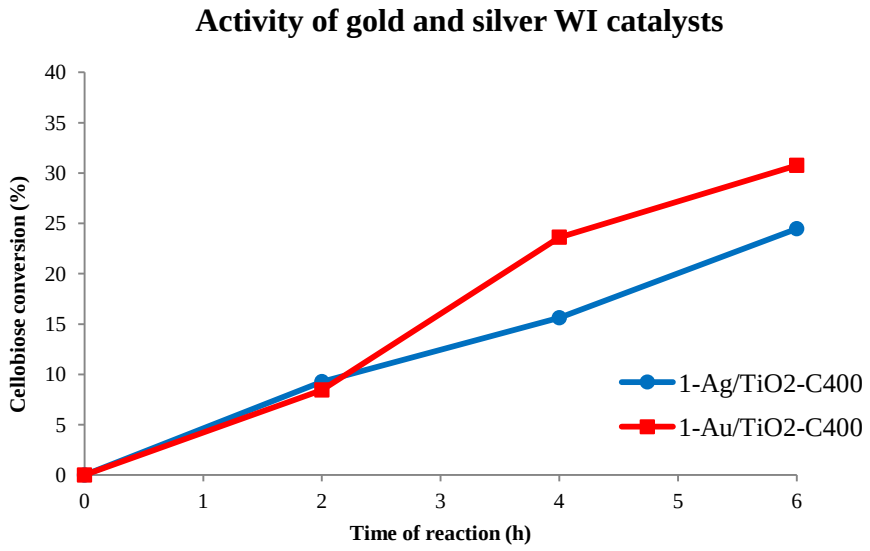

Figure 61: Catalytic performances of 1-Au/TiO_2-C400 and 1-Ag/TiO_2-C400 catalysts.

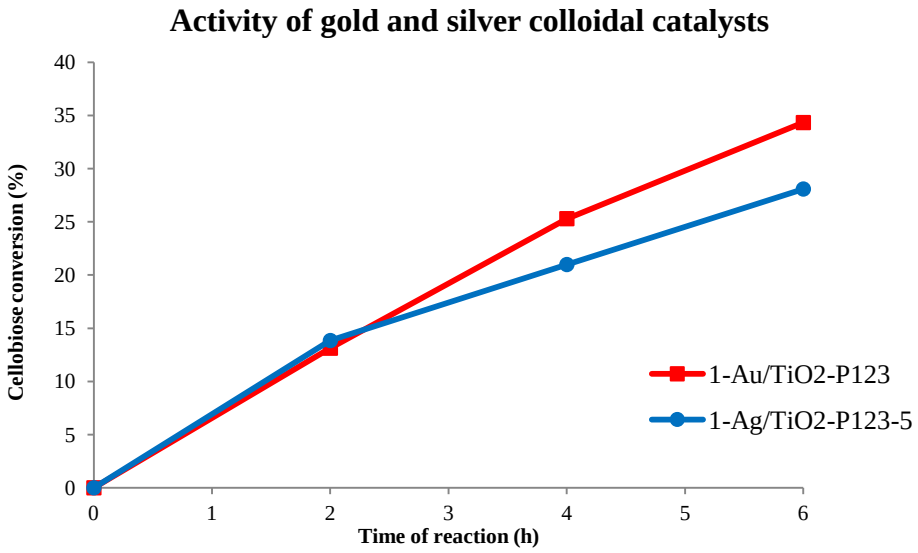

Figure 62: Catalytic performances of 1-Ag/TiO_2-P123-5 and 1-Au/TiO_2-P123 catalysts.

Bimetallic alloys were also tested to try to combine the good catalytic activity of gold with the tunable properties of silver SPR band. Different ratios were examined with a total metal loading of 1% w/w on titania and synthesized by wetness impregnation and sol methods. The activity ratio between the two pathways is reported as an example in Figure 63, indicating higher values for the preformed nanoparticles catalyst, as reported for the monometallic samples.

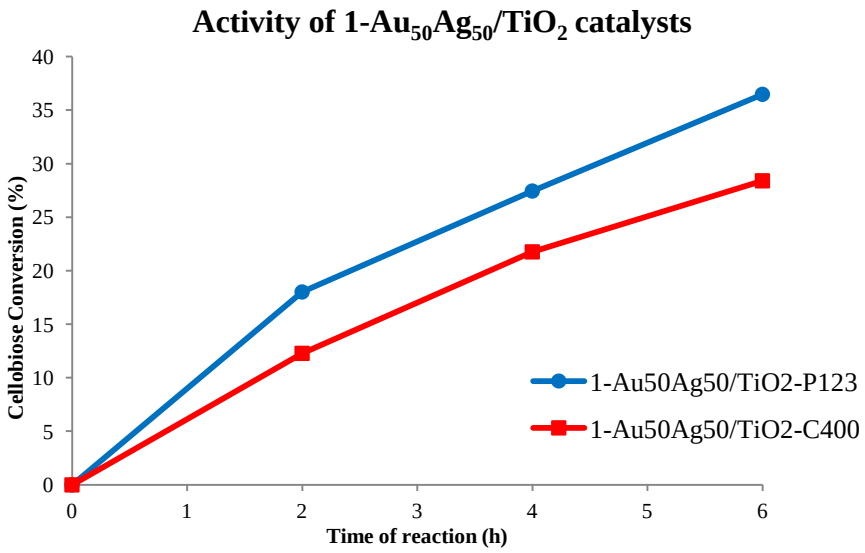

Figure 63: Catalytic performances of 1-$Au_{50}Ag_{50}$/TiO_2-C400 and 1-$Au_{50}Ag_{50}$/TiO_2 catalysts.

The synthesized sols were analyzed with UV-VIS spectrophotometry to check the effective alloying of the two metal before and after immobilisation. Moreover the position of the maxima of the SPR band was found to be in a linear relation with the

percentage of the two metals in the alloy. In Figure 64 is reported the catalytic activity trend of the different alloys in the performed reaction after 6h.

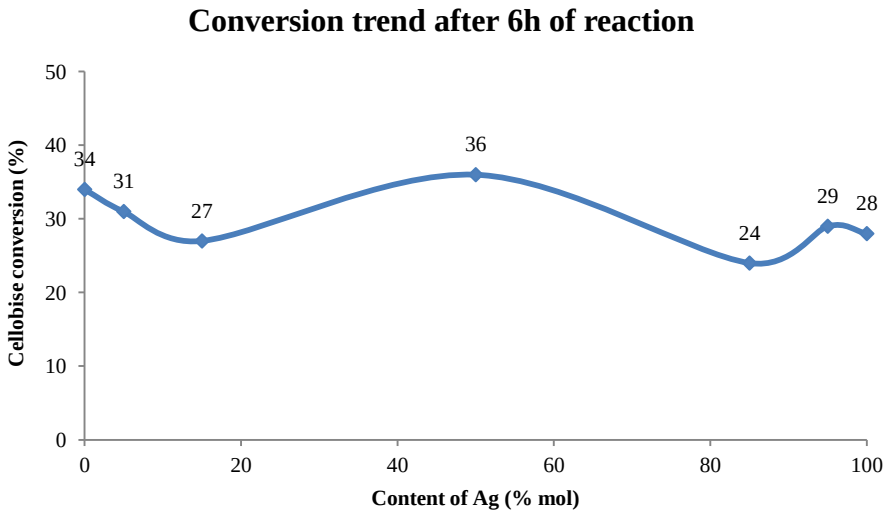

Figure 64: Conversion trend for 1-AuAg/TiO_2 catalysts after 6h of reaction.

The conversion suggests that when a small amount of silver is added to a catalyst principally composed of gold it acts like a poison causing a decrease in the activity. The same symmetrical trend can be seen for large amounts of silver and small of gold both for conversion values and for the production of the oxidation product. On the other hand the *1-*$Au_{50}Ag_{50}/TiO_2$ catalyst slightly increases the conversion value compared with the two monometallic catalysts.

In conclusion, metal nanoparticles supported on titania are promising catalysts for the reaction of selective oxidation of cellobiose, but do not have good yields in the hydrolysis reaction. Nonetheless, further characterisation is necessary to define and quantify the products of reaction, to better characterise the synthesized catalysts and to explain the mechanism. Furthermore, alloying seems a good way to enhance the activity of the catalysts and to decrease its cost with the use of cheaper metals than gold, in particular when preformed nanoparticles are supported on titania.

5. APPENDIX

5.1. Mass spectroscopy and products analysis

There are reported the hypothesis on the possible products of reaction. The second oxidation is possible on different alcohols of the same type (primary and secondary) on the molecule, but it is reported only an example of product because they present the same molecular weight. Subsequently are reported also the possible fragmentation patterns of the reagents and the ESI^+ spectra of reaction mixture.

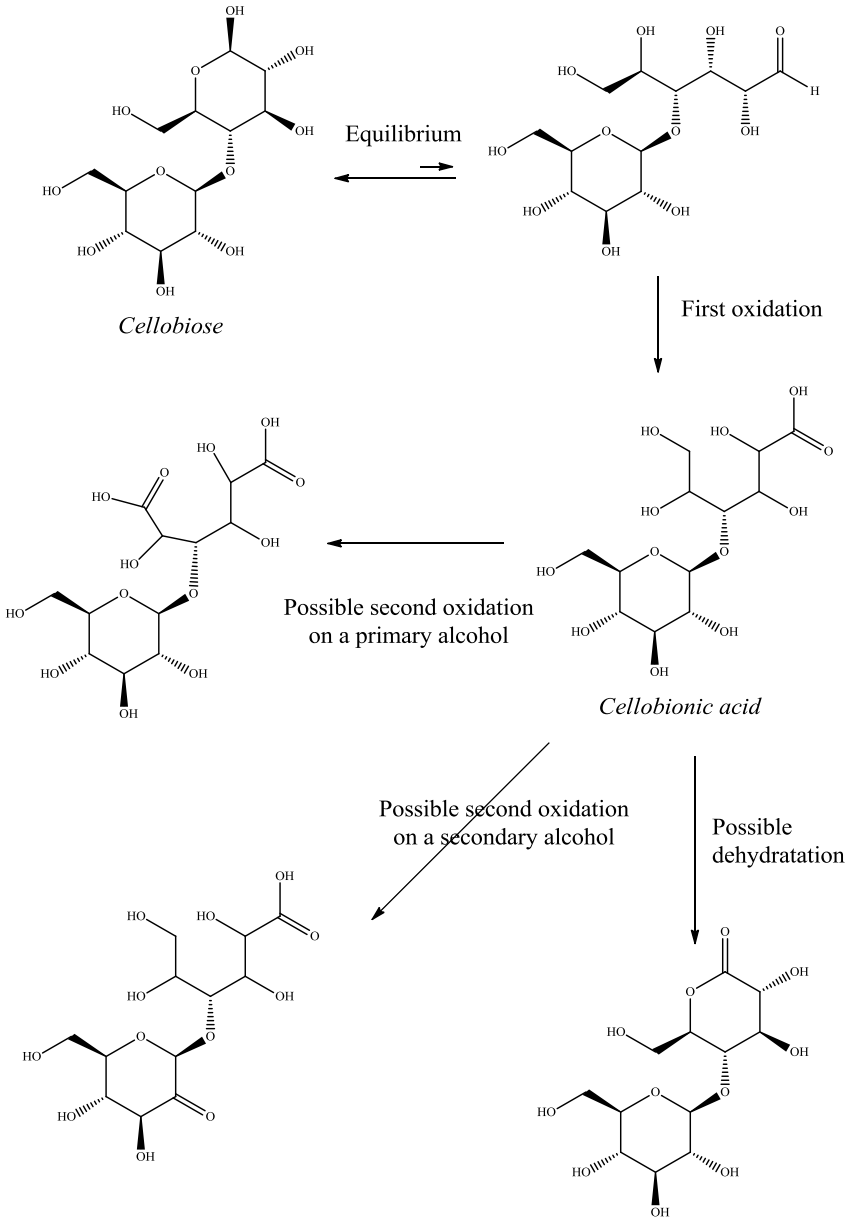

Scheme 4: Hypothesis on the second oxidation products of the performed reaction.

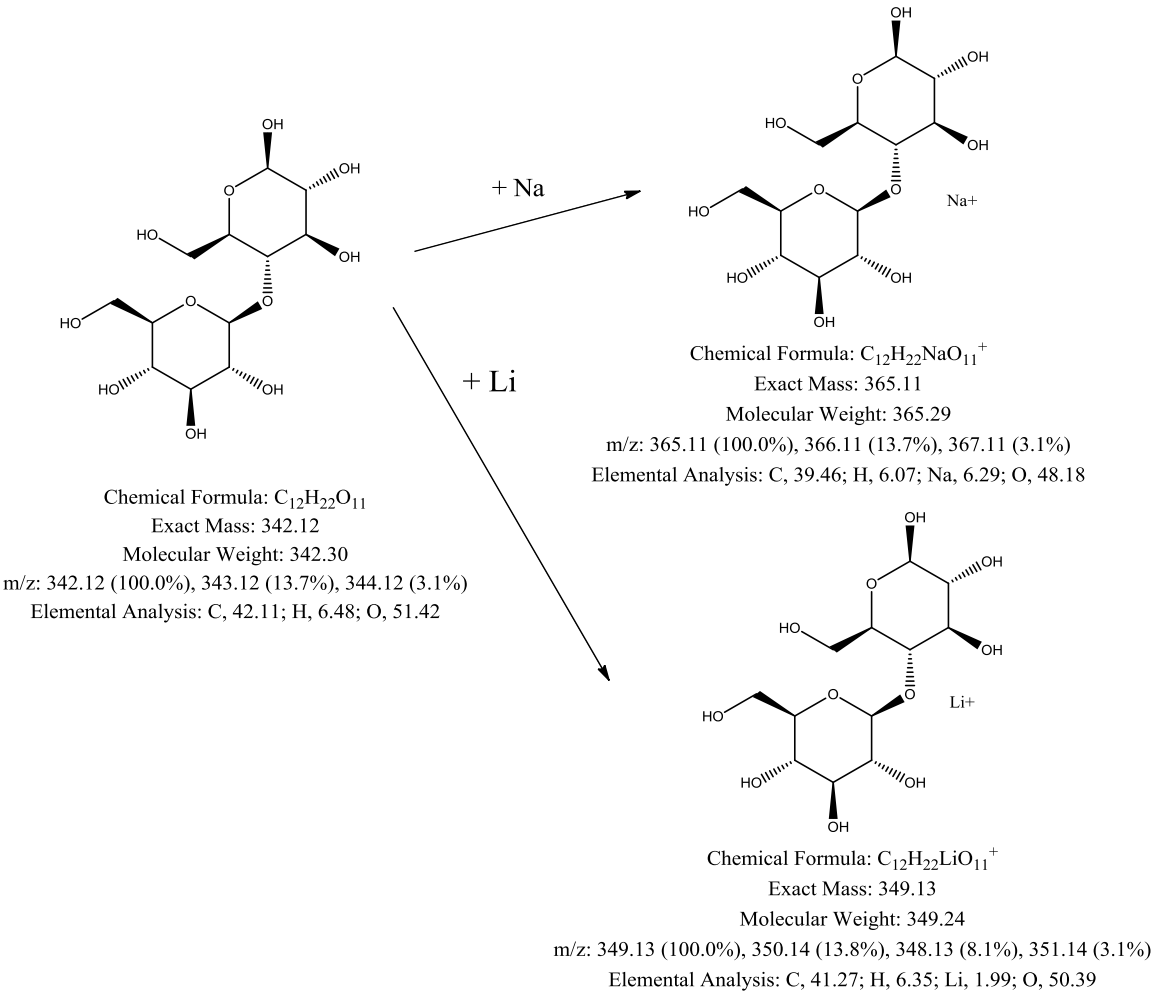

Scheme 5: Possible fragmentation pattern of cellobiose.

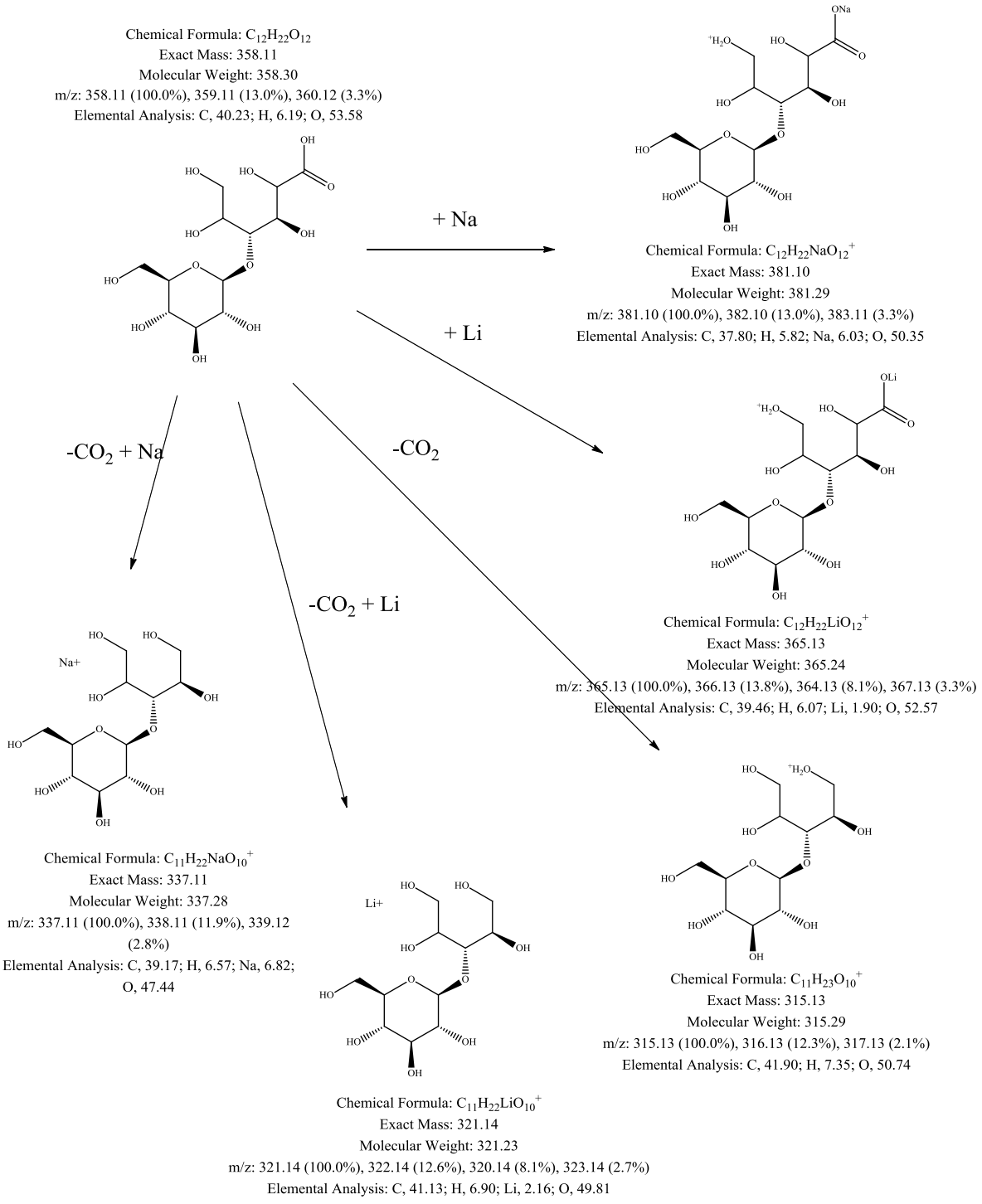

Scheme 6: Possible fragmentation pattern of the cellobionic acid.

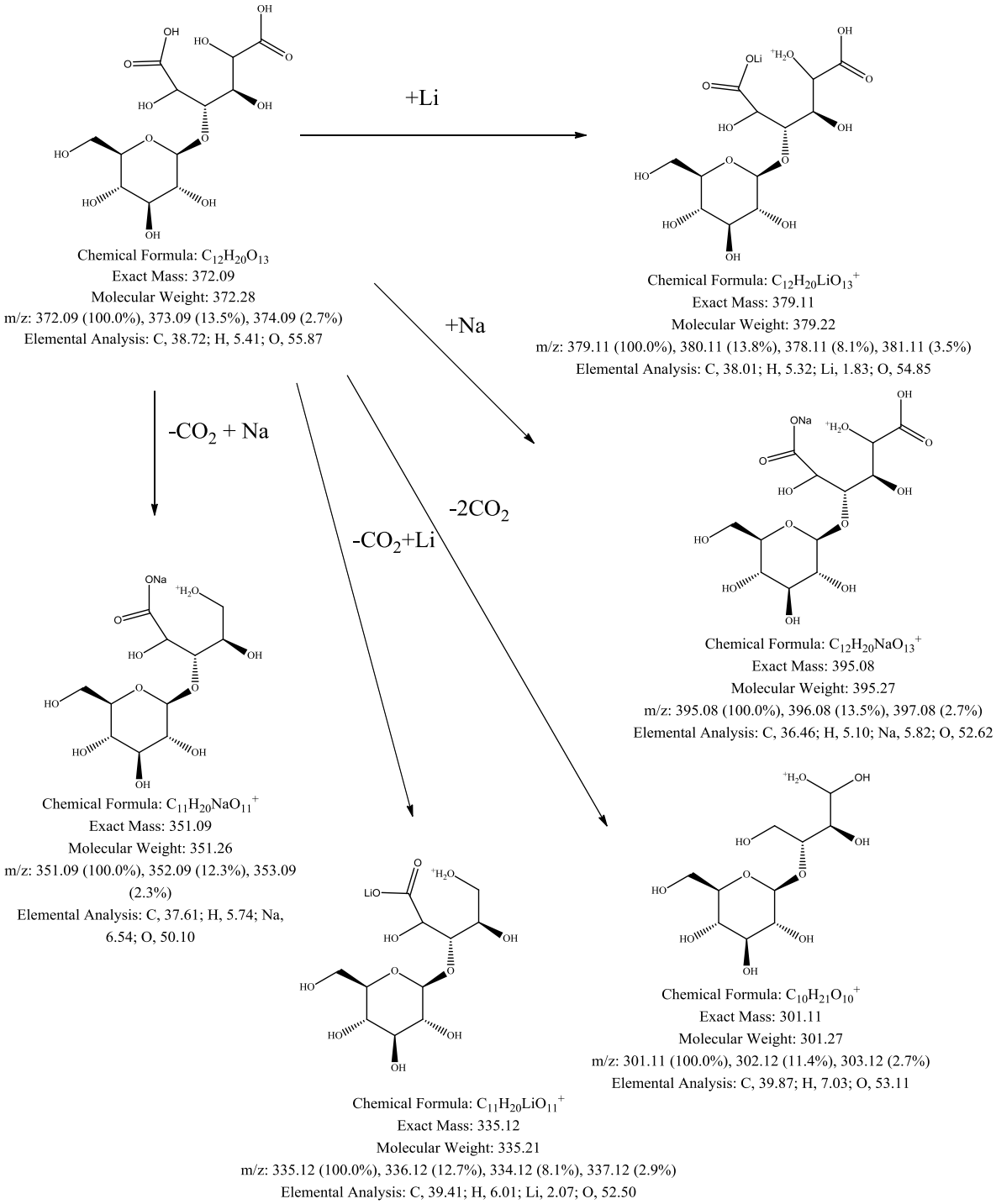

Scheme 7: Possible fragmentation pattern of the secondary oxidation product from cellobionic acid. It is supposed a reaction on a primary alcohol of the molecule.

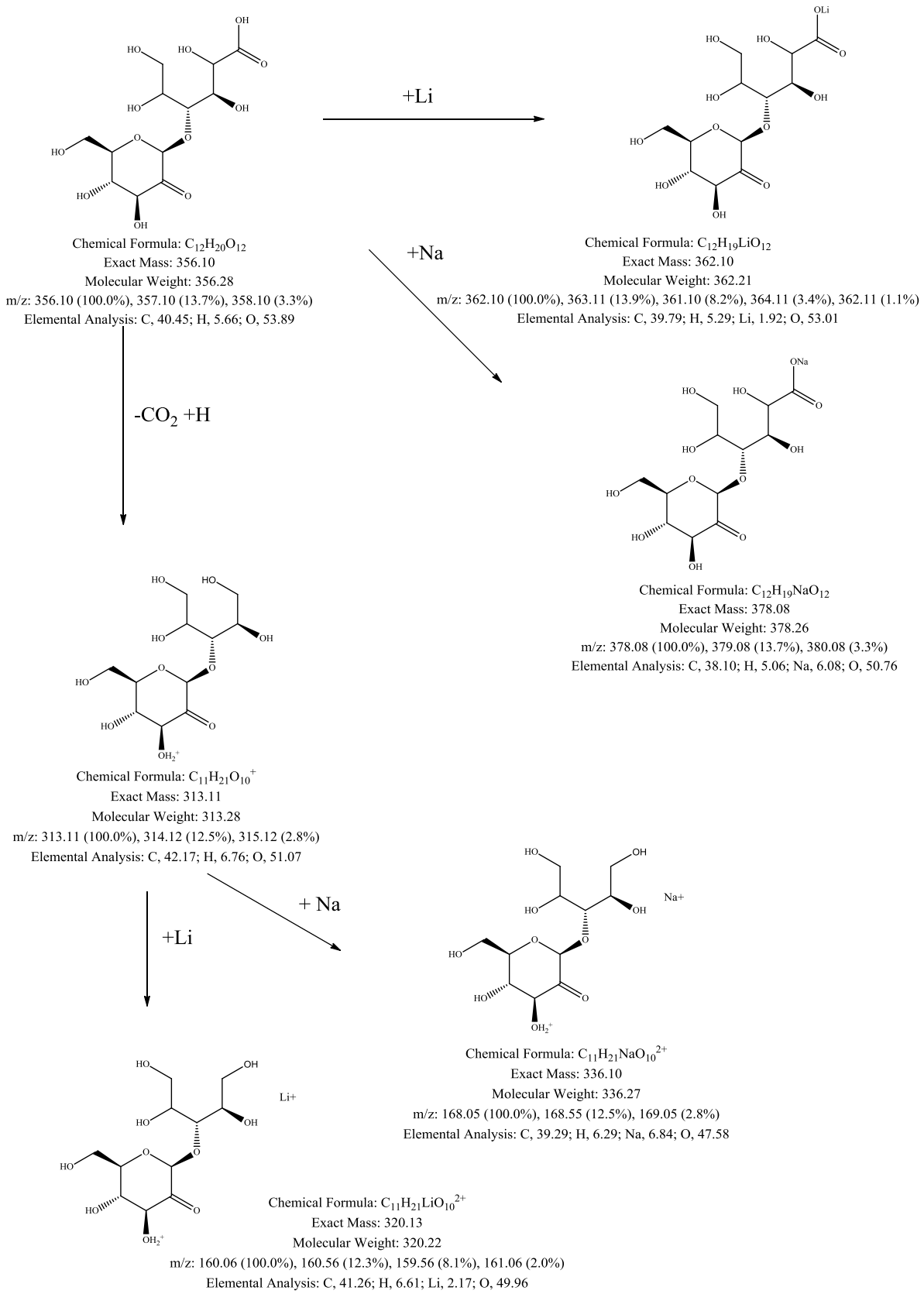

Chemical Formula: $C_{12}H_{20}O_{12}$
Exact Mass: 356.10
Molecular Weight: 356.28
m/z: 356.10 (100.0%), 357.10 (13.7%), 358.10 (3.3%)
Elemental Analysis: C, 40.45; H, 5.66; O, 53.89

Chemical Formula: $C_{12}H_{19}LiO_{12}$
Exact Mass: 362.10
Molecular Weight: 362.21
m/z: 362.10 (100.0%), 363.11 (13.9%), 361.10 (8.2%), 364.11 (3.4%), 362.11 (1.1%)
Elemental Analysis: C, 39.79; H, 5.29; Li, 1.92; O, 53.01

Chemical Formula: $C_{12}H_{19}NaO_{12}$
Exact Mass: 378.08
Molecular Weight: 378.26
m/z: 378.08 (100.0%), 379.08 (13.7%), 380.08 (3.3%)
Elemental Analysis: C, 38.10; H, 5.06; Na, 6.08; O, 50.76

Chemical Formula: $C_{11}H_{21}O_{10}^{+}$
Exact Mass: 313.11
Molecular Weight: 313.28
m/z: 313.11 (100.0%), 314.12 (12.5%), 315.12 (2.8%)
Elemental Analysis: C, 42.17; H, 6.76; O, 51.07

Chemical Formula: $C_{11}H_{21}NaO_{10}^{2+}$
Exact Mass: 336.10
Molecular Weight: 336.27
m/z: 168.05 (100.0%), 168.55 (12.5%), 169.05 (2.8%)
Elemental Analysis: C, 39.29; H, 6.29; Na, 6.84; O, 47.58

Chemical Formula: $C_{11}H_{21}LiO_{10}^{2+}$
Exact Mass: 320.13
Molecular Weight: 320.22
m/z: 160.06 (100.0%), 160.56 (12.3%), 159.56 (8.1%), 161.06 (2.0%)
Elemental Analysis: C, 41.26; H, 6.61; Li, 2.17; O, 49.96

Scheme 8: Possible fragmentation pattern of the secondary oxidation product from cellobionic acid. It is supposed a reaction on a secondary alcohol of the molecule.

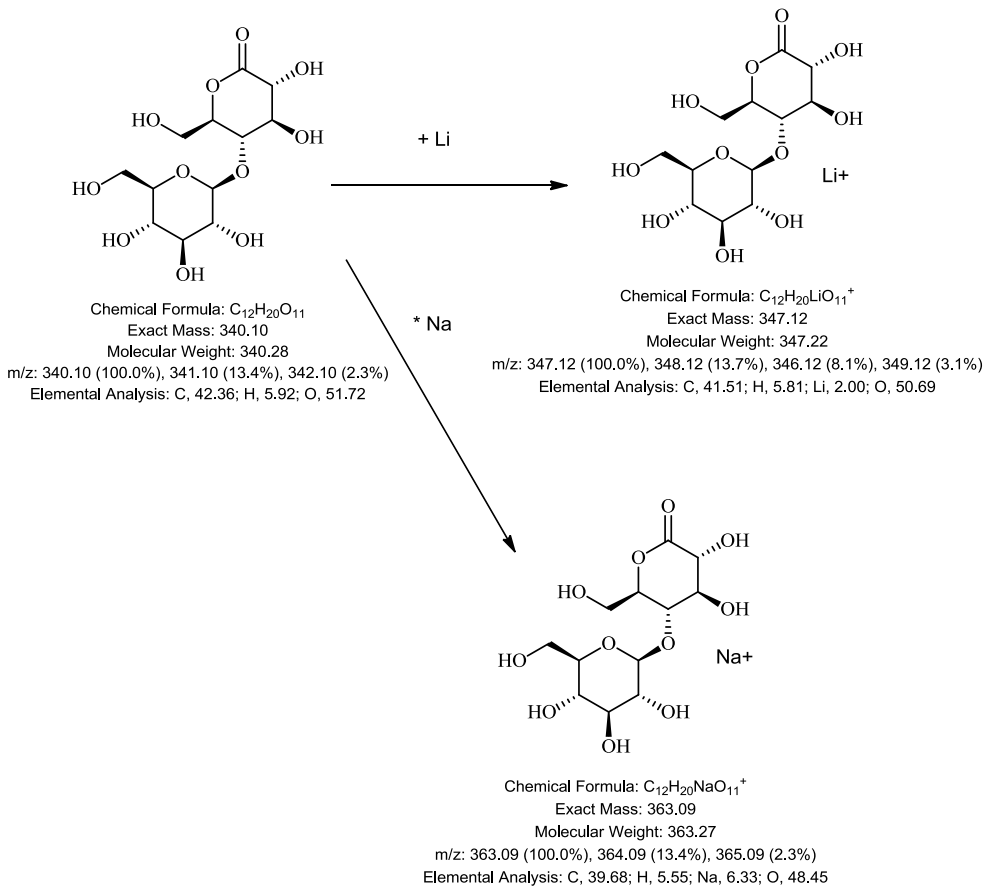

Scheme 9: Possible fragmentation pattern of the cellobionolactone, deriving from dehydratation of cellobionic acid.

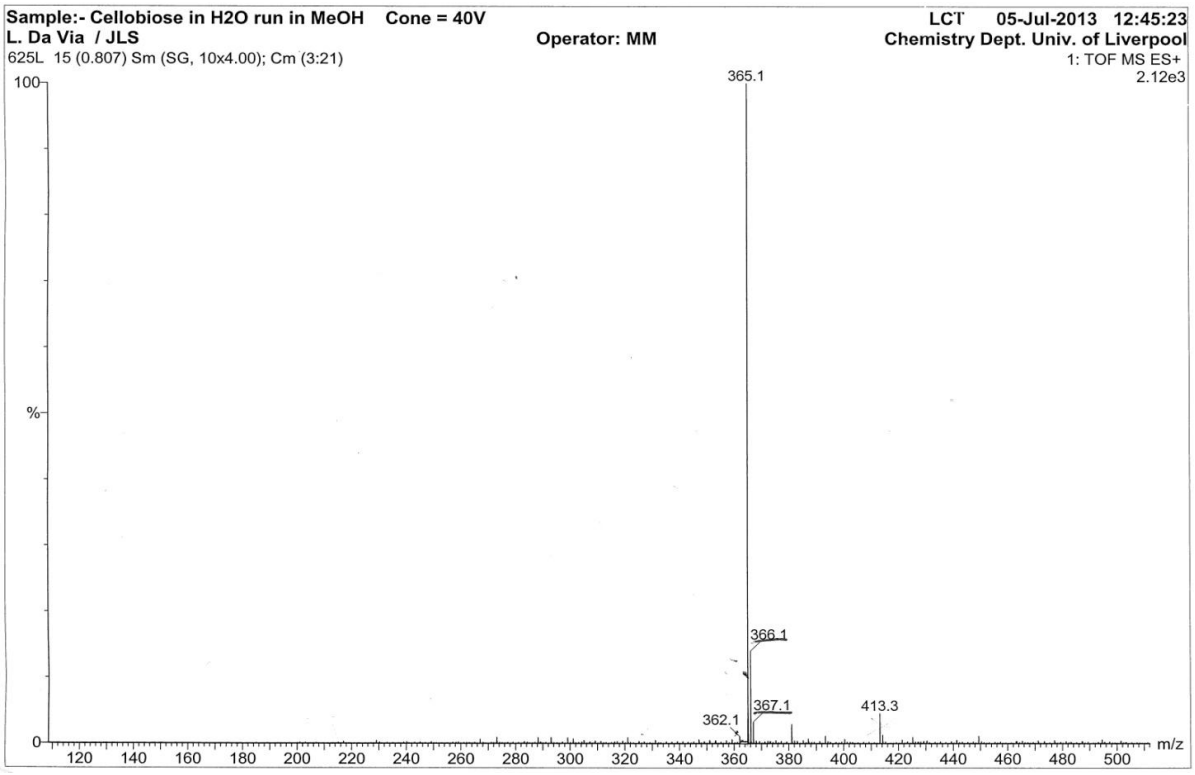

Figure 65: ESI+ spectrum of cellobiose standard 2.8mM.

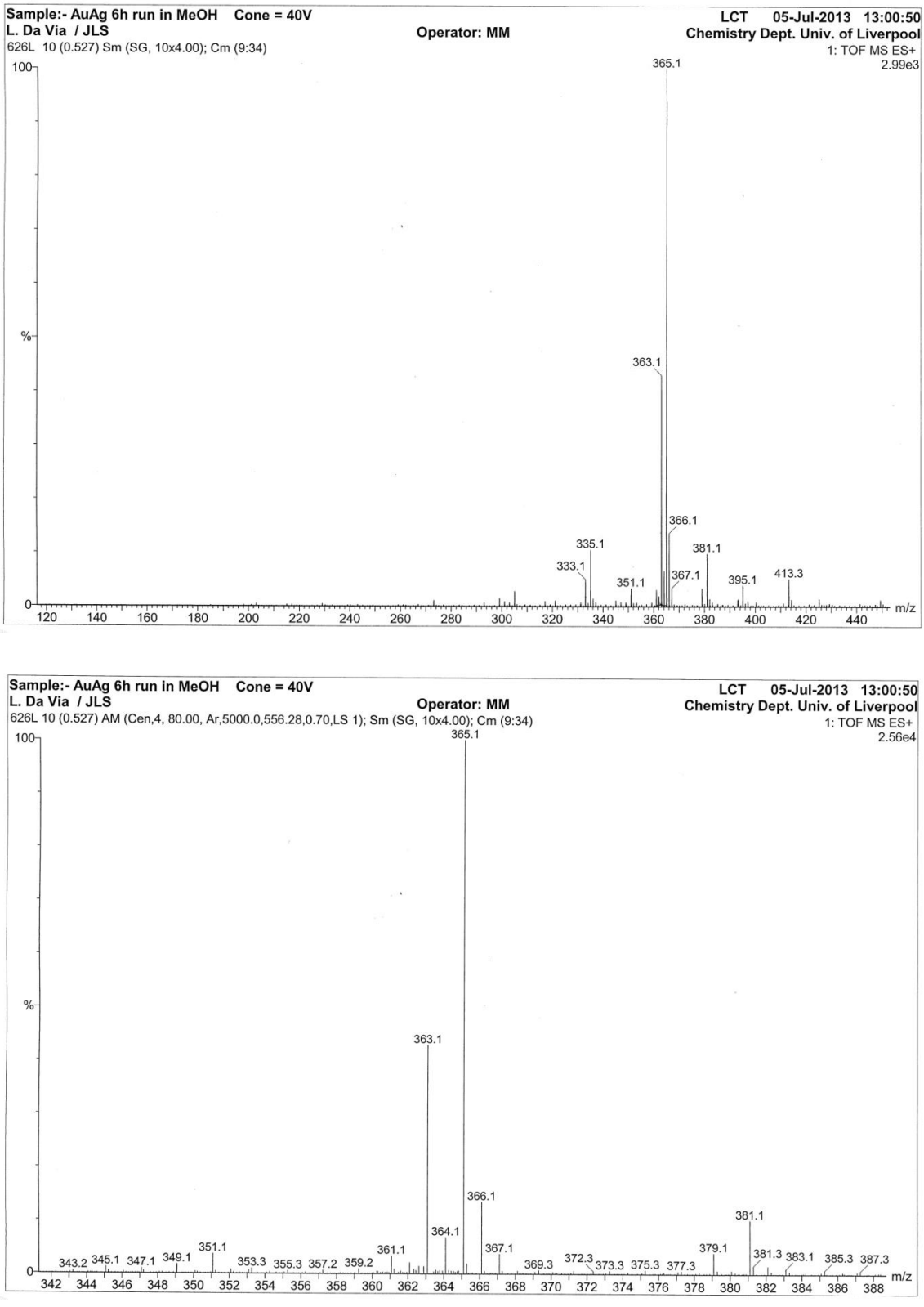

Figure 66: ESI+ spectra of reaction performed with 1-$Au_{50}Ag_{50}/TiO_2$ catalyst in the Luzchem photoreactor for 6h.

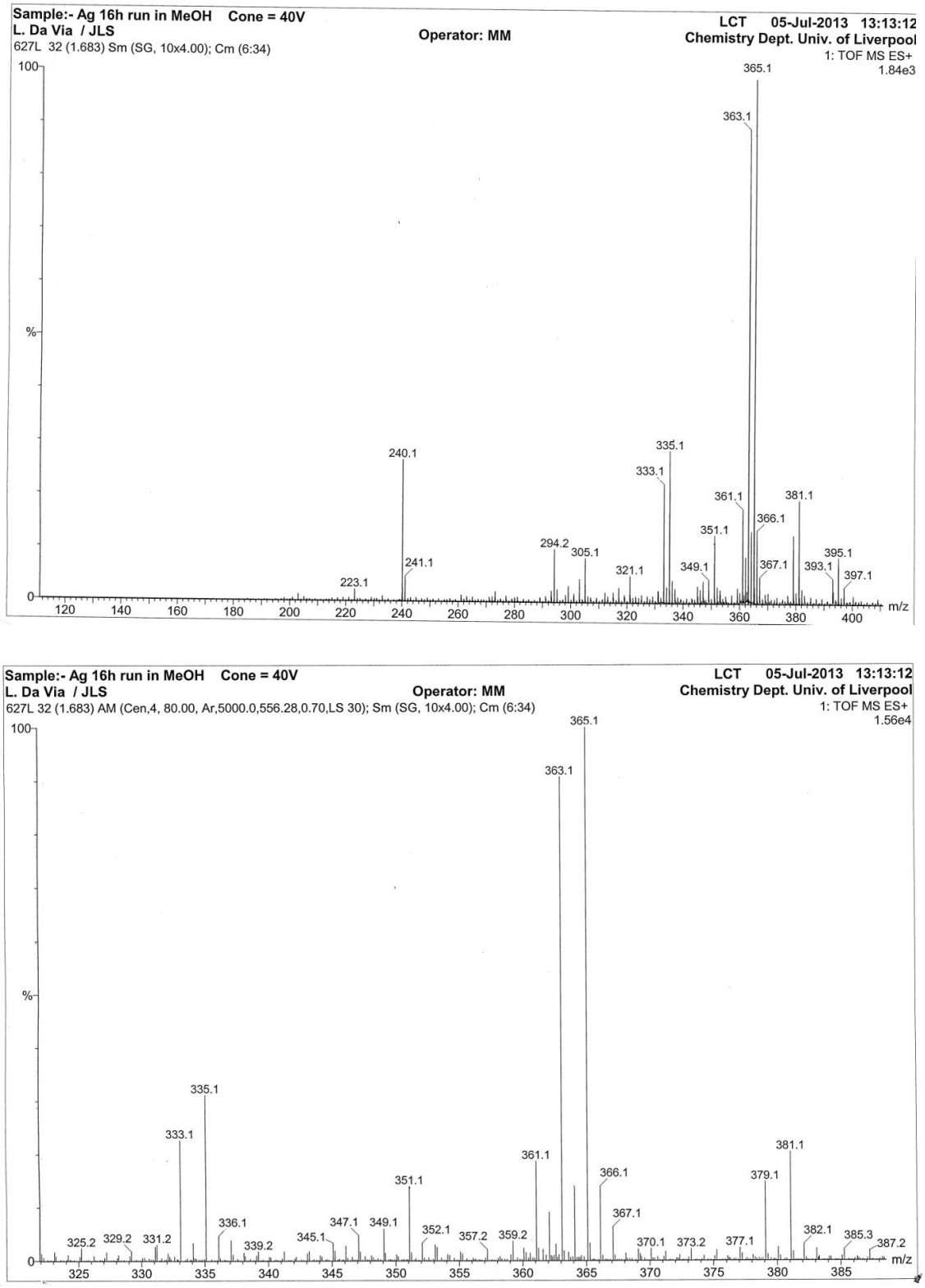

Figure 67: ESI+ spectra of reaction performed with 1-Ag/TiO_2-P123-5 catalyst in the Luzchem photoreactor for 16h.

5.2. Identification of gluconic acid

Here is reported the peak of production of gluconic acid detected by VWD HPLC detector. Before 6h of reaction the peak is not detectable from instrumental noise.

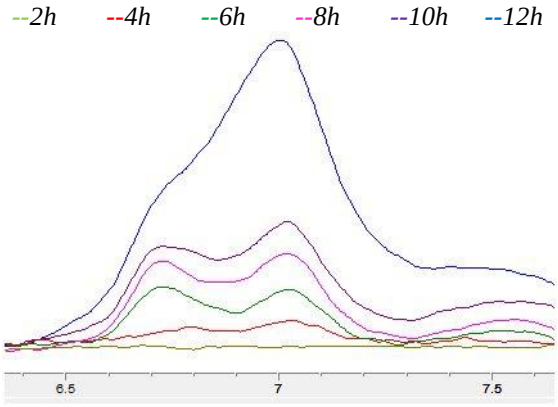

Figure 68: HPLC VWD chromatogram of anatase tested in the Luzchem photoreactor under visible irradiation for 12h.

5.3. Water hydrolysis and dark reactions

Table 22: Cellobiose conversion and products yield for some reactions performed in thermal conditions at 70°C (section 2.3.5).

Catalyst	Time of reaction (h)	Cellobiose conversion (%)	Peak area at 7.5min	Peak area at 7.8min	Glucose yield (%)
1-Ag/TiO_2-C200	2	-	-	-	-
1-Ag/TiO_2-C200	4	-	-	-	-
1-Ag/TiO_2-C200	6	-	-	-	-
1-Au/TiO_2-P123	2	5	-	-	-
1-Au/TiO_2-P123	4	3	-	-	-
1-Au/TiO_2-P123	6	4	-	-	-
1-$Au_{85}Ag_{15}/TiO_2$	2	5	-	-	-
1-$Au_{85}Ag_{15}/TiO_2$	4	5	-	-	-
1-$Au_{85}Ag_{15}/TiO_2$	6	6	-	-	-
1-$Au_{50}Ag_{50}/TiO_2$	2	-	-	-	-
1-$Au_{50}Ag_{50}/TiO_2$	4	-	-	-	-
1-$Au_{50}Ag_{50}/TiO_2$	6	-	-	-	-
1-Ag/TiO_2-P123-5	2	-	-	-	-
1-Ag/TiO_2-P123-5	4	-	-	-	-
1-Ag/TiO_2-P123-5	6	-	-	-	-

Table 23: Cellobiose conversion and products yield for some reactions performed in dark conditions in Luzchem photoreactor for 13h. (section 2.3.4)

Catalyst	Cellobiose conversion (%)	Peak area at 7.5min	Peak area at 7.8min	Glucose yield (%)
TiO_2	0	-	-	-
1-Au/TiO_2-C200	2	-	-	-
1-Ag/TiO_2-C200	5	-	-	-
5-Ag/TiO2-C200	4	-	-	-
1-Ag/TiO_2-C400	5	-	-	-
5-Ag/TiO2-C400	3	-	-	-
1-Au/TiO_2-PVA	4	-	-	-
1-Ag/TiO_2-P123-5	1	-	-	-

ACKNOWLEDGEMENTS

I would like to thank first Tony, for his availability to receive me in his group and for the advices he has given to me during my period in Liverpool. Many thanks also to Luigi for every day help and patience in the lab, and to Maria for her satisfying explanations and experience. Thanks also to Stefania, for her help and availability at any time.

A great acknowledge goes to my family, to Simone and my friends for their support and help during the drafts of my work.

6. BIBLIOGRAPHY

6.1. Literature articles

1 V. Amendola, and M. Meneghetti, 'Size Evaluation of Gold Nanoparticles by Uv-Vis Spectroscopy', Journal of Physical Chemistry C, 113 (2009), 4277-85.

2 A. Amtout, and R. Leonelli, 'Optical-Properties of Rutile near Its Fundamental-Band Gap', Physical Review B, 51 (1995), 6842-51.

3 K. An, S. Alayoglu, T. Ewers, and G. A. Somorjai, 'Colloid Chemistry of Nanocatalysts: A Molecular View', Journal of Colloid and Interface Science, 373 (2012), 1-13.

4 Linda Aschwanden, Tamas Mallat, Marek Maciejewski, Frank Krumeich, and Alfons Baiker, 'Development of a New Generation of Gold Catalysts for Amine Oxidation', Chemcatchem, 2 (2010), 666-73.

5 V. Augugliaro, H. Kisch, V. Loddo, M. J. Lopez-Munoz, C. Marquez-Alvarez, G. Palmisano, L. Palmisano, F. Parrino, and S. Yurdakal, 'Photocatalytic Oxidation of Aromatic Alcohols to Aldehydes in Aqueous Suspension of Home Prepared Titanium Dioxide 2. Intrinsic and Surface Features of Catalysts', Applied Catalysis a-General, 349 (2008), 189-97.

6 V. Augugliaro, V. Loddo, M. J. Lopez-Munoz, C. Marquez-Alvarez, G. Palmisano, L. Palmisano, and S. Yurdakal, 'Home-Prepared Anatase, Rutile, and Brookite Tio2 for Selective Photocatalytic Oxidation of 4-Methoxybenzyl Alcohol in Water: Reactivity and Atr-Ftir Study', Photochemical & Photobiological Sciences, 8 (2009), 663-69.

7 K. Awazu, M. Fujimaki, C. Rockstuhl, J. Tominaga, H. Murakami, Y. Ohki, N. Yoshida, and T. Watanabe, 'A Plasmonic Photocatalyst Consisting of Sliver Nanoparticles Embedded in Titanium Dioxide', Journal of the American Chemical Society, 130 (2008), 1676-80.

8 Inga Bannat, Katrin Wessels, Torsten Oekermann, Jiri Rathousky, Detlef Bahnemann, and Michael Wark, 'Improving the Photocatalytic Performance of Mesoporous Titania Films by Modification with Gold Nanostructures', Chemistry of Materials, 21 (2009), 1645-53.

9 M. A. Barakat, R. I. Al-Hutailah, M. H. Hashim, E. Qayyum, and J. N. Kuhn, 'Titania-Supported Silver-Based Bimetallic Nanoparticles as Photocatalysts', Environmental science and pollution research international, 20 (2013), 3751-9.

10 W. Bhagathsingh, and A. Samson Nesaraj, 'Low Temperature Synthesis and Thermal Properties of Ag-Cu Alloy Nanoparticles', Transactions of Nonferrous Metals Society of China, 23 (2013), 128-33.

11 S. Biella, L. Prati, and M. Rossi, 'Selective Oxidation of D-Glucose on Gold Catalyst', Journal of Catalysis, 206 (2002), 242-47.

12 M. I. bin Saiman, G. L. Brett, R. Tiruvalam, M. M. Forde, K. Sharples, A. Thetford, R. L. Jenkins, N. Dimitratos, J. A. Lopez-Sanchez, D. M. Murphy, D. Bethell, D. J. Willock, S. H. Taylor, D. W. Knight, C. J. Kiely, and G. J. Hutchings, 'Involvement of Surface-Bound Radicals in the Oxidation of Toluene Using Supported Au-Pd Nanoparticles', Angewandte Chemie-International Edition, 51 (2012), 5981-85.

13 X. Bokhimi, R. Zanella, V. Maturano, and A. Morales, 'Nanocrystalline Ag, and Au-Ag Alloys Supported on Titania for Co Oxidation Reaction', Materials Chemistry and Physics, 138 (2013), 490-99.

14 F. Bonet, V. Delmas, S. Grugeon, R. H. Urbina, P. Y. Silvert, and K. Tekaia-Elhsissen, 'Synthesis of Monodisperse Au, Pt, Pd, Ru and Ir Nanoparticles in Ethylene Glycol', Nanostructured Materials, 11 (1999), 1277-84.

15 Michael Bowker, Abdullahi Nuhu, and Jorge Soares, 'High Activity Supported Gold Catalysts by Incipient Wetness Impregnation', Catalysis Today, 122 (2007), 245-47.

16 Charles T. Campbell, Stephen C. Parker, and David E. Starr, 'The Effect of Size-Dependent Nanoparticle Energetics on Catalyst Sintering', Science, 298 (2002), 811-14.

17 Nirmalya K. Chaki, Hironori Tsunoyama, Yuichi Negishi, Hidehiro Sakurai, and Tatsuya Tsukuda, 'Effect of Ag-Doping on the Catalytic Activity of Polymer-Stabilized Au Clusters in Aerobic Oxidation of Alcohol', Journal of Physical Chemistry C, 111 (2007), 4885-88.

18 S. Chowdhury, V. R. Bhethanabotla, and R. Sen, 'Effect of Ag-Cu Alloy Nanoparticle Composition on Luminescence Enhancement/Quenching', Journal of Physical Chemistry C, 113 (2009), 13016-22.

19 Phillip Christopher, David B. Ingram, and Suljo Linic, 'Enhancing Photochemical Activity of Semiconductor Nanoparticles with Optically Active Ag Nanostructures: Photochemistry Mediated by Ag Surface Plasmons', Journal of Physical Chemistry C, 114 (2010), 9173-77.

20 J. C. Colmenares, A. Magdziarz, and A. Bielejewska, 'High-Value Chemicals Obtained from Selective Photo-Oxidation of Glucose in the Presence of Nanostructured Titanium Photocatalysts', Bioresource Technology, 102 (2011), 11254-57.

21 D. P. Colombo, D. E. Skinner, J. J. Cavaleri, and R. M. Bowman, 'Femtosecond Spectroscopy of Quantum-Sized and Bulk-Sized Semiconductor Particles', Abstracts of Papers of the American Chemical Society, 210 (1995), 37-PHYS.

22 A. Corma, and H. Garcia, 'Supported Gold Nanoparticles as Catalysts for Organic Reactions', Chemical Society Reviews, 37 (2008), 2096-126.

23 Avelino Corma, Pedro Serna, and Hermenegildo Garcia, 'Gold Catalysts Open a New General Chemoselective Route to Synthesize Oximes by Hydrogenation of Alpha,Beta-Unsaturated Nitrocompounds with H-2', Journal of the American Chemical Society, 129 (2007), 6358-+.

24 J. A. Creighton, and D. G. Eadon, 'Ultraviolet Visible Absorption-Spectra of the Colloidal Metallic Elements', Journal of the Chemical Society-Faraday Transactions, 87 (1991), 3881-91.

25 D. Dambournet, I. Belharouak, and K. Amine, 'Tailored Preparation Methods of Tio2 Anatase, Rutile, Brookite: Mechanism of Formation and Electrochemical Properties', Chemistry of Materials, 22 (2010), 1173-79.

26 Laurent Delannoy, Nissrine El Hassan, Andrea Musi, Nga Nguyen Le To, Jean-Marc Krafft, and Catherine Louis, 'Preparation of Supported Gold Nanoparticles by a Modified Incipient Wetness Impregnation Method', Journal of Physical Chemistry B, 110 (2006), 22471-78.

27 Weiping Deng, Mi Liu, Xuesong Tan, Qinghong Zhang, and Ye Wang, 'Conversion of Cellobiose into Sorbitol in Neutral Water Medium over Carbon Nanotube-Supported Ruthenium Catalysts', Journal of Catalysis, 271 (2010), 22-32.

28 H. Dimitroula, V. M. Daskalaki, Z. Frontistis, D. I. Kondarides, P. Panagiotopoulou, N. P. Xekoukoulotakis, and D. Mantzavinos, 'Solar Photocatalysis for the Abatement of Emerging Micro-Contaminants in Wastewater: Synthesis, Characterization and Testing of Various Tio2 Samples', Applied Catalysis B-Environmental, 117 (2012), 283-91.

29 T. A. Egerton, and I. R. Tooley, 'Effect of Changes in Tio2 Dispersion on Its Measured Photocatalytic Activity', Journal of Physical Chemistry B, 108 (2004), 5066-72.

30 D. I. Enache, D. W. Knight, and G. J. Hutchings, 'Solvent-Free Oxidation of Primary Alcohols to Aldehydes Using Supported Gold Catalysts', Catalysis Letters, 103 (2005), 43-52.

31 P. Engel, R. Mladenov, H. Wulfhorst, G. Jager, and A. C. Spiess, 'Point by Point Analysis: How Ionic Liquid Affects the Enzymatic Hydrolysis of Native and Modified Cellulose', Green Chemistry, 12 (2010), 1959-66.

32 S. Eustis, and M. A. El-Sayed, 'Why Gold Nanoparticles Are More Precious Than Pretty Gold: Noble Metal Surface Plasmon Resonance and Its Enhancement of the Radiative and Nonradiative Properties of Nanocrystals of Different Shapes', Chemical Society Reviews, 35 (2006), 209-17.

33 David D. Evanoff, and George Chumanov, 'Synthesis and Optical Properties of Silver Nanoparticles and Arrays', Chemphyschem, 6 (2005), 1221-31.

34 H. X. Fan, G. Li, F. Yang, L. Yang, and S. M. Zhang, 'Photodegradation of Cellulose under Uv Light Catalysed by Tio2', Journal of Chemical Technology and Biotechnology, 86 (2011), 1107-12.

35 Hongxian Fan, Gang Li, Fang Yang, Lei Yang, and Songmei Zhang, 'Photodegradation of Cellulose under Uv Light Catalysed by Tio2', Journal of Chemical Technology and Biotechnology, 86 (2011), 1107-12.

36 A. Fujishima, and K. Honda, 'Electrochemical Photolysis of Water at a Semiconductor Electrode', Nature, 238 (1972), 37-+.

37 J. Geboers, S. Van de Vyver, K. Carpentier, K. de Blochouse, P. Jacobs, and B. Sels, 'Efficient Catalytic Conversion of Concentrated Cellulose Feeds to Hexitols with Heteropoly Acids and Ru on Carbon', Chemical Communications, 46 (2010), 3577-79.

38 S. K. Ghosh, S. Nath, S. Kundu, K. Esumi, and T. Pal, 'Solvent and Ligand Effects on the Localized Surface Plasmon Resonance (Lspr) of Gold Colloids', Journal of Physical Chemistry B, 108 (2004), 13963-71.

39 D. G. Gong, W. C. J. Ho, Y. X. Tang, Q. Tay, Y. K. Lai, J. G. Highfield, and Z. Chen, 'Silver Decorated Titanate/Titania Nanostructures for Efficient Solar Driven Photocatalysis', Journal of Solid State Chemistry, 189 (2012), 117-22.

40 E. Grabowska, A. Zaleska, S. Sorgues, M. Kunst, A. Etcheberry, C. Colbeau-Justin, and H. Remita, 'Modification of Titanium(Iv) Dioxide with Small Silver Nanoparticles: Application in Photocatalysis', Journal of Physical Chemistry C, 117 (2013), 1955-62.

41 A. Grirrane, A. Corma, and H. Garcia, 'Gold-Catalyzed Synthesis of Aromatic Azo Compounds from Anilines and Nitroaromatics', Science, 322 (2008), 1661-64.

42 S. M. Gupta, and M. Tripathi, 'An Overview of Commonly Used Semiconductor Nanoparticles in Photocatalysis', High Energy Chemistry, 46 (2012), 1-9.

43 D. A. H. Hanaor, and C. C. Sorrell, 'Review of the Anatase to Rutile Phase Transformation', Journal of Materials Science, 46 (2011), 855-74.

44 M. Haruta, 'Size- and Support-Dependency in the Catalysis of Gold', Catalysis Today, 36 (1997), 153-66.

45 M. Haruta, N. Yamada, T. Kobayashi, and S. Iijima, 'Gold Catalysts Prepared by Coprecipitation for Low-Temperature Oxidation of Hydrogen and of Carbon-Monoxide', Journal of Catalysis, 115 (1989), 301-09.

46 A. S. K. Hashmi, 'Gold-Catalyzed Organic Reactions', Chemical Reviews, 107 (2007), 3180-211.

47 A. Stephen K. Hashmi, and Graham J. Hutchings, 'Gold Catalysis', Angewandte Chemie-International Edition, 45 (2006), 7896-936.

48 A. Hattori, Y. Tokihisa, H. Tada, and S. Ito, 'Acceleration of Oxidations and Retardation of Reductions in Photocatalysis of a Tio2/Sno2 Bilayer-Type Catalyst', Journal of the Electrochemical Society, 147 (2000), 2279-83.

49 H. Hirai, and N. Yakura, 'Protecting Polymers in Suspension of Metal Nanoparticles', Polymers for Advanced Technologies, 12 (2001), 724-33.

50 M. R. Hoffmann, S. T. Martin, W. Y. Choi, and D. W. Bahnemann, 'Environmental Applications of Semiconductor Photocatalysis', Chemical Reviews, 95 (1995), 69-96.

51 H. H. Huang, X. P. Ni, G. L. Loy, C. H. Chew, K. L. Tan, F. C. Loh, J. F. Deng, and G. Q. Xu, 'Photochemical Formation of Silver Nanoparticles in Poly(N-Vinylpyrrolidone)', Langmuir, 12 (1996), 909-12.

52 X. Huang, X. Wang, X. Wang, X. Wang, M. Tan, W. Ding, and X. Lu, 'P123-Stabilized Au-Ag Alloy Nanoparticles for Kinetics of Aerobic Oxidation of Benzyl Alcohol in Aqueous Solution', Journal of Catalysis, 301 (2013), 217-26.

53 Kosuke Kaizuka, Hiroyuki Miyamura, and Shu Kobayashi, 'Remarkable Effect of Bimetallic Nanocluster Catalysts for Aerobic Oxidation of Alcohols: Combining Metals Changes the Activities and the Reaction Pathways to Aldehydes/Carboxylic Acids or Esters', Journal of the American Chemical Society, 132 (2010), 15096-98.

54 K. L. Kelly, E. Coronado, L. L. Zhao, and G. C. Schatz, 'The Optical Properties of Metal Nanoparticles: The Influence of Size, Shape, and Dielectric Environment', Journal of Physical Chemistry B, 107 (2003), 668-77.

55 K. Kimura, S. Naya, Y. Jin-nouchi, and H. Tada, 'Tio2 Crystal Form-Dependence of the Au/Tio2 Plasmon Photocatalyst's Activity', Journal of Physical Chemistry C, 116 (2012), 7111-17.

56 Hirokazu Kobayashi, Tasuku Komanoya, Kenji Hara, and Atsushi Fukuoka, 'Water-Tolerant Mesoporous-Carbon-Supported Ruthenium Catalysts for the Hydrolysis of Cellulose to Glucose', Chemsuschem, 3 (2010), 440-43.

57 E. Kowalska, O. O. P. Mahaney, R. Abe, and B. Ohtani, 'Visible-Light-Induced Photocatalysis through Surface Plasmon Excitation of Gold on Titania Surfaces', Physical Chemistry Chemical Physics, 12 (2010), 2344-55.

58 Ewa Kowalska, Ryu Abe, and Bunsho Ohtani, 'Visible Light-Induced Photocatalytic Reaction of Gold-Modified Titanium(Iv) Oxide Particles: Action Spectrum Analysis', Chemical Communications (2009), 241-43.

59 U. Kreibig, and L. Genzel, 'Optical Absorption of Small Metallic Particles', Surface Science, 156, Part 2 (1985), 678-700.

60 S. G. Kumar, and L. G. Devi, 'Review on Modified Tio2 Photocatalysis under Uv/Visible Light: Selected Results and Related Mechanisms on Interfacial Charge Carrier Transfer Dynamics', Journal of Physical Chemistry A, 115 (2011), 13211-41.

61 Da-ming Lai, Li Deng, Jiang Li, Bing Liao, Qing-Xiang Guo, and Yao Fu, 'Hydrolysis of Cellulose into Glucose by Magnetic Solid Acid', Chemsuschem, 4 (2011), 55-58.

62 M. Landmann, E. Rauls, and W. G. Schmidt, 'The Electronic Structure and Optical Response of Rutile, Anatase and Brookite Tio2', Journal of Physics-Condensed Matter, 24 (2012).

63 G. F. Liang, C. Y. Wu, L. M. He, J. Ming, H. Y. Cheng, L. H. Zhuo, and F. Y. Zhao, 'Selective Conversion of Concentrated Microcrystalline Cellulose to Isosorbide over Ru/C Catalyst', Green Chemistry, 13 (2011), 839-42.

64 Suljo Linic, Phillip Christopher, and David B. Ingram, 'Plasmonic-Metal Nanostructures for Efficient Conversion of Solar to Chemical Energy', Nature Materials, 10 (2011), 911-21.

65 S. Link, and M. A. El-Sayed, 'Size and Temperature Dependence of the Plasmon Absorption of Colloidal Gold Nanoparticles', Journal of Physical Chemistry B, 103 (1999), 4212-17.

66 A. L. Linsebigler, G. Q. Lu, and J. T. Yates, 'Photocatalysis on Tio2 Surfaces - Principles, Mechanisms, and Selected Results', Chemical Reviews, 95 (1995), 735-58.

67 J. A. Lopez-Sanchez, N. Dimitratos, P. Miedziak, E. Ntainjua, J. K. Edwards, D. Morgan, A. F. Carley, R. Tiruvalam, C. J. Kiely, and G. J. Hutchings, 'Au-Pd Supported Nanocrystals Prepared by a Sol Immobilisation Technique as Catalysts for Selective Chemical Synthesis', Physical Chemistry Chemical Physics, 10 (2008), 1921-30.

68 Jose A. Lopez-Sanchez, Nikolaos Dimitratos, Ceri Hammond, Gemma L. Brett, Lokesh Kesavan, Saul White, Peter Miedziak, Ramchandra Tiruvalam, Robert L. Jenkins, Albert F. Carley, David Knight, Christopher J. Kiely, and Graham J. Hutchings, 'Facile Removal of Stabilizer-Ligands from Supported Gold Nanoparticles', Nature Chemistry, 3 (2011), 551-56.

69 Chen Luo, Shuai Wang, and Haichao Liu, 'Cellulose Conversion into Polyols Catalyzed by Reversibly Formed Acids and Supported Ruthenium Clusters in Hot Water', Angewandte Chemie-International Edition, 46 (2007), 7636-39.

70 Michelle Duval Malinsky, K. Lance Kelly, George C. Schatz, and Richard P. Van Duyne, 'Chain Length Dependence and Sensing Capabilities of the Localized Surface Plasmon Resonance of Silver Nanoparticles Chemically Modified with Alkanethiol Self-Assembled Monolayers', Journal of the American Chemical Society, 123 (2001), 1471-82.

71 Thomas Maschmeyer, and Michel Che, 'Catalytic Aspects of Light-Induced Hydrogen Generation in Water with Tio2 and Other Photocatalysts: A Simple and Practical Way Towards a Normalization?', Angewandte Chemie-International Edition, 49 (2010), 1536-39.

72 A. Mattsson, and L. Osterlund, 'Adsorption and Photoinduced Decomposition of Acetone and Acetic Acid on Anatase, Brookite, and Rutile Tio2 Nanoparticles', Journal of Physical Chemistry C, 114 (2010), 14121-32.

73 M. Messaoud, E. Chadeau, C. Brunon, T. Ballet, L. Rappenne, F. Roussel, D. Leonard, N. Oulahal, and M. Langlet, 'Photocatalytic Generation of Silver Nanoparticles and Application to the Antibacterial Functionalization of Textile Fabrics', Journal of Photochemistry and Photobiology a-Chemistry, 215 (2010), 147-56.

74 Gustav Mie, 'Beiträge Zur Optik Trüber Medien, Speziell Kolloidaler Metallösungen', Annalen der Physik, 330 (1908), 377-445.

75 C. Milone, R. Ingoglia, A. Pistone, G. Neri, and S. Galvagno, 'Activity of Gold Catalysts in the Liquid-Phase Oxidation of O-Hydroxybenzyl Alcohol', Catalysis Letters, 87 (2003), 201-09.

76 Agnes Mirescu, and Ulf Pruesse, 'A New Environmental Friendly Method for the Preparation of Sugar Acids Via Catalytic Oxidation on Gold Catalysts', Applied Catalysis B-Environmental, 70 (2007), 644-52.

77 N. F. Mott, and R. S. Allgaier, 'Localized States in Disordered Lattices', physica status solidi (b), 21 (1967), 343-56.

78 Radha Narayanan, and Mostafa A. El-Sayed, 'Some Aspects of Colloidal Nanoparticle Stability, Catalytic Activity, and Recycling Potential', Topics in Catalysis, 47 (2008), 15-21.

79 K. Niu, P. Chen, X. Zhang, and W. S. Tan, 'Enhanced Enzymatic Hydrolysis of Rice Straw Pretreated by Alkali Assisted with Photocatalysis Technology', Journal of Chemical Technology and Biotechnology, 84 (2009), 1240-45.

80 Ayumu Onda, Takafumi Ochi, and Kazumichi Yanagisawa, 'Selective Hydrolysis of Cellulose into Glucose over Solid Acid Catalysts', Green Chemistry, 10 (2008), 1033-37.

81 L. D. Pachon, and G. Rothenberg, 'Transition-Metal Nanoparticles: Synthesis, Stability and the Leaching Issue', Applied Organometallic Chemistry, 22 (2008), 288-99.

82 G. S. Pang, S. G. Chen, Y. Koltypin, A. Zaban, S. H. Feng, and A. Gedanken, 'Controlling the Particle Size of Calcined Sno2 Nanocrystals', Nano Letters, 1 (2001), 723-26.

83 Jifeng Pang, Aiqin Wang, Mingyuan Zheng, and Tao Zhang, 'Hydrolysis of Cellulose into Glucose over Carbons Sulfonated at Elevated Temperatures', Chemical Communications, 46 (2010), 6935-37.

84 I. Paramasivam, H. Jha, N. Liu, and P. Schmuki, 'A Review of Photocatalysis Using Self-Organized Tio2 Nanotubes and Other Ordered Oxide Nanostructures', Small, 8 (2012), 3073-103.

85 O. O. Prieto-Mahaney, N. Murakami, R. Abe, and B. Ohtani, 'Correlation between Photocatalytic Activities and Structural and Physical Properties of Titanium(Iv) Oxide Powders', Chemistry Letters, 38 (2009), 238-39.

86 A. Primo, A. Corma, and H. Garcia, 'Titania Supported Gold Nanoparticles as Photocatalyst', Physical Chemistry Chemical Physics, 13 (2011), 886-910.

87 A. J. Ragauskas, C. K. Williams, B. H. Davison, G. Britovsek, J. Cairney, C. A. Eckert, W. J. Frederick, J. P. Hallett, D. J. Leak, C. L. Liotta, J. R. Mielenz, R. Murphy, R. Templer, and T. Tschaplinski, 'The Path Forward for Biofuels and Biomaterials', Science, 311 (2006), 484-89.

88 L. U. Rahman, R. Qureshi, M. M. Yasinzai, and A. Shah, 'Synthesis and Spectroscopic Characterization of Ag-Cu Alloy Nanoparticles Prepared in Various Ratios', Comptes Rendus Chimie, 15 (2012), 533-38.

89 D. Reyes-Luyanda, J. Flores-Cruz, P. J. Morales-Perez, L. G. Encarnacion-Gomez, F. Y. Shi, P. M. Voyles, and N. Cardona-Martinez, 'Bifunctional Materials for the Catalytic Conversion of Cellulose into Soluble Renewable Biorefinery Feedstocks', Topics in Catalysis, 55 (2012), 148-61.

90 R. Rinaldi, R. Palkovits, and F. Schuth, 'Depolymerization of Cellulose Using Solid Catalysts in Ionic Liquids', Angewandte Chemie-International Edition, 47 (2008), 8047-50.

91 R. Rinaldi, and F. Schuth, 'Design of Solid Catalysts for the Conversion of Biomass', Energy & Environmental Science, 2 (2009), 610-26.

92 Vera P. Santos, Sónia A. C. Carabineiro, Pedro B. Tavares, Manuel F. R. Pereira, José J. M. Órfão, and José L. Figueiredo, 'Oxidation of Co, Ethanol and Toluene over Tio2 Supported Noble Metal Catalysts', Applied Catalysis B: Environmental, 99 (2010), 198-205.

93 A. Sclafani, and J. M. Herrmann, 'Comparison of the Photoelectronic and Photocatalytic Activities of Various Anatase and Rutile Forms of Titania in Pure Liquid Organic Phases and in Aqueous Solutions', Journal of Physical Chemistry, 100 (1996), 13655-61.

94 S. Tamil Selvan, Tomokatsu Hayakawa, and Masayuki Nogami, 'Remarkable Influence of Silver Islands on the Enhancement of Fluorescence from Eu3+ Ion-Doped Silica Gels', The Journal of Physical Chemistry B, 103 (1999), 7064-67.

95 N. Serpone, E. Borgarello, and M. Gratzel, 'Visible-Light Induced Generation of Hydrogen from H2s in Mixed Semiconductor Dispersions - Improved Efficiency through Inter-Particle Electron-Transfer', Journal of the Chemical Society-Chemical Communications (1984), 342-44.

96 N. Serpone, and A. V. Emeline, 'Semiconductor Photocatalysis - Past, Present, and Future Outlook', Journal of Physical Chemistry Letters, 3 (2012), 673-77.

97 Yihong Shen, Shenghong Zhang, Hongjia Li, Yuan Ren, and Haichao Liu, 'Efficient Synthesis of Lactic Acid by Aerobic Oxidation of Glycerol on Au-Pt/Tio2 Catalysts', Chemistry-a European Journal, 16 (2010), 7368-71.

98 C. G. Silva, R. Juá rez, T. Marino, R. Molinari, and H. García, 'Influence of Excitation Wavelength (Uv or Visible Light) on the Photocatalytic Activity of Titania Containing Gold Nanoparticles for the Generation of Hydrogen or Oxygen from Water', Journal of the American Chemical Society, 133 (2011), 595-602.

99 E. Stathatos, P. Lianos, P. Falaras, and A. Siokou, 'Photocatalytically Deposited Silver Nanoparticles on Mesoporous Tio2 Films', Langmuir, 16 (2000), 2398-400.

100 Yoshitsune Sugano, Yasuhiro Shiraishi, Daijiro Tsukamoto, Satoshi Ichikawa, Shunsuke Tanaka, and Takayuki Hirai, 'Supported Au-Cu Bimetallic Alloy Nanoparticles: An Aerobic Oxidation Catalyst with Regenerable Activity by Visible-Light Irradiation', Angewandte Chemie (International ed. in English), 52 (2013), 5295-9.

101 Satoshi Suganuma, Kiyotaka Nakajima, Masaaki Kitano, Daizo Yamaguchi, Hideki Kato, Shigenobu Hayashi, and Michikazu Hara, 'Hydrolysis of Cellulose by Amorphous Carbon Bearing So3h, Cooh, and Oh Groups', Journal of the American Chemical Society, 130 (2008), 12787-93.

102 J. M. Sun, and X. H. Bao, 'Textural Manipulation of Mesoporous Materials for Hosting of Metallic Nanocatalysts', Chemistry-a European Journal, 14 (2008), 7478-88.

103 C. Suwanchawalit, and S. Wongnawa, 'Triblock Copolymer-Templated Synthesis of Porous Tio2 and Its Photocatalytic Activity', Journal of Nanoparticle Research, 12 (2010), 2895-906.

104 A. Takagaki, C. Tagusagawa, and K. Domen, 'Glucose Production from Saccharides Using Layered Transition Metal Oxide and Exfoliated Nanosheets as a Water-Tolerant Solid Acid Catalyst', Chemical Communications (2008), 5363-65.

105 A. Takagaki, C. Tagusagawa, S. Hayashi, M. Hara, and K. Domen, 'Nanosheets as Highly Active Solid Acid Catalysts for Green Chemical Syntheses', Energy & Environmental Science, 3 (2010), 82-93.

106 Atsuhiro Tanaka, Satoshi Sakaguchi, Keiji Hashimoto, and Hiroshi Kominami, 'Preparation of Au/Tio2 with Metal Cocatalysts Exhibiting Strong Surface Plasmon Resonance Effective for Photoinduced Hydrogen Formation under Irradiation of Visible Light', Acs Catalysis, 3 (2013), 79-85.

107 H. Tang, F. Lévy, H. Berger, and P. E. Schmid, 'Urbach Tail of Anatase Tio_{2}', Physical Review B, 52 (1995), 7771-74.

108 Andrea Tao, Franklin Kim, Christian Hess, Joshua Goldberger, Rongrui He, Yugang Sun, Younan Xia, and Peidong Yang, 'Langmuir−Blodgett Silver Nanowire Monolayers for Molecular Sensing Using Surface-Enhanced Raman Spectroscopy', Nano Letters, 3 (2003), 1229-33.

109 Na Tian, Zhi-You Zhou, Shi-Gang Sun, Yong Ding, and Zhong Lin Wang, 'Synthesis of Tetrahexahedral Platinum Nanocrystals with High-Index Facets and High Electro-Oxidation Activity', Science, 316 (2007), 732-35.

110 Y. Tian, and T. Tatsuma, 'Mechanisms and Applications of Plasmon-Induced Charge Separation at Tio2 Films Loaded with Gold Nanoparticles', Journal of the American Chemical Society, 127 (2005), 7632-37.

111 ———, 'Plasmon-Induced Photoelectrochemistry at Metal Nanoparticles Supported on Nanoporous Tio2', Chemical Communications (2004), 1810-11.

112 X. L. Tong, Y. Ma, and Y. D. Li, 'Biomass into Chemicals: Conversion of Sugars to Furan Derivatives by Catalytic Processes', Applied Catalysis a-General, 385 (2010), 1-13.

113 S. Tsubota, D. A. H. Cunningham, Y. Bando, and M. Haruta, Preparation of Nanometer Gold Strongly Interacted with Tio2 and the Structure Sensitivity in Low-Temperature Oxidation of Co. ed. by G. Poncelet, J. Martens, B. Delmon, P. A. Jacobs and P. Grange. Vol. 91, Preparation of Catalysts Vi: Scientific Bases for the Preparation of Heterogeneous Catalysts, 1995), pp. 227-35.

114 S. Van De Vyver, J. Geboers, P. A. Jacobs, and B. F. Sels, 'Recent Advances in the Catalytic Conversion of Cellulose', Chemcatchem, 3 (2011), 82-94.

115 S. Van de Vyver, L. Peng, J. Geboers, H. Schepers, F. de Clippel, C. J. Gommes, B. Goderis, P. A. Jacobs, and B. F. Sels, 'Sulfonated Silica/Carbon Nanocomposites as Novel Catalysts for Hydrolysis of Cellulose to Glucose', Green Chemistry, 12 (2010), 1560-63.

116 Y. F. Wang, and T. Asefa, 'Poly(Allylamine)-Stabilized Colloidal Copper Nanoparticles: Synthesis, Morphology, and Their Surface-Enhanced Raman Scattering Properties', Langmuir, 26 (2010), 7469-74.

117 Bo Wen, JiaHai Ma, ChunCheng Chen, WanHong Ma, HuaiYong Zhu, and JinCai Zhao, 'Supported Noble Metal Nanoparticles as Photo/Sono-Catalysts for Synthesis of Chemicals and Degradation of Pollutants', Science China Chemistry, 54 (2011), 887-97.

118 R. J. White, R. Luque, V. L. Budarin, J. H. Clark, and D. J. Macquarrie, 'Supported Metal Nanoparticles on Porous Materials. Methods and Applications', Chemical Society Reviews, 38 (2009), 481-94.

119 Guang-nian Xu, Xue-liang Qiao, Xiao-lin Qiu, and Jian-guo Chen, 'Preparation and Characterization of Stable Monodisperse Silver Nanoparticles Via Photoreduction', Colloids and Surfaces A: Physicochemical and Engineering Aspects, 320 (2008), 222-26.

120 Junqing Yan, Guangjun Wu, Naijia Guan, Landong Li, Zhuoxin Li, and Xingzhong Cao, 'Understanding the Effect of Surface/Bulk Defects on the Photocatalytic Activity of Tio2: Anatase Versus Rutile', Physical chemistry chemical physics : PCCP, 15 (2013), 10978-88.

121 Wenfu Yan, Bei Chen, S. M. Mahurin, V. Schwartz, D. R. Mullins, Andrew R. Lupini, S. J. Pennycook, Sheng Dai, and S. H. Overbury, 'Preparation and Comparison of Supported Gold Nanocatalysts on Anatase, Brookite, Rutile, and P25 Polymorphs of Tio2 for Catalytic Oxidation of Co', The Journal of Physical Chemistry B, 109 (2005), 10676-85.

122 J. C. Yu, J. G. Yu, W. K. Ho, and L. Z. Zhang, 'Preparation of Highly Photocatalytic Active Nano-Sized Tio2 Particles Via Ultrasonic Irradiation', Chemical Communications (2001), 1942-43.

123 X. M. Zhang, Y. L. Chen, R. S. Liu, and D. P. Tsai, 'Plasmonic Photocatalysis', Reports on Progress in Physics, 76 (2013).

124 J. C. Zhao, T. X. Wu, K. Q. Wu, K. Oikawa, H. Hidaka, and N. Serpone, 'Photoassisted Degradation of Dye Pollutants. 3. Degradation of the Cationic Dye Rhodamine B in Aqueous Anionic Surfactant/Tio2 Dispersions under Visible Light Irradiation: Evidence for the Need of Substrate Adsorption on Tio2 Particles', Environmental Science & Technology, 32 (1998), 2394-400.

125 C. H. Zhou, X. Xia, C. X. Lin, D. S. Tong, and J. Beltramini, 'Catalytic Conversion of Lignocellulosic Biomass to Fine Chemicals and Fuels', Chemical Society Reviews, 40 (2011), 5588-617.

126 M. H. Zhou, J. G. Yu, S. W. Liu, P. C. Zhai, and L. Jiang, 'Effects of Calcination Temperatures on Photocatalytic Activity of Sno2/Tio2 Composite Films Prepared by an Epd Method', Journal of Hazardous Materials, 154 (2008), 1141-48.

127 W. Zhou, and H. G. Fu, 'Mesoporous Tio2: Preparation, Doping, and as a Composite for Photocatalysis', Chemcatchem, 5 (2013), 885-94.

128 X. M. Zhou, G. Liu, J. G. Yu, and W. H. Fan, 'Surface Plasmon Resonance-Mediated Photocatalysis by Noble Metal-Based Composites under Visible Light', Journal of Materials Chemistry, 22 (2012), 21337-54.

129 H. Y. Zhu, X. Chen, Z. F. Zheng, X. B. Ke, E. Jaatinen, J. C. Zhao, C. Guo, T. F. Xie, and D. J. Wang, 'Mechanism of Supported Gold Nanoparticles as Photocatalysts under Ultraviolet and Visible Light Irradiation', Chemical Communications (2009), 7524-26.

130 J. Zhu, Z. Konya, V. F. Puntes, I. Kiricsi, C. X. Miao, J. W. Ager, A. P. Alivisatos, and G. A. Somorjai, 'Encapsulation of Metal (Au, Ag, Pt) Nanoparticles into the Mesoporous Sba-15 Structure', Langmuir, 19 (2003), 4396-401.

131 Junjiang Zhu, Tao Wang, Xuelian Xu, Ping Xiao, and Jinlin Li, 'Pt Nanoparticles Supported on Sba-15: Synthesis, Characterization and Applications in Heterogeneous Catalysis', Applied Catalysis B-Environmental, 130 (2013), 197-217.

6.2. Books

132 B. Kamm, P. R. Gruber, M. Kamm, 'Biorefineries – Industrial Process and Products', Wiley-VCH, Weinheim, vol. 1, 2006, p. 15.

133 D. Fengel, G. Wegener, Wood: Chemistry, 'Ultrastructure', Reactions, Berlin, 1984, p. 613.

134 U. Kreibig, M. Vollmer, 'Optical Properties of Metal Clusters', Springer, Berlin, 1995.